Advanced Space Concepts Laboratory

Department of Mechanical and Aerospace Engineering

Faculty of Engineering

University of Strathclyde

Station-keeping and orbital transfers in the vicinity of the Moon exploiting quasi-periodic orbit dynamics

Marcel Duering

Submitted in fulfilment of the requirements for the degree of

Doctor of Philosophy

2018

This thesis is the result of the author's original research. It has been composed by the author and has not been previously submitted for examination which has led to the award of a degree.

Marcel Duering
Glasgow, United Kingdom, 2018

Abstract

Future manned space exploration sets a focus on the long-term goal of landing humans on a foreign planet in particular on Mars. Translating this ambitious plan into practice is a major challenge, and beforehand several milestones have to be achieved. One major objective in the years ahead will be a return to the vicinity of the Moon with robotic exploration missions and crewed space vehicles. Not only is returning to the Moon an inspiring challenge but also and more importantly a return to the Moon opens the possibility to prove new technologies, gain scientific knowledge, and identify key requirements for further endeavours. As a consequence it is possible that traditional mission scenarios considering the use of low lunar orbits or transfer arcs to the surface are replaced by new mission scenarios exploiting the potentialities of the collinear Earth-Moon libration point orbits. In addition, solutions considering multiple coordinated spacecraft with disaggregated payloads are becoming more and more interesting for a variety of space missions. The cooperation between spacecraft will increase redundancy and will enable new navigation and remote sensing solutions that can hardly be achieved with single monolithic spacecraft. A key element of missions considering the collaborative interaction among groups of spacecraft is the ability to transfer them between orbits. This might include rendezvous and docking for on-orbit assembling. In this context, the vision is to have a transport system in the Earth-Moon environment that allows transferring components from the Earth to the Moon and assembling large infrastructures in the vicinity of the Moon. This infrastructure serves as stepping stone or gateway to the exploration of the solar system. A fundamental understanding of existing orbits and transfer possibilities becomes critical for exploring and accessing the vicinity of the Moon. A transport system in this described context offers regular access to all orbits between the Earth and the Moon, which includes transfers from the Earth to the Moon, transfers among orbits in the proximity of the Moon and transfers from the Moon to interplanetary space. From a mission design point of

view it is paramount to understand the intricate interaction between the Earth's and the Moon's gravity field. Projects also benefit from the unique dynamical environment prevailing at the libration point regions enabling to choose from a huge variety of operational orbits with greatly varying parameters. The utilisation of quasi-periodic orbits increase the flexibility in planning future missions, reduces the complexity of long-term space missions by enabling larger windows for manoeuvre execution for orbital transfers. Furthermore, properties of operational orbits might be changed by manoeuvres enabling to achieve mission objectives. Based on this assumption a variety of problems are addressed in this work. Numerical tools are presented to study and assess quasi-periodic bounded orbits in the vicinity of the Moon, in particular libration point and distant periodic orbits. On the basis of a description of quasi-periodic orbits, mission analysis aspects studied are the identification of suitable operational orbits, transfer opportunities among those orbits, and the handling of quasi-periodic orbits in a high-fidelity dynamical model. A method is presented to systematically compute any type of transfer either for changing properties of the operational orbit or to re-phase spacecraft along the orbit. The proposed orbital transfers utilise hyperbolic invariant manifolds of orbits that exist in a three-body regime. Parameters have been identified that have a substantial impact on the existent range of orbits and figure of merits are presented for reference scenarios that comprises the elements of an exploration mission travelling to L_2 libration point orbits in the proximity of the Moon.

Table of Contents

Nomenclature

Throughout this work scalar quantities are denoted as italic letters (a) or (A). Vectors are featured as italic and bold lower-case letters ($\boldsymbol{a}$). Matrices are termed with italic bold capital letters ($\boldsymbol{A}$).

t	Time
G	Universal gravitational constant
L_n	Libration point n
m_n	Mass of body n
r_n	Radius of body n
$\boldsymbol{r_n}$	Radius vector of body n
μ_n	Gravitational parameter of body n
ω	Angular velocity of the rotating frame
$\boldsymbol{\omega}$	Frequency vector of a quasi-periodic orbit
U	Pseudo potential function
U_{ij}	Partial derivatives of the pseudo potential function
a_n	Eigenvectors
H	Hamiltonian
p_n	Partial derivatives of the momentum
C	Jacobian integral
E	Total orbital energy
l^*	Characteristic length
m^*	Characteristic mass
t^*	Characteristic time
$\boldsymbol{Q}_{ri}$	Euler rotation matrix
$\boldsymbol{I}$	Identity matrix
$\boldsymbol{\Theta}$	State transition matrix

$\boldsymbol{M}$	Monodromy matrix
$\boldsymbol{\lambda_i}$	Eigenvector i
T_p	Orbital period
A_i	Orbital amplitudes
A_1	Stable component of the linear Lissajous motion
A_2	Unstable component of the linear Lissajous motion
$\boldsymbol{\theta}$	Quasi-periodic phase angles
$\boldsymbol{s}$	Singular state vector on a quasi-periodic orbit
$\boldsymbol{p}$	Arranged vector containing multiple torus states
$\boldsymbol{u}$	Parametric state vector function
$\alpha,\ \beta$	Quasi-periodic phase angles, similar to $\boldsymbol{\theta}$
$\boldsymbol{D}$	Fourier transform matrix
$\boldsymbol{k}$	Fourier coefficient vector
$\boldsymbol{R}$	Rotation matrix
$N,\ M$	Discretisation parameters
n_{max}	Number of harmonics
s	Stepping parameter
$\boldsymbol{\psi^s},\ \boldsymbol{\psi^u}$	Stable and unstable directions
l	Selection of the hyperbolic invariant manifold branch
τ	Transfer time
J	Objective functions

List of Figures

List of Tables

CHAPTER 1

Introduction

Advanced orbital transportation capabilities and co-operation between spacecraft are key enabling technologies to achieve future complex and ambitious objectives in space science and exploration. These capabilities include transfers from the proximity of the Earth to the proximity of the Moon and transfers among orbits in the proximity of the Moon. Utilising them enable the exploration of the solar system in a much more cost-effective way than what is done today. Considered scenarios for the following years include a return to the Moon and missions to Near Earth Objects (Chesley et al. [2002]) and other asteroids with the purpose of harvesting materials (Adamo et al. [2010]) or protecting our planet from an impact. The Moon serves as a gateway to the exploration of the solar system and a test-bed to validate new technologies, gain scientific knowledge, and identify key developments for further endeavours. Therefore, instead of landing on the surface of the Moon, it is desirable that an orbit about one of the collinear Earth-Moon libration points will be the next destination. Another capability is to provide regular access with low propellant expenditures to operational orbits enabling re-phasing of spacecraft, regular in-space operations, rendezvous, and docking manoeuvres. This may include multi-spacecraft missions demanding rendezvous scenarios e.g. for in orbit-assemblies.

A return to the Moon will result in important breakthroughs in understanding the Earth-Moon system and in gaining knowledge in fundamental science across multiple disciplines. From a mission design point of view, a key enabling technology is the dynamic interaction between the gravity field of nearby celestial bodies. This interaction enables new mission concepts that were never tested nor explored in the years of the first lunar landing. In this context orbital transfers can benefit from hyperbolic invariant manifolds that exist in a three-body regime. The dynamical behaviour and the strategic location of libration points make them ideal locations for future exploration endeav-

ours and scientific missions, such as space telescopes, space stations, and other traffic management activities (Catlin and McLaughlin [2007]). An orbital staging location in the vicinity of L_1 or L_2 would provide a platform for science and logistic purposes, and multi-destination flexible exploration strategies can be derived. Libration points are also ideal locations, for assembly, loitering and staging. A spacecraft can be placed in orbit around one of the libration points to serve as a gateway station in order to store required propellant and cargo. By docking another spacraft to this gateway station, cargo and propellant can be distributed to other spacecraft before heading off to interplanetary space. Furthermore, the Earth and the Moon's surface are easily accessible without severe launch window constraints or entering an orbit around the Moon can be simplified once the libration point regions are an intermediate step from travelling from Earth to the Moon. A currently discussed proposal is a lunar surface robotic missions which is technologically feasible within a realistic budget and would benefit from design aspects considering the libration points. A major step in the return to the Moon will be a sample return mission to a location at the South pole, a geographically and scientifically interesting region with a combination of craters permanently in the dark and peaks always in sunlight. The knowledge and competencies learned in a lunar environment are potentially adaptable to farther destinations in interplanetary space such as Mars, Near Earth Objects and outer planets or beyond. The motivation for the analysis of quasi-periodic in the Earth-Moon system is triggered by the need to include the unique properties of the libration point regions in the design of missions aiming to explore farther destinations.

The libration point regions are spaces where the balance of forces offers a dynamical environment where small perturbations have a large effect on the motion of spacecraft and the evolution of their operational orbits. This sensitivity allows for low propellant orbital and station-keeping manoeuvres. Transport phenomena among Earth-Moon libration points have been proven in the past (Ozimek and Howell [2010]) and play an important role in the aforementioned transportation infrastructure. Key dynamical structures associated with libration points are periodic and quasi-periodic orbits and hyperbolic invariant manifolds that allow travelling through space at minimal cost (Gómez and Masdemont [2000]).

One design aspect is the identification of nominal orbits. There are the classical non-keplerian libration point orbits, e.g. lissajous, halo and lyapunov orbits. Another class are distant periodic orbits (DPO). These orbits are, seen from an Earth-centric reference frame, in resonance with the Earth motion about the Sun (Hirani and Russell [2006]). Unfortunately, quasi-periodic orbits lack of a description by Keplerian elements. This is due to the fact that these are solutions exist in a three-body regime and no analytical

solution as for the two-body is problem is available. This prohibits the derivation of Keplerian elements. Libration point orbits are usually described by six-dimensional state vectors. This shortfall is addressed in this work by the introduction of parametric functions representing quasi-periodic orbits. Novel in this work is the definition of a well defined set of parameters, in particular amplitudes, frequencies and phase definitions.

1.1 Current state of research

The challenge in designing missions with operational orbits around one of the libration points comes from the location in space and the instability of these points. Different operational libration point orbits have been studied in the past. The family of halo orbits were the first periodic set identified with a direct application to enable communication from behind the Moon. Barden and Howell [1998] investigated libration point regions in the circular restricted three-body problem with a focus on the determination of the natural behaviour at the centre manifold. Unique for these orbits is the set of asymptotic trajectories that approach or depart the orbit, which are the hyperbolic invariant manifolds. Numerical methods are utilised to generate periodic and quasi-periodic orbits within the vicinity of libration points, see Canalias Vila [2007]. More complex quasi-periodic orbits and proposed numerical procedures for their generation and continuation were studied by Kolemen et al. [2011] and Kolemen [2008]. Multiple Poincaré maps were used to approximate invariant circles. Olikara [2016] proposed a different approach in obtaining quasi-periodic solutions. Howell and Pernicka presented a numerical shooting approach and Gómez et al. [2010] later developed a scheme for computing quasi-periodic orbits by utilising Fourier coefficients to approximate invariant circles. The fundamentals about invariant tori can be found in Schilder [2002].

Transfers of spacecraft from one orbit to another have been studied extensively for many years and is directly associated with optimality being either defined as minimum propellant costs, a minimum transfer time, or other parameters. The analysis and design of transfer orbits using invariant manifolds associated with periodic orbits around the libration points have been a topic of many publications. Transfers between libration point orbits of the same energy level utilising invariant manifolds are presented in Gómez et al. [2004]. Other works by Davis [2009], Canalias Vila [2007] and Marsden and Ross [2005] study orbital transfers in this dynamical regime employing invariant manifolds. The introduction of pseudo-manifolds by Davis et al. [2011] considers larger offsets constructing the manifold branches and their impact on the transfer design. A technique using invariant manifolds for near Earth objects retrieval missions

is presented by Yárnoz et al. [2013]. The utilisation of invariant manifolds for transfers between libration point orbits and distant retrograde orbit has been studied by Mingotti et al. [2010]. Another way of constructing transfers between orbits without the use of invariant manifolds, are two-manoeuvre transfers where the first manoeuvre is performed at departure, and the second one at arrival, see Gómez et al. [2004]. Recently, the use of Earth-Moon libration points as staging nodes for further human expeditions were studied by Alessi [2010].

Regardless of the selection of operational orbits, station-keeping is required to maintain the spacecraft on the desired path. Station-keeping strategies have been studied for several dynamical frameworks and missions in the past by Gómez et al. [2001], Infeld [2005], and Pavlak [2010]. Methods using theoretical knowledge based on modal Floquet theory have been explored by Farrés and Jorba [2014]. With these techniques, the motion can be described by centre components, stable and unstable modes. The cancellation of the unstable components is used to maintain a spacecraft at a libration point orbit. A similar methodology is already applied in the past utilising a linearisation of the equations of motion (Hechler [2002]). For periodic orbits dominant manoeuvre directions can be determined by the eigenvectors of the monodromy matrix, see Simo et al. [1987]. Guidelines related to station-keeping methods are given by Lo et al. [2000] and Pavlak and Howell [2012].

Relative spacecraft formations and configurations have been studied from the beginning of space projects but the focus changed from proximity manoeuvring for e.g. staging two spacecraft within the Apollo programme to, in recent years, larger telescopes building a large aperture by having sensor and collector on different spacecraft. Howell and Pernicka [1993] derived natural regions where the geometry of spacecraft formations is maintained. Coping with multiple satellites achieving specific geometries is a significant technical challenge as described by Tolbert [2009]. The first multi-spacecraft formations were proposed by Howell [2004] to demonstrate that quasi-periodic trajectories evolving on invariant tori can be utilised for such purpose. Further analyses considered natural and non-natural arcs for formation applications. Héritier and Howell [2011] explore quasi-periodic Lissajous trajectories near a given reference orbit in the vicinity the Sun-Earth libration point L_2 for the placement of large formations of spacecraft, see Héritier and Howell [2012], Marchand [2004], and Héritier [2012]. Examples are astronomical apertures in telescope assemblies with a reflector and collector on different spacecraft to assure a physical distance. In particular potential telescope configurations benefit from apertures created by long distances between spacecraft.

1.2 Research objectives

Current research conducted focus on different approaches to calculate quasi-periodic orbits. However, what is missing is a suitable method to describe the entity of state vectors belonging to one quasi-periodic solution. To fill in this gap, the main objective is to introduce a parametric function that is in a following step utilised to calculate orbital transfers among quasi-periodic orbits. One high-level objective of this work is to systematically describe the properties such as amplitudes and frequencies of quasi-periodic orbits including libration point and distant periodic orbits existing within the vicinity of the Moon and to identify for which parameters solutions exist. The assessment of properties of bounded motion near the equilibrium points, which includes periodic and quasi-periodic orbits, is difficult as no Keplerian elements can be defined.

A characterisation of quasi-periodic orbits and their asymptotic trajectories is done by using time-dependent phases and amplitudes, which originates from the dynamical description of quasi-periodic orbits as invariant tori. When reducing the orbits to a Poincaré section or to a stroboscopic map, a quasi-periodic trajectory is described by a so-called invariant curve. This is a contrarily approach compared to periodic orbits that can be described by fixed points. In this work, the proposed method to determine quasi-periodic orbits utilises stroboscopic maps in combination with complex two-dimensional truncated Fourier series. This method allows to be used for different families of quasi-periodic solutions.

A parametric representation of quasi-periodic orbits by state vectors in angular phase space builds the foundation. On this basis, mission analysis aspects studied are the identification of suitable operational orbits, transfer opportunities among those orbits, station keeping and the identification of suitable formation flying trajectories. These ideas have the goal to systematising the computation of any type of mission involving quasi-periodic orbits and orbital transfers. The previously studied quasi-periodic orbits exist in the restricted dynamical description of the three-body problem. The dynamical instabilities of most of these orbits disrupt exact solutions known from the restricted problem. Therefore, a numerical method is proposed to construct quasi-periodic orbits in a high-fidelity dynamical model.

A major contribution of this dissertation includes the introduction of lunar orbital transfer manoeuvres for a variety of purposes from changing parameters of operational orbits, such as their amplitudes, to identifying manoeuvre sequences resulting in propellant savings. The specific focus is on transfers from one quasi-periodic orbit to

another. In a more generic way, spacecraft manoeuvres are introduced with the objective of transferring a spacecraft from one orbit to another taking into account the lowest possible propellant expenses, phasing conditions, and transfer times.

1.3 Conception of this work

Methodologically, first of all, Chap. 2 presents the Moon as a destination highlighting future exploration scenarios and unique characteristics of the lunar vicinity. In Chap. 3 state of the art methods and basic principles of n-body dynamics are introduced and important issues related to the dynamical framework are discussed.

The primary goal of Chap. 4 is to introduce new and innovative methods for designing spacecraft trajectories with a focus on quasi-periodic motion. A numerical method is presented to obtain the parametric representation of quasi-periodic orbits. Orbits are then generated for the Lagrange point L_1 and L_2 in the Earth-Moon system.

Chap. 5 addresses the problem of station-keeping and handling of quasi-periodic orbits in an accurate dynamic model based on planetary ephemeris data. Fortunately, quasi-periodic solutions also exist in high-fidelity dynamical models and a methodology is proposed to transfer solutions from the circular restricted three-body problem to this model. Additionally, frequent manoeuvres are demanded in order to keep a spacecraft on orbit for several revolutions. Strategies to maintain these unique orbits are proposed and its applicability is discussed.

Chap. 6 builds up on results of the previous chapters to finally design orbital transfers. A method is proposed that is necessary to design orbital transfers and to assess realistic Δv requirements. First guesses are obtained by a differential evolution algorithm. In a second step, accurate solutions and continous trajectories are obtained by a gradient-based optimisation method. Examples of transfers with minimised propellant consumption are presented for the circular restricted three-body problem and in an high-fidelity dynamical model. Single-manoeuvre transfers reveal to be efficient in their performance and simple in realisation. This work aims to draw up recommendations for future missions, which includes guidelines for manoeuvre scheduling and station-keeping strategies.

PhD co-funding agreement

This research project was co-funded under a Networking and Partnership Initiative (NPI) provided by the European Space Agency (ESA) and the University of Strathclyde. A common initial statement of work was defined to examine mid- and large-scale

spacecraft formations near Langragian points. The research proposal covered many aspects of the conceptual design of space missions. On the basis of regular meetings of both co-funding stakeholders, the review of the literature, the author's focus led to the work presented in this thesis, which in some parts has evolved from the initial statement of work. This was agreed by both co-funding stakeholders.

Publication history

Prior to publication of this thesis some results of the research have been presented and published. Below is a summary of these papers:

- M. Duering, M. Landgraf, M. Vasile, Station-keeping for quasi-periodic orbits, 65th International Astronautical Congress, Toronto, Canada, 2014
- M. Landgraf, M. Duering, F. Renk, Mission Design Aspects of European Elements in the International Space Exploration Framework, 24th International Symposium on Space Flight Dynamics, 2014
- M. Duering, M. Landgraf, M. Vasile, Manoeuvre considerations for quasi-periodic orbits, 64th International Astronautical Congress, Beijing, China, 2013
- M. Duering, M. Vasile, M. Landgraf, Optimal manoeuvring between quasi-periodic orbits, 5th International Conference on Spacecraft Formation Flying Missions and Technologies, Munich, Germany, 2013
- M. Duering, M. Vasile, M. Landgraf, Uncontrolled spacecraft formations on two-dimensional invariant tori, 5th International Symposium on Space Flight Dynamics, Pasadena, United States, 2012

CHAPTER 2

Destination Moon

The Moon is our closest companion visible throughout day and night, revealing only slightly more than half of its surface to an observer on Earth. Some part of its surface is lit by light from the Sun, whereas the dark part of the crescent-shaped Moon seen from Earth is lit by faint reflected light. The mean distance from Earth varies from about three-hundred sixty thousand to four-hundred thousand kilometres at the extreme perigee and apogee points depending on the location of the Moon with respect to Earth and the Sun. Centuries ago, explorers already knew how to make use of the phases of the Moon for navigating across sea and land. With the view on future space travel, a return to the lunar environment is a major milestone towards the exploration to farther planets and beyond.

> 'The fact that humans have walked on the Moon, and will again, should not diminish but enhance the sense of wonder. In the modern perspective, seeking a lunar foothold for science and technology could be a natural step after establishing bases in the harsh but splendid landscapes of Antarctica. *'

This inspiration bridges the gap between scientific results and the broader vision of space exploration. It is a challenging process to prepare, build and operate exploration missions. The process is on the one hand influenced by Agencies and political aspects, and on the other hand detailed scientific knowledge is hidden in every decision and is the driving factor for the majority of projects.

2.1 Science and inspiration of past missions

The technological feasibility of lunar spacecraft missions have been proven decades ago with the first Surveyor missions to explore the lunar surroundings. Early missions to

*Science and Lunar Sample Return, Workshop outcomes and recommendations, ESA Report, 2014

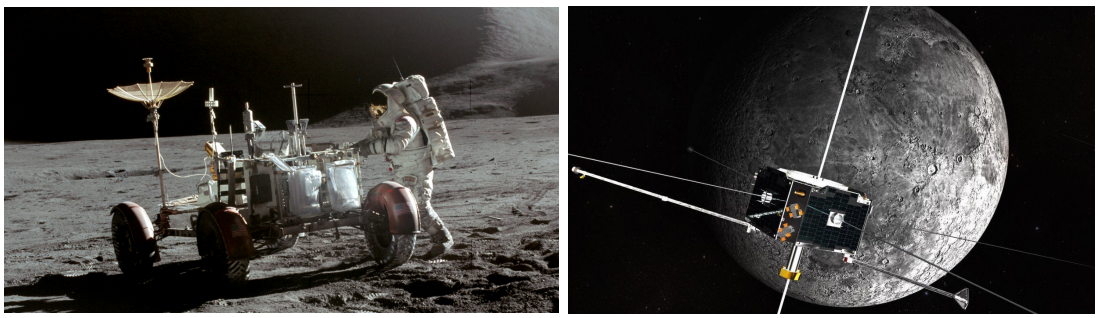

(a) **(b)**

Figure 2.1: Past exploration and science missions to the Moon (a) Apollo 15 (Credit: NASA), (b) the Artemis mission exploiting the properties of multi-body dynamics (Credit: NASA).

the Moon, Apollo and Surveyor from the American space programme to the Lunochod spacecraft from the Russian programme (Nayler [1971]), achieved great results and the picture of our close companion changed fundamentally, see Fig. 2.1a. The term 'marble Earth' was coined with the first pictures from Earth as seen from a Moon's perspective. The first view of the far side of the Moon resulted from lunar exploration in the 1960s. Space exploration beyond Low Earth Orbit is an expensive endeavour and only the main space-faring countries, the United States, Russia and Europe through the European Space Agency can lead and pave the way for exploration programmes. The first missions to the Moon distinguished themselves by a monolithic approach and a reuse of orbital equipment once launch into space was never part of the program nor intended. In the following years other concepts have been studied and realised. The European Space Agency was involved in the endeavour to return to the Moon with the SMART-1 spacecraft proving low-thrust propulsion (Racca et al. [2002]).

It was probably Arthur C. Clarke in 1961 that describes the utilisation of the first and second Earth-Moon libration points in the book 'A Fall of Moondust'. He describes a habitat that can be utilised for various purposes. Ten years later in 1971 Robert Farquhar studied and proposed a detailed architecture for extended human operations at collinear Earth-Moon libration points after a major contribution three years before by describing the halo orbit family (Farquhar et al. [1972] and Farquhar [1971]). Farquhar already mentioned aspects of long-duration habitats, on-orbit depots and tugs, and the benefits of a control of robotic systems on the lunar surface from this remote location. Dunham and Farquhar [2003] described a plan to use the Sun-Earth libration point as the primary hub for future human space activities in the Earth neighbourhood. The Japan Aerospace Exploration Agency (JAXA) has started investigating a deep-space port built in the vicinity of the $L_{2,Sun}$ Lagrange point in the Sun-Earth system.

The first libration point targeted by a spacecraft mission was $L_{1,Sun}$ in the Sun-Earth system. It hosts the 1995 launched, and still in operation, Solar and Heliospheric Observatory (SOHO), a joint mission of NASA and the European Space Agency (Domingo and Poland [1992]). The Earth-Moon Libration Orbiter ARTEMIS (an acronym for 'Acceleration, Reconnection, Turbulence and Electrodynamics of the Moon's Interaction with the Sun') was the first to operate at the libration points L_1 and L_2 in the Earth-Moon system proving concepts being studied on paper before, see Fig. 2.1b. This includes navigating aspects and station-keeping operations. ARTEMIS used in their measurements two spacecraft from another NASA Heliophysics mission that are in orbit since 2007.

The Chinese Space Programme known as Chang'E also focus on a lunar return. Remarkable objectives and achievements of the programme are the utilisation of properties of the Earth-Moon libration points and the carefully selected step by step exploitation of these properties utilising orbiters, landers and rovers. The first spacecraft within the programme was launched in 2007 and the second satellite Chang'E-2 followed in October 2010. Mission phases are a direct cis-lunar transfer by a rocket, a cis-lunar transfer trajectory, and a lunar capture phase to enter a 100 km altitude circular polar lunar orbit. In April 2011, the satellite mission had come to the end of its half-year design life and had achieved all scheduled engineering and scientific goals. A mission extension of transferring Chang'E-2 to the Sun-Earth L_2 libration point was put forward to further expand the lunar and deep-space exploration. The latest spacecraft within the programme Chang'E 5-T1, designed to test the lunar return spacecraft, was launched in October 2014.

2.2 The uniqueness of the libration point regions

In the 18^{th} century the mathematicians Leonhard Euler and Joseph-Louis Lagrange identified gravitational equilibrium points in a specific rotating reference frame associated with the three-body problem. Euler discovered the collinear libration points, whereas Lagrange identified the triangular configurations. The location of these points with respect to Moon and Earth is a unique characteristic and huge advantage compared to e.g. Low Lunar Orbits.

A spacecraft placed in a bounded orbit around one of the libration points can maintain the same position with respect to the two bodies, whereas a direct placement of a spacecraft at one of the libration points is not desirable or even not feasible. The main reason for this is the large manoeuvre required to decelerate the spacecraft to zero and the high cost of station-keeping to maintain the spacecraft at its location. The collinear

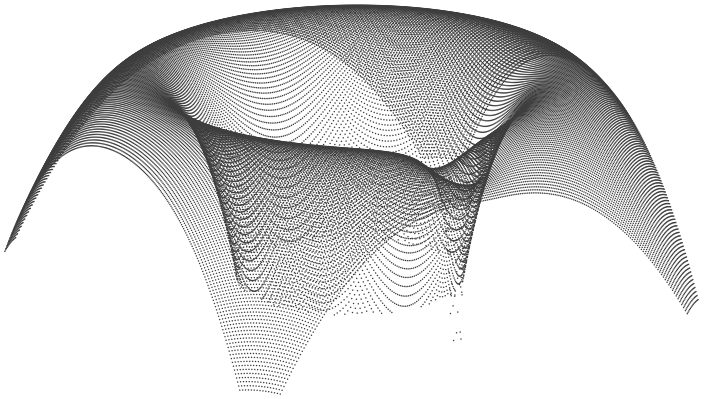

Figure 2.2: Effective potential identifying the location of the libration points, here for a mass parameter equivalent to the one of the Earth-Moon system.

libration points L_1, L_2 and L_3 have similar properties, the gravity of the Moon either increases or decreases the orbital period of a particle at those locations in a way that it moves with the same speed as the secondary around the primary. An interesting aspect of the triangular libration points L_4 and L_5 is the stability of their orbits that can be exploited in spacecraft missions reducing the station-keeping budget. A downfall is that thousands of bodies populate this region of the solar system and the risk of collisions prevent scientist to consider those triangular points for exploration studies although their inherent stability. Various groups of periodic and quasi-periodic orbits exist with the libration point regions, some circling around one of the points, others move around the Moon and cross the libration points. These orbits enable access to the surface of the Moon, and it is feasible to observe the Moon at close distance without landing. Furthermore, libration point and distant retrograde orbits require less Δv than low lunar orbits to maintain them. This behaviour, in particular, is beneficial for spacecraft missions that rely on regular orbital manoeuvres and transfers. Operational orbits near the collinear libration points offer interesting opportunities and using them might enable many space mission scenarios. What the gravity assist manoeuvre is for interplanetary mission is the shallow gravity gradient is for libration points missions.

Fig. 2.2 shows the contour plot of the effective potential. The effective potential energy is an expression combining multiple effects into a single potential. In classical mechanics it is defined as the sum of the centrifugal potential energy and the potential energy of a dynamical system. The saddle points define the locations of the libration points, where the centripetal acceleration of the spacecraft balances the gravitational forces.

A spacecraft escaping one of the equilibrium points either falls in the gravity well of the Moon or the Earth.

2.3 A view on future exploration endeavours and scenarios

The Moon is an important exploration destination for the European Space Agency, who is working to secure roles in future exploration missions *. Current and future programmatic approaches for a future in-orbit infrastructure for human and robotic space exploration programmes, to near Earth objects and asteroid retrieval missions favour the Moon as basis. However, before or even instead of landing on the Moon, it is more likely that an orbit about one of the collinear Earth-Moon libration points will be the next destination. The motivation for the analysis of lunar orbital manoeuvres in Earth-Moon system is the involvement of the European Space Agency in the design of the Multi-Purpose Crew Vehicle, providing the required capabilities for reaching operational orbit in the lunar vicinity. The Multi-Purpose Crew Vehicle is providing the crew transportation and exploration infrastructure, and concepts are required for crew and cargo access and storing beyond Earth orbit in conjunction with payloads delivery.

Huge progress is made with the Chinese Chang'E programme, it is ongoing and up to now it will conclude with the landing on the surface of the Moon and a sample return mission. The past missions are previously mention in Sec. 2.1 and future missions within the programme will build up on them. The next step is the launch of Chang'E-5 expected to be in 2017 aboard a Long March 5 rocket. The spacecraft design includes a lunar lander with the capability of retrieving up to $2\,kg$ of lunar samples and returning them to the Earth. Chang'E-6 is expected to launch in 2020. The technological milestones and achievements of each Chang'E spacecraft are listed in the following:

- The Chang'E-2 extended mission to the Sun-Earth libration point with a flyby at the Toutatis asteroid. First satellite travelling from a lunar orbit to the L_2 libration point.
- Chang'E-3 will perform an unmanned lunar soft-landing and rover mission, crucial to the Chang'E-3 mission. The first Chinese lunar soft-landing and rover mission.
- Launch of Chang'E-5 expected to be in 2017. Capable of retrieving lunar samples and bringing them to Earth.
- Chang'E-6 is expected to launch in 2020.

*Science and Lunar Sample Return, Workshop outcomes and recommendations, ESA Report, 2014

Another challenge in the future is to identify the technology required to enable missions that have been cancelled in the past. Several multi-spacecraft space missions have been studied that include formation flying aspects, they all never left the design phase. In particular telescope assemblies flying in spacecraft formation e.g. TPF, LISA (Danzmann et al. [1996]), and STEREO (Kaiser et al. [2008]) assessed opportunities to have operational orbits within the libration point regions. The libration point offer unique properties in order to control large baseline formations, the trajectories ideally follow natural spacecraft paths. Most of the projects are on hold, e.g. Spectrum-M (Millimetron) as mentioned in Smirnov et al. [2012] and Kardashev et al. [2007], and may be considered again in future projects.

In the coming years there will be research conducted at lunar polar regions and other unexplored regions on the lunar surface. Once the Earth view fades on the far side of the Moon, scientific experiments can be conducted without background noise from the Earth.

> 'A sustainable infrastructure is required, similar to Antarctic missions, a place where people come together. Onto next destinations, an infrastructure in vicinity of the Moon enables the step into next destinations in our cosmos. *'

In the future missions to the Moon will be one step towards more ambitious projects such as the protection of the Earth from Near Earth objects and observing distant stars. Other concepts go further and include the utilisation of in-situ resources like hydrogen-containing regolith or oxygen from iron oxide. Another resource is water that could be processed at the lunar poles and serve as propellant for human missions beyond the Earth-Moon system, as well as provide radiation shielding for crew members. Such concepts will reduce the amount of mass needed to be launched from the Earth's surface, see Spudis and Lavoie [2010] and Spudis [2011].

*Science and Lunar Sample Return, Workshop outcomes and recommendations, ESA Report, 2014

CHAPTER 3

Review of the dynamics in a three-body regime

The design process of a space mission in the early study phase consists of defining and consolidating science requirements and conducting preliminary trade-off studies. Later on in the process, more and more details are included to the design and definition of the overall system and subsystems. The first step of this process is the modelling of the dynamics. This thesis is concerned with the dynamics in the proximity of the Moon and the Earth-Moon system. The major forces in this region are the gravity of the Earth and the Moon.

3.1 Derivation of equations of motion

The classical Newtonian approach portrays the environment by accounting each planetary body as point mass and evaluating the resulting forces acting on a body in space. High fidelity models, including all forces, provide a very accurate description of the motion of a body, but make the study of the properties and governing laws of the dynamical system rather complicated. Reduced models provide a powerful tool to derive results of general validity and first guess solutions. The three-body problem arose from the work of Newton and facilitates the problem of three bodies orbiting in many ways leading to time-invariant equations of motion. It is important to find the right balance between a model being precise enough to represent the environment and on the other side simple enough to generalise the results. Whenever applicable the facilitated dynamical model is applied, the high-fidelity dynamical model based on the classical Newtonian approach is utilised whenever it is required to accurately picture the dynamical environment and resolve effects caused by e.g. variations in distance between the Earth and the Moon. For references to previous works on this topic, see Renk [2008]. Libration point orbits and Earth-Moon transfers are studied in this work applying the classical Newtonian equations of motion.

Peturbed two-body motion in the Earth system

This dynamical model is founded in the heliocentric MEE2000 inertial reference frame, see Sec. 3.2. In this model, the Earth is the central body, and gravities of other planets are added as third-body perturbations. The actual dynamical equations are

$$\ddot{\boldsymbol{r}} = \frac{\mu_{Earth}}{r_{Earth}^3} \pm \sum_{n=[Sun,\ Moon]} \mu_n \left(\frac{\boldsymbol{r}_n - \boldsymbol{r}}{|\boldsymbol{r}_n - \boldsymbol{r}|^3} - \frac{\boldsymbol{r}_n}{|\boldsymbol{r}_n|^3} \right), \tag{3.1}$$

where μ_n is the standard gravitational parameters for the planets and $\boldsymbol{r}_n$ the corresponding position vector, here in an Earth-centred coordinate system. The position and velocity of the planets accounted in this model are given by the DE421 ephemeris data from the Jet Propulsion Laboratory (Folkner et al. [2008]). In this thesis the DE421 ephemeris model is utilised to prove the existence of quasi-periodic motion similar to those identified in the circular restricted three-body problem and to more accurately predict station-keeping costs. The dominating accelerations in the libration point regions stem from the central body and from third-body perturbations. Each contribution to the acceleration is illustrated in Fig. 3.1. In this example, the contribution to the overall acceleration of the Sun in minor. The initial conditions correspond to a periodic halo orbit around L_2 that stays in the vicinity of the Moon for about 38 days and finally escapes towards the Sun. The escape phase is identified by a fading influence of the acceleration contribution of the Moon. Here, the Moon affects the spacecraft with a period of $12 - 14$ days, which is the distance between the peaks. The solid line represents the acceleration level with all perturbing effects removed except for the two-body gravity field. Further details on third-body interactions are found in Bosanac et al. [2013].

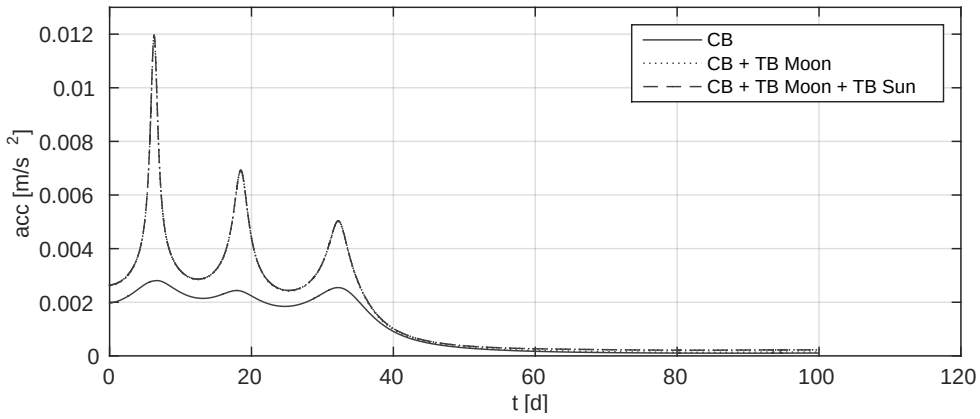

Figure 3.1: Contribution to the overall acceleration from the central body (CB) Earth and the third-body perturbations (TB) from Moon and Sun.

Circular restricted three-body problem

Although the motion of a spacecraft in a multi-body regime can be analysed from the equations of motion given by Newtonian mechanics adding up the gravitational forces of each celestial body, here, the starting point is the reduced model of the circular restricted three-body problem. This model gives a relatively comprehensive picture of the motion around the libration points.

The model describes a spacecraft moving under the gravitational forces of a primary and a secondary body. The motion of m_1 and m_2 is given by the two-body problem. It is *restricted* in the sense that the particle has no mass, and *circular* indicates that the motion of the secondary with respect to the primary is idealised as a circular orbit. The motion of the spacecraft is described in a rotating, so-called synodic, coordinate frame centred in the barycentre (*centre of mass*) of the primary and secondary body with a rotating x axis. The primary and secondary body are at rest in this frame. The reference system rotates at a constant angular frequency of the bodies about the barycentre. The position of the centre of mass can be determined from initial conditions because of the constant angular velocity. For the sake of simplicity the mass unit is chosen such that

$$G^* = \mu_1 + \mu_2 = 1, \tag{3.2}$$

where μ_1 and μ_2 are the gravitational parameters of the primary and secondary body in the circular restricted three-body problem. The universal gravitational constant G^*

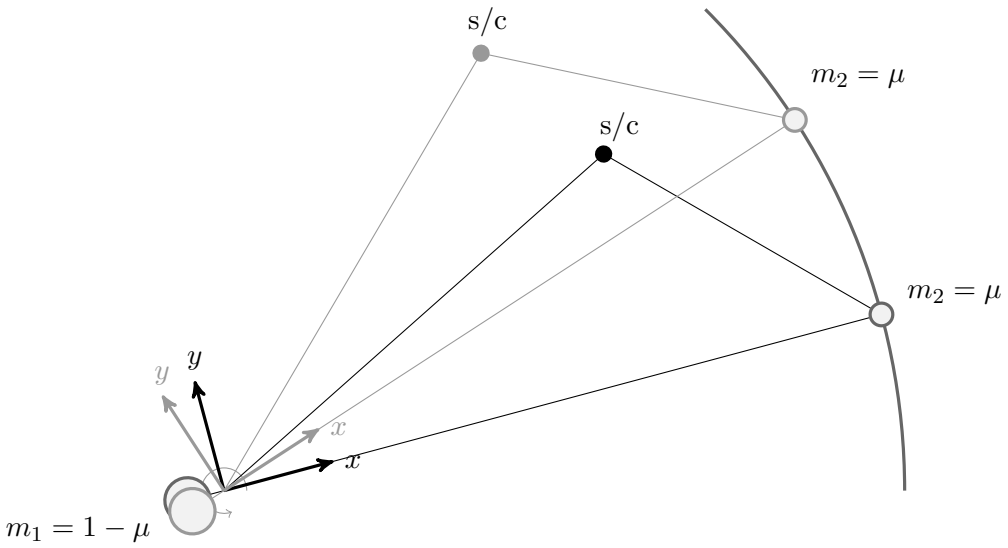

Figure 3.2: Description of the synodic reference frame utilised for the circular restricted three-body problem.

is equal to one. Fig. 3.2 shows the geometry and the relation of both coordinate frames.

In the rotating reference frame, if one accounts only for gravity and centrifugal force, the following balance holds true in the inertial reference frame

$$G\frac{m_1 m_2}{R_{ps}^2} = m_1 D_1 \omega^2 = m_2 D_2 \omega^2, \tag{3.3}$$

where

$$D_1 = r_{12}\frac{m_2}{m_1+m_2} \text{ and } D_2 = r_{12}\frac{m_1}{m_2+m_1}. \tag{3.4}$$

The distance between the primary and secondary body is defined as r_{12}, the angular velocity of the rotating frame is $\omega = \sqrt{G\frac{m_1+m_2}{R_{12}^3}}$. The equations of motions for the third body with m_3 in the inertial frame are

$$\ddot{\zeta} = \mu_1\frac{\zeta_1-\zeta}{r_1^3} + \mu_2\frac{\zeta_2-\zeta}{r_2^3} \tag{3.5}$$

$$\ddot{\eta} = \mu_1\frac{\eta_1-\eta}{r_1^3} + \mu_2\frac{\eta_2-\eta}{r_2^3} \tag{3.6}$$

$$\ddot{\xi} = \mu_1\frac{\xi_1-\xi}{r_1^3} + \mu_2\frac{\xi_2-\xi}{r_2^3}. \tag{3.7}$$

The relation between the inertial and rotating reference frame is

$$\begin{pmatrix}\zeta\\ \eta\\ \xi\end{pmatrix} = \begin{pmatrix}\cos(t) & -\sin(t) & 0\\ \sin(t) & \cos(t) & 0\\ 0 & 0 & 1\end{pmatrix}\begin{pmatrix}x\\ y\\ z\end{pmatrix}. \tag{3.8}$$

The conservation of angular momentum allows the computation of the angular velocity from initial conditions. The second-order differential equations of motion are derived in the Euler-Lagrange form as

$$\ddot{x} = 2\dot{y} + x - \frac{1-\mu}{r_1^3}(x+\mu) - \frac{\mu}{r_2^3}(x-1+\mu) \tag{3.9}$$

$$\ddot{y} = -2\dot{x} + y - \frac{1-\mu}{r_1^3}y - \frac{\mu}{r_2^3}y \tag{3.10}$$

$$\ddot{z} = -\frac{1-\mu}{r_1^3}z - \frac{\mu}{r_2^3}z, \tag{3.11}$$

where $r_1^2 = (x-\mu)^2+y^2+z^2$ represents the distance from the spacecraft to the primary, and $r_2^2 = (x+1-\mu)^2+y^2+z^2$ to the secondary body.

Up to this point the system was written as a set of second-order differential equations. In this reference system, the forces that act on a particle are the two gravitational attractions, the centrifugal force and the Coriolis force. It is often useful to express the equations of motion as a vector field, which is easily done by rewriting the equations.

A pseudo potential function is derived from Eq. 3.9-3.11, which is defined as

$$U = \frac{1-\mu}{r_1} + \frac{\mu}{r_2} + \frac{1}{2}(x^2 + y^2), \tag{3.12}$$

where $\frac{1}{2}(x^2 + y^2)$ is the centrifugal and $\frac{1-\mu}{r_1} + \frac{\mu}{r_2}$ the gravitational component. The function U is visualised in Fig. 2.2.

The Hamiltonian function is written as

$$H = \frac{1}{2}\left\{(p_x + y)^2 + (p_y - x)^2 + p_z^2\right\} - \frac{1}{2}(x^2 + y^2) + \frac{1-\mu}{r_1} - \frac{\mu}{r_2} + \frac{\mu(1-\mu)}{2}, \tag{3.13}$$

where $p_x = \dot{x} - y$, $p_y = \dot{x} + x$ and $p_z = \dot{z}$ are partial derivatives of the momenta.

The Eq. 3.9-3.11 define the motion of the spacecraft in a rotating coordinate system that is normalised, therefore dimensionless. The non-dimensional orbital period is normalised to 2π by the factor t^*, which is the inverse of the mean motion of the primaries. The factor for distance quantities is the characteristic length l^*, which is the distance between the primaries. The factor for mass is the characteristic mass m^*, which is the total mass of the system. The notation for units throughout this work is as follows: *length unit LU*, *time unit TU*, and the *mass unit MU*. Although only the Earth/Moon and in some parts the Sun/Earth+Moon three-body problem is considered, for completeness the parameters for a variety of systems are stated in Tab. 3.1.

The total energy, angular momentum and the linear momentum are conserved, but the lack of sufficient integrals of motion prohibits a general analytical solution of the dynamical system. One integral of motion for the circular restricted three-body problem is the Jacobian constant C, which connects the relative speed of the third body to the location constraint by the potential energy. The quantity is directly related to the conserved energy defined by

$$\frac{C}{2} = -E = \frac{1}{2}(\dot{x}^2 + \dot{y}^2) - \left\{\frac{1}{2}(x^2 + y^2) + \frac{1-\mu}{r_1} - \frac{\mu}{r_2}\right\}. \tag{3.14}$$

Note that the Jacobi integral is minus twice the total energy per unit mass in the rotating frame of reference. In Eq. 3.14 the first term from left to right is the kinetic energy, the centrifugal energy, and the gravitational potential energy. Since the first two

Primary body	Secondary body	μ	l^* $[km]$	t^* $[s]$	m^* $[kg]$
		$\frac{m_s}{m_p+m_s}$	d_{p-s}	$\left(\frac{l^{*3}}{Gm^*}\right)^{-1/2}$	m_p+m_s
Earth	Luna	0.0123	$3.84 \cdot 10^5$	$3.774 \cdot 10^5$	$6.047 \cdot 10^{24}$
Sun	Earth+Luna	$3.0404 \cdot 10^{-6}$	$1.4960 \cdot 10^8$	$5.0228 \cdot 10^6$	$1.9889 \cdot 10^{30}$
Jupiter	Europa	$7.8072 \cdot 10^{-5}$	$1.07 \cdot 10^6$	$9.8332 \cdot 10^4$	$1.8983 \cdot 10^{27}$

Table 3.1: Summary of the gravitational parameter μ and characteristic values for different relevant three-body systems.

can be derived from potentials and the last one is perpendicular to the trajectory, they are all conservative, so the energy measured in this system of reference is a constant of motion. The Jacobi value has no unit, but an energy equivalent may be given. An example is: $C = 3.12$ is equal to a total energy of $E = -1.56 = -1.6176\,\frac{kJ}{kg}\,[\frac{m^2}{s^2}]$.

The Jacobi constant is later on used to classify periodic and quasi-periodic trajectories. From the Jacobi integral one can derive the so-called zero velocity curves by setting the kinetic component to zero. The corresponding equation is

$$C = -2 \cdot E = x^2 + y^2 + 2\left\{\frac{1-\mu}{r_1} + \frac{\mu}{r_2}\right\}. \tag{3.15}$$

The Jacobi constant is valuable in gaining information about regions in which a spacecraft can be found. The station-keeping methodology proposed in this work benefits from this definition.

Location of the libration points

One initial analysis of a dynamical system is to solve for the equilibrium points and investigate the nature of the phase space near these solutions. The full three-body problem in an inertial reference system has no equilibrium points, but in its simplified form as circular restricted three-body problem five equilibrium points can be identified. The libration points are characterised by a zero velocity and a no acceleration environment. Their position can be identified by local maxima of the pseudo-potential function U, see Fig. 2.2 for a visualisation. The locations are determined by setting the partial derivatives of U equal to zero. The following equation

$$x - \frac{(1-\mu)(x+\mu)}{|x+\mu|^3} - \frac{\mu(x-(1-\mu))}{|x-(1-\mu)|^3} = 0 \tag{3.16}$$

leads to the location of the three collinear libration points assuming $y = 0$ for the collinear equilibrium points with its three solutions at $x_{L_2} > 1-\mu > x_{L_1} > -\mu > x_{L_3}$.

Fig. 3.3 illustrates a planar view of the rotating reference frame. In literature, this region is referred to the bottleneck region, the name originates from the definition of zero velocity curves. The black lines represents zero velocity curves each indicating the boundary for a certain energy level between reachable and forbidden regions.

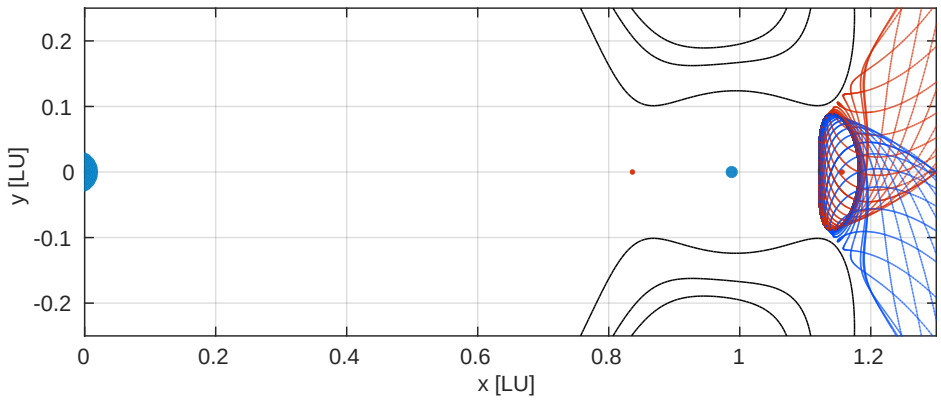

Figure 3.3: Bottleneck region with the Moon, the libration point L_1 and L_2. Stable (blue) and unstable (red) manifold branches are shown for a periodic Northern halo orbit.

Linear Lissajous motion

Another case to be considered is when the equations of motion are linearised about one of the libration points. A new reference frame with the same axis definition as the synodic frame introduced above is applicable. Only the new origin at one of the equilibrium points differs. Here, the equations are given for the second libration point L_2. The linearised equations of motion have the form

$$\begin{aligned} \ddot{x} &= 2\dot{y} + (1 + 2c_2)x \\ \ddot{y} &= -2\dot{x} + (c_2 - 1)y \\ \ddot{z} &= -c_2 z \end{aligned} \tag{3.17}$$

with

$$c_2 = \frac{1}{\gamma_2^3}(\mu + (1-\mu)\frac{\gamma_2^3}{(1-\gamma_2^3)^3}, \tag{3.18}$$

where γ_2 is the distance from the libration point L_2 to the closer body (either the primary or secondary one). The constant value c_2 only depends on the mass parameter and the location of the Lagrange point. Note that the expression for c_2 is only valid for the Lagrange point L_2. The linearised system is characterised by a coupled motion in the x-y plane and a decoupled one in the z direction, as seen in Eq. 3.17. An analytic solution to the linear equation of motion is known, see Richardson [1980]. The periodic part of the analytic solution is written with the help of the amplitudes A_x, A_y, and A_z and the phases θ_1 and θ_2 as

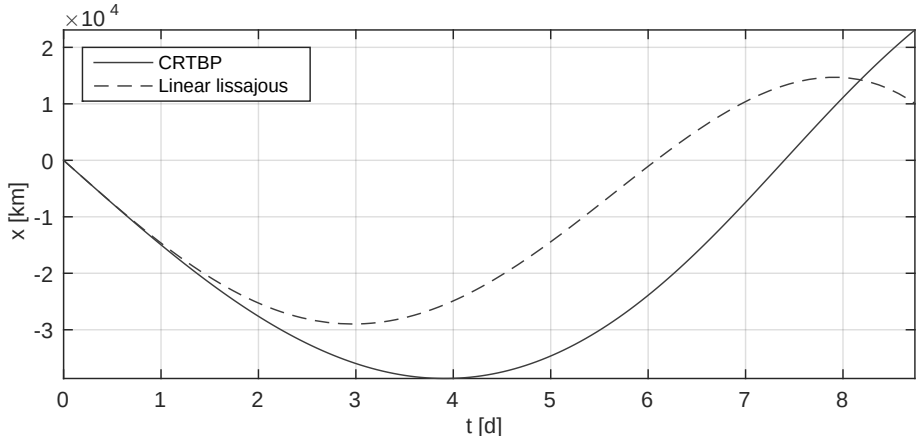

Figure 3.4: Example of the drift between the linearised dynamics around the libration point L_2 and the circular restricted three-body problem.

$$
\begin{aligned}
x &= A_1 e^{\lambda t} + A_2 e^{-\lambda t} + A_x \cos(\omega_2 t + \theta_2) \\
y &= c A_1 e^{\lambda t} - c A_2 e^{-\lambda t} + \kappa A_x \sin(\omega_2 t + \theta_2) \\
z &= A_z \cos(\omega_1 t + \theta_1)
\end{aligned} \tag{3.19}
$$

with

$$
\lambda^2 = \frac{c_2 - 2 + \sqrt{9c_2^2 - 8c_2}}{2} \qquad \omega_1^2 = c_2 \qquad \omega_2^2 = \frac{2 - c_2 + \sqrt{9c_2^2 - 8c_2}}{2} \tag{3.20}
$$

and $c = \frac{\lambda - 1 - 2c_2}{2\lambda}$, $\kappa = \frac{\omega_2 - 1 - 2c_2}{2\omega_2}$ (Richardson [1980]). The amplitudes establish the overall dimensions, while the angular quantities establish a given location on the orbit. The equation of motions contain an oscillatory part and hyperbolic exponential parts. The hyperbolic exponential parts comprise of an exponential part with a positive exponent, and a part with a negative exponent. The in-plane phases and amplitudes relate to the motion in the x-y plane, whereas the out-of-plane parameters describe the motion in z direction. The integral of motion A_1 and A_2 are related to the unstable and stable component. This components decays exponentially to zero, if A_1 is zero and a A_2 component exists. When selecting initial condition vectors, the unstable component in the integral A_1 is set to zero in order to not move along an unstable manifold.

A comparison of the linearised motion versus the circular restricted three-body problem is shown for an example trajectory in Fig. 3.4. Evaluating the delta between the two solutions for multiple initial state vectors belonging to different sized orbits showed that for small orbital amplitudes the linearised equations deliver acceptable results, whereas for large orbital amplitudes the solution diverge after a few days.

Summary

The benefit of the introduction of the time-invariant dynamical model in Eq. 3.9-3.11 is the possibility to use dynamical system theory for the study of the system, e.g. Poincaré and stroboscopic maps, see Sec. 3.3. Another advantage is the described coordinate frame removing the basic rotation of the Moon around the Earth. This enables to investigate orbits that are close to the Moon but heavily influenced by the gravity of the Earth. In this thesis solutions are mainly derived form the circular restricted three-body problem. In some cases the solutions are recomputed in a high-fidelity dynamical model.

For studies presented in this work, the equations of motion are integrated numerically by a finite difference method employing an explicit seventh-order Dormand and Prince

method with step-size adaptation (Dormand and Prince [1980]). This method provides the required numerical stability and an error estimation by step size adaptation for this problem. The equation of motions previously introduced are smooth ordinary differential equations and the integration scheme is computationally fast and achieves a good accuracy.

3.2 A matter of perspective

A prerequisite for the mathematical description of the state of a dynamical system is the definition of appropriate reference frames. The previously introduced dynamical systems were formulated in different reference frames. The high-fidelity model is founded in the MEE2000 system, which is an inertial reference frame, here with its origin at the Earth centre. In case of the CRTBP, it is a non-inertial reference frame exhibiting fictitious forces, which are the centrifugal force and the Coriolis force. For a non-uniformly rotation about the centre, the fictitious Euler force exists. The introduction of the rotation frame further enables the search for periodic orbits, therefore it is a unique tool to picture the phase space of the circular restricted three-body problem. The same way it offers insight into the problem, an inertial view is required as it finally offers the geometry e.g. an observer sees a spacecraft orbiting on such an orbit from Earth. The relation between positions and velocities in both frames is defined as

$$\begin{cases} \boldsymbol{x}^i &= \boldsymbol{Q}_{ri}\boldsymbol{x}^r d_{12} + \boldsymbol{r}^i_{bc} \\ \dot{\boldsymbol{x}}^i &= \boldsymbol{Q}_{ri}\dot{\boldsymbol{x}}^r \frac{d_{12}}{t^*} + (\dot{k}\boldsymbol{Q}_{ri} + d_{12}\dot{\boldsymbol{Q}}_{ri})\boldsymbol{x}^r + \dot{\boldsymbol{x}}^i_{bc}, \end{cases} \tag{3.21}$$

where $\boldsymbol{x}^i$ and $\boldsymbol{v}^i$ are inertial quantities, and $\boldsymbol{x}^r$ and $\boldsymbol{v}^r$ are relative position and velocity vectors. The Euler rotation matrix $\boldsymbol{Q}_{ri}$ represents the rotation of the Moon around the Earth. The coordinates are finally shifted, by adding the translation elements $\boldsymbol{r}^i_{bc}$ and $\dot{\boldsymbol{x}}^i_{bc}$. Aside from the barycentre, other possible origins of the reference frames are $\boldsymbol{r}_{L1}$, $\boldsymbol{r}_{L2}$, or $\boldsymbol{r}_{Moon}$. To account for variations in the rotation rate $(\dot{k}\boldsymbol{Q}_{ri} + d_{12}\dot{\boldsymbol{Q}}_{ri})$ are required. The terms d_{12} and $\frac{d_{ps}}{t^*}$ are required due to the normalisation of position and velocity quantities. The values of $\dot{k}$ and $\dot{\boldsymbol{Q}}_{ri}$ are obtained by numerical differentiation by

$$\dot{k} = \frac{\Delta k}{\Delta t} = \frac{d^+_{12} - d^-_{12}}{\Delta t}, \tag{3.22}$$

and

$$\dot{\boldsymbol{Q}}_{ri} = \frac{\Delta \boldsymbol{Q}_{ri}}{\Delta t} = \frac{\boldsymbol{Q}^+_{ri} - \boldsymbol{Q}^-_{ri}}{\Delta t}. \tag{3.23}$$

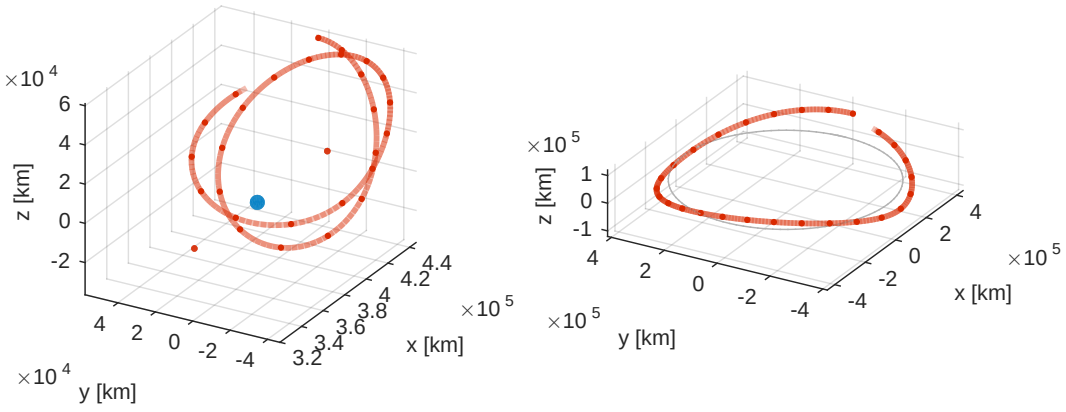

(a) **(b)**

Figure 3.5: Trajectory in the (a) rotating reference frame, and (b) in the inertial reference frame. Ticks along trajectory represent equal time steps. Trajectory of the Moon plotted in light red.

The rotation matrix $\boldsymbol{Q}_{ri} = [\hat{\boldsymbol{e}_1},\ \hat{\boldsymbol{e}_2},\ \hat{\boldsymbol{e}_3}]$ is assembled by

$$\hat{\boldsymbol{e}_1} = \frac{\boldsymbol{R}}{|\boldsymbol{R}|}, \quad \hat{\boldsymbol{e}_2} = \frac{\boldsymbol{\omega}}{|\boldsymbol{\omega}|}, \quad \hat{\boldsymbol{e}_3} = \frac{\hat{\boldsymbol{e}_1} \times \hat{\boldsymbol{e}_3}}{|\hat{\boldsymbol{e}_1} \times \hat{\boldsymbol{e}_3}|} \tag{3.24}$$

Note also that the transformation from the synodic reference frame to an inertial frame is simplified, if variations in the distance between the primary and secondary, and in the angular motion are neglected. With this assumption the components $\dot{\boldsymbol{Q}}_{ri}$ and $\dot{k}$ are zero and the transformation is simplified to

$$\begin{cases} \boldsymbol{x}^i &= \hat{\boldsymbol{Q}}_{ri}\boldsymbol{x}_r l^* - \boldsymbol{x}_p^i \\ \dot{\boldsymbol{x}}^i &= \hat{\boldsymbol{Q}}_{ri}\dot{\boldsymbol{x}}_r l^*/t^* + \omega \times \boldsymbol{x}_i - \dot{\boldsymbol{x}}_p^i, \end{cases} \tag{3.25}$$

where here $\hat{\boldsymbol{Q}}_{ri}$ represents an Euler rotation around the z axis. The rotating and inertial coordinate frame are instantaneously aligned for $t = 0$.

In most of the cases, if the motion is modelled in the circular restricted three-body problem, trajectories are expressed in natural units. Different dynamical models, reference frames and units are used throughout the thesis:

- Dynamics: CRTBP or EPHEM
- Reference frame: index $_r$ for rotating (*synodic*) frame, index $_i$ for inertial frame
- Units: dimensionless, SI-units (*natural*).

The rotation frame is applicable when the focus is on bounded orbits in the proximity of the Moon. The inertial frame MEE2000 finds application when time dependencies

and variations and general precise system knowledge is required. The time system as applied in this work is the Universial Time (UT1) or ephemeris time. The time frame UT1 considers the Earth's axial rotation and differs from the Greenwich Mean Time (GMT).

For a better understanding of both reference frames, Fig. 3.5 shows the same trajectory in a rotating and inertial reference frames, the location of the primary and secondary body are highlighted (blue). Additionally, the libration points L_1 and L_2 are represented by dots (red). The ticks along the trajectory indicate equal time steps with a one day interval.

3.3 Dynamical behaviour

Analytic solutions are rare for ordinary differential equations (ODE) and numerical methods are applied to solve the system to a specific accuracy. The dynamical system theory provides a solid framework to understand the dynamics, orbital motion and other phenomena in the autonomous description of the restricted three-body problem. Certain characteristics such as stability, equilibria or periodicity can be derived.

3.3.1 Continuous flows - State transition matrix

Starting with an autonomous ordinary differential equation, with a right hand side $\boldsymbol{f}$ as

$$\dot{\boldsymbol{x}}(t) = \boldsymbol{f}(t, \boldsymbol{x}). \tag{3.26}$$

A solution of this equation depending on initial conditions is called the flow of the differential equation. It is defined as

$$\boldsymbol{\rho}(t, \boldsymbol{x}_0). \tag{3.27}$$

For a n-dimensional non-linear system a linear differential equation can be derived about an equilibrium point using Taylor expansions and ignoring higher-order terms. The linear variational equations in its general form are

$$\delta\boldsymbol{x}(t) = \boldsymbol{\rho}(t, \boldsymbol{x}_0 + \partial\boldsymbol{x}_0) - \boldsymbol{\rho}(t, \boldsymbol{x}_0), \tag{3.28}$$

where $\delta\boldsymbol{x}(t)$ are variations with respect to a reference orbit. The equation can be formulated as

$$\frac{d}{dt}\frac{\partial \boldsymbol{\rho}(t,\boldsymbol{x}_0)}{\partial \boldsymbol{x}_0} = \begin{pmatrix} & \mathbf{0}_3 & & & \boldsymbol{I}_3 & \\ & & & & & \\ U_{1,1} & U_{1,2} & U_{1,3} & 0 & 2 & 0 \\ U_{2,1} & U_{2,2} & U_{2,3} & -2 & 0 & 0 \\ U_{3,1} & U_{3,2} & U_{3,3} & 0 & 0 & 0 \end{pmatrix} \frac{\partial \boldsymbol{\rho}(t,\boldsymbol{x}_0)}{\partial \boldsymbol{x}_0}, \tag{3.29}$$

where $\boldsymbol{I}$ is the identity matrix, and U_{ij} are the second partial derivatives of the potential function U with respect to i and j building a symmetric sub-matrix. The result is a state vector with a dimension of 42 consisting of the six-dimensional state vector (6 elements) and the first variation matrix with 36 elements. It is defined as

$$\begin{cases} \dot{\boldsymbol{x}} = \boldsymbol{f}(t,\boldsymbol{x}) & \boldsymbol{x}(t_0) = \boldsymbol{x}_0 \\ \dot{\boldsymbol{\Phi}} = \dfrac{\partial \boldsymbol{f}}{\partial \boldsymbol{x}}\boldsymbol{\Phi} & \boldsymbol{\Phi}(t_0) = \boldsymbol{I}, \end{cases} \tag{3.30}$$

where $\boldsymbol{\Phi}$ is the state transition matrix, $\boldsymbol{x}_0$ the initial state vector, and $\boldsymbol{I}$ the identity matrix. The state transition matrix $\boldsymbol{\Phi}(t,t_0)$ is a linear map from the initial state at t_0 to a time t correlating a variation $\delta\boldsymbol{x}$ of an initial state $\boldsymbol{x}_i$ to states downstream the flow.

A special form of the state transition matrix is the Monodromy matrix, which is a state transition matrix for a time equal to the period of a periodic orbit. Later in this thesis a method is proposed to derive a matrix with similar properties for a quasi-periodic orbit, see Chap. 4. The Monodromy matrix $\boldsymbol{M}$ of a periodic orbit is essentially a linear discrete map of a fix point. From this discrete mapping the characteristics of the local geometry of the phase space can be determined from the eigenvalues of the matrix $\boldsymbol{M}$ and their eigenvectors. These characteristics not only apply to the fix point but also to the corresponding periodic orbit.

Since the dynamical system has a Hamiltonian character and $\boldsymbol{M}$ is a symplectic matrix, the eigenvalues of this matrix occur in quadruples. The eigenvalue that are different from one describe the characteristics and stability of the fix point. The eigenvalues λ_i indicate the stability of the equilibrium point. They exhibit the following structure:

If $\lambda = e^{j\phi}$ the fix point is elliptic, in the other case for $\lambda = 2$ it is parabolic. One real-valued reciprocal pair $\lambda_1, \lambda_1^{-1}$ and one complex-valued reciprocal pair $\lambda_2, \lambda_2^{-1}$ of eigenvalues exists, if the fix point is a hyperbolic equilibrium point and the corresponding orbit possesses stable and unstable manifolds. One very small and large eigenvalues building a real-valued reciprocal pair always means instability. These values indicate the stable and unstable directions of the hyperbolic invariant manifolds. The conjugate complex-valued eigenvalues $\lambda = e^{j\phi}$ represent circles on the imaginary plane and they

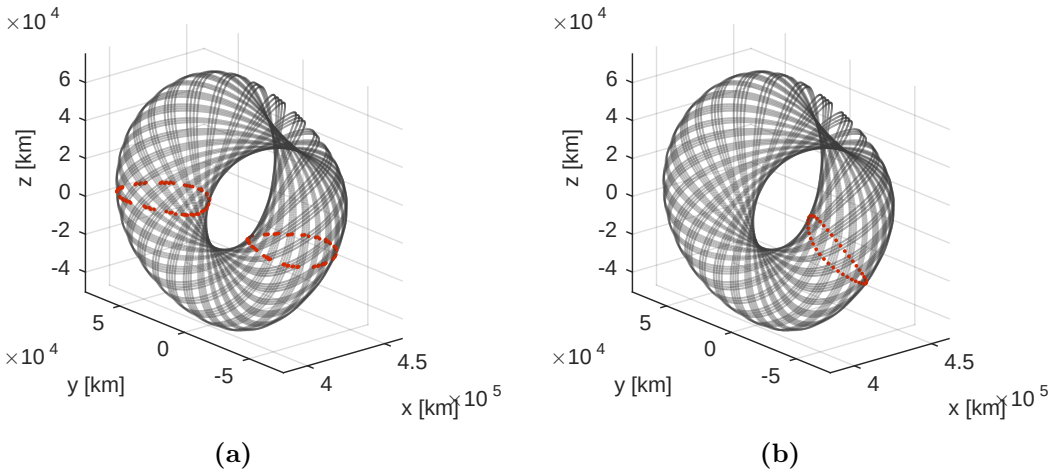

Figure 3.6: (a) Poincaré map with consecutive plane crossings of a trajectory. (b) Stroboscopic map created by states returning at a time t.

remain close to the centre orbit at any time. The local approximation of the stable and unstable manifolds is derived from the eigenvectors. In the case of complex characteristic roots, stability holds only, if all roots have unit modulus one, which means the roots lie on the unit circle.

3.3.2 Discrete maps

The flow of a n^{th}-order continuous-time system can be reduced to a map representation of a discrete-time system by a classical technique due to Poincaré. A Poincaré map is a return map in phase space on a lower dimensional subspace usually defined by a plane (Scheeres [1999]). This map is the link between a continuous- and a discrete-time system. The stability of a fixed point on a Poincaré map indicates the stability of the related periodic orbit. An extension to Poincaré maps are stroboscopic maps, where the underlying flow of a continuous-time system is observed at periodic intervals. This finds its application in the determination of quasi-periodic orbits in the extend of this work. Fig. 3.6 shows the difference between a Poincaré and a stroboscopic map with consecutive plane crossings of a trajectory belonging to a quasi-periodic orbit. The Poincaré map lies in the x-y plane, whereas the stroboscopic map is represented by a three-dimensional curve.

3.3.3 The invariant manifold

An invariant manifold describes a subspace (Jorba and Masdemont [1999]) that is created by a perturbation around an invariant subspace of an equilibrium. Describing

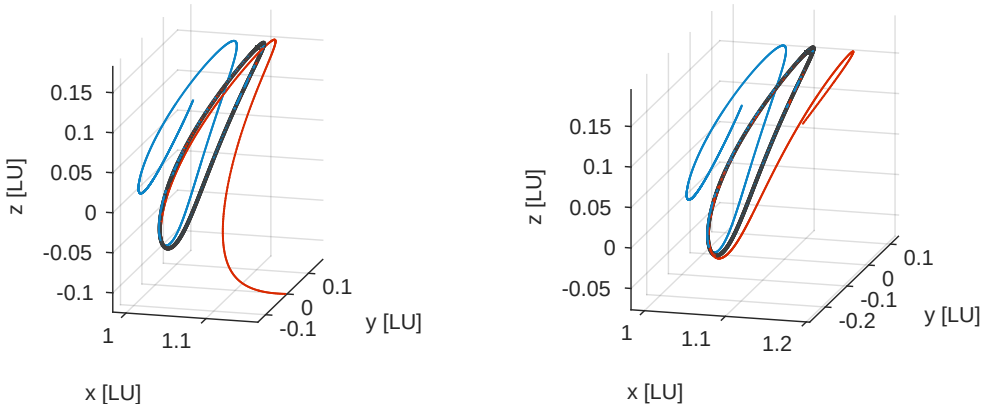

(a) **(b)**

Figure 3.7: (a) Periodic orbit (black) with trajectories departing on positive (blue) and negative (red) branches of (a) a stable and (b) an unstable hyperbolic manifold.

them with the help of a trajectory, a particular manifold may be described as the collectivity of trajectories building a surface. During the evolution of the dynamics the trajectories do not leave this particular surface. In general, centre modes are indicative of the existence of additional bounded solutions in the vicinity of the reference orbit. For instance, modes associated with the complex eigenvalues span a two-dimensional subspace giving rise to quasi-periodic solutions. The hyperbolic invariant manifold is formed by trajectories asymptotically approaching or departing other invariant manifolds. These are called stable and unstable manifolds, respectively. Stable and unstable manifolds are associated to unstable periodic orbits. The unstable manifold is the set of all trajectories that results, if an orbit is perturbed in the direction of the unstable

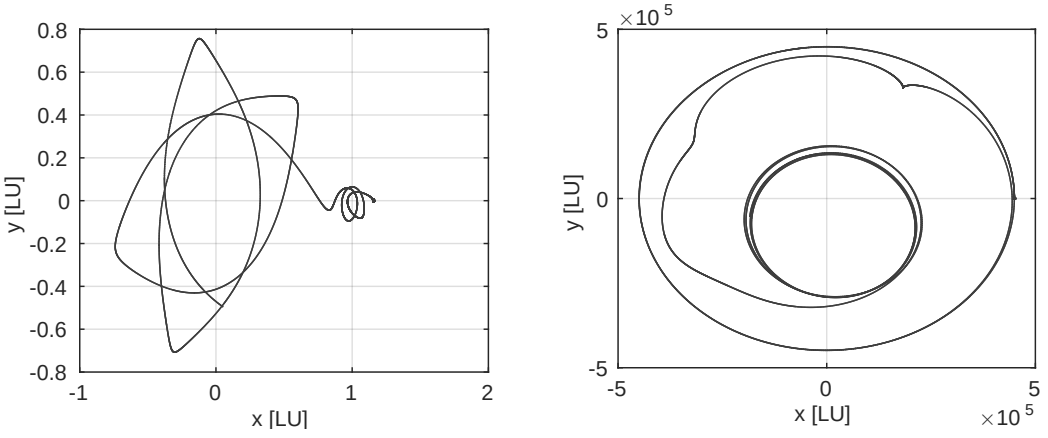

(a) **(b)**

Figure 3.8: Illustration of invariant manifold escape routes, (a) in the rotating frame, and (b) in an inertial view.

eigenvector. The stable manifold is a set of trajectories leading a particle to the corresponding orbit. Each manifold has two branches, a positive one and negative one, depending on the sign of the perturbation. As a trajectory of a stable or unstable hyperbolic invariant manifold enables a spacecraft to enter or depart a libration point orbit. Major contributions in the field of designing orbital transfer arcs are due to the stable and unstable manifolds associated with periodic and quasi-periodic orbits.

The computation of the stable and unstable manifolds associated with a particular orbit can be accomplished numerically in a straightforward manner. The calculation of a trajectory of a stable or unstable manifold starts with taking a state on the orbit and creating an initial guess by perturbing it. An infinitesimal offset is applied and integrating backward or forward in time results in the desired trajectories. The initial guess for the stable and unstable manifold is achieved by

$$\begin{aligned} \boldsymbol{x}^s &= \boldsymbol{x} \pm \Delta \boldsymbol{x}^{\boldsymbol{s}} \\ \boldsymbol{x}^u &= \boldsymbol{x} \pm \Delta \boldsymbol{x}^{\boldsymbol{u}}, \end{aligned} \tag{3.31}$$

where $\Delta \boldsymbol{x}^{\boldsymbol{s}}$ is an offset in the direction of the eigenvector $\boldsymbol{v_1}$, and $\Delta \boldsymbol{x}^{\boldsymbol{u}}$ in the direction of $\boldsymbol{v_2}$, respectively. Suggested values for its length in the Earth-Moon system is $10^{-6}\,LU$ (approximately $0.38\,km$).

Trajectories of the stable and unstable hyperbolic invariant manifolds are visualised in Fig. 3.7a and Fig. 3.7b showing the manifold spreads out to the inner and outer region towards the secondary body. The entity of an invariant manifold tube can be determined and visualised by propagating various states along the orbit. Fig. 3.8a and Fig. 3.8b show the trajectory of a spacecraft initially travelling around the Moon with an escape towards the Earth. The path of a spacecraft is perturbed as it passes by the secondary and is bound within the zero velocity surface. The spacecraft performs two passes around the primary before escaping towards the interior region.

3.4 The region around L_1 and L_2

The CRTBP possesses five equilibrium points named ($L_1 - L_5$), which are also called Lagrange or libration points. L_1 and L_2 are the closest points to the secondary body. In the framework of the circular restricted three-body problem the linear six-dimensional phase space around the collinear libration points can mathematically be described by a centre-centre-saddle structure. This structure enables the classification of different periodic orbits that exist within the four-dimensional centre manifold. For the following work it is convenient to distinguish between *distant periodic orbits* (dpo) and *libration point orbits* (lpo), the different families of existing orbits in both classes are described in the following. A numerical scheme has been implemented from scratch for this study in order to calculate the periodic orbits in this chapter. Existing symmetries have been exploited and the continuation were the orbital period T_p, the corresponding frequency ω_1, and the Jacobian constant J.

3.4.1 Distant periodic and periodic libration point orbits

Periodic orbits are characterised by returns to a fix point once one orbital revolution is conducted. The time between the returns defines the orbital period T_p. In the circular restricted three-body problem these orbits are determined by numerically solving a boundary-value problem. The continuation of one-parameter families is realised by the Jacobian constant C. Another option is to take the orbital period T_p as continuation parameter, which has the disadvantage of a non-monotonous behaviour, which requires to change sign of the step size within the process. Several types of periodic orbits exist for a range of the Jacobian or other orbital identifiers. Some of them are two-dimensional (*planar*) others are three-dimensional (*spatial*).

Libration point orbits cannot be described by Keplerian elements. The term *libration* implies an oscillating motion. Hence, it seems logical to introduce amplitudes and frequencies to characterise the size of such an orbit. As a first guess, the amplitudes are usually in the order of the distance from L_1 or L_2 to the Moon. For periodic orbits the frequency $\omega_1 = \frac{2\pi}{T_p}$ can be defined. It is usually between 1.5 and 2.5 for libration point orbits, as it is approximately the half the orbital period of the motion of the Moon around the Earth.

Libration point orbits

Each libration point gives raise to a set of periodic *libration point orbits*. Namely, horizontal and vertical Lyapunov orbits, Northern and Southern halo orbits. Halo

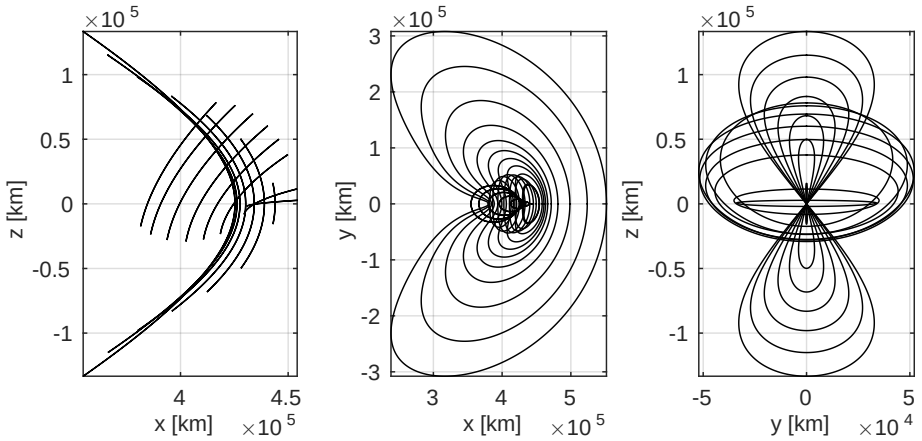

Figure 3.9: Axiometric view of periodic libration point orbits around L_2 in the rotating reference frame in natural units. This includes families of Northern halo, vertical and horizontal Lyapunov orbits.

orbits bifurcate from the horizontal Lyapunov orbits as the energy increases and non-linear terms become dominant. The Northern and Southern family of halo orbits are distinguishable by their direction of motion and the naming stems from the fact that the main part of the orbits is either South or North of the ecliptic, which is the x-y plane in the synodic reference frame. Fig. 3.9 shows an axiometric view of the families of periodic orbits in the Earth-Moon system. The y-z view reveals the geometry of the orbits as they would appear from Earth when keeping the Earth-Moon line in the centre.

Periodic orbits can be grouped in one-parameter families. Either the Jacobian constant, a frequency, or the orbital period can be used to uniquely describe a periodic orbit. The orbital periods vary from 12.87 to 14.8 days for the northern halo orbits at the

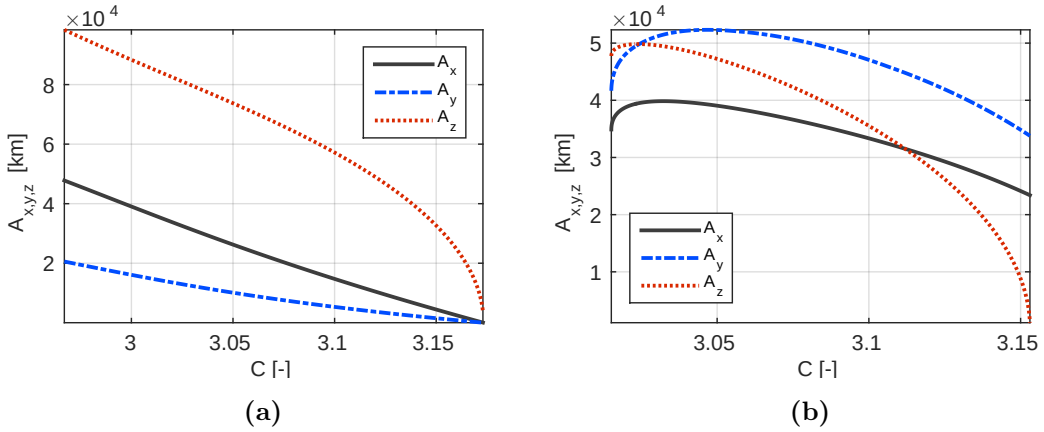

Figure 3.10: Orbital amplitudes A_x, A_y, and A_z for (a) vertical Lyapunov orbits and (b) Northern halo orbits around the L_2 Earth-Moon libration point.

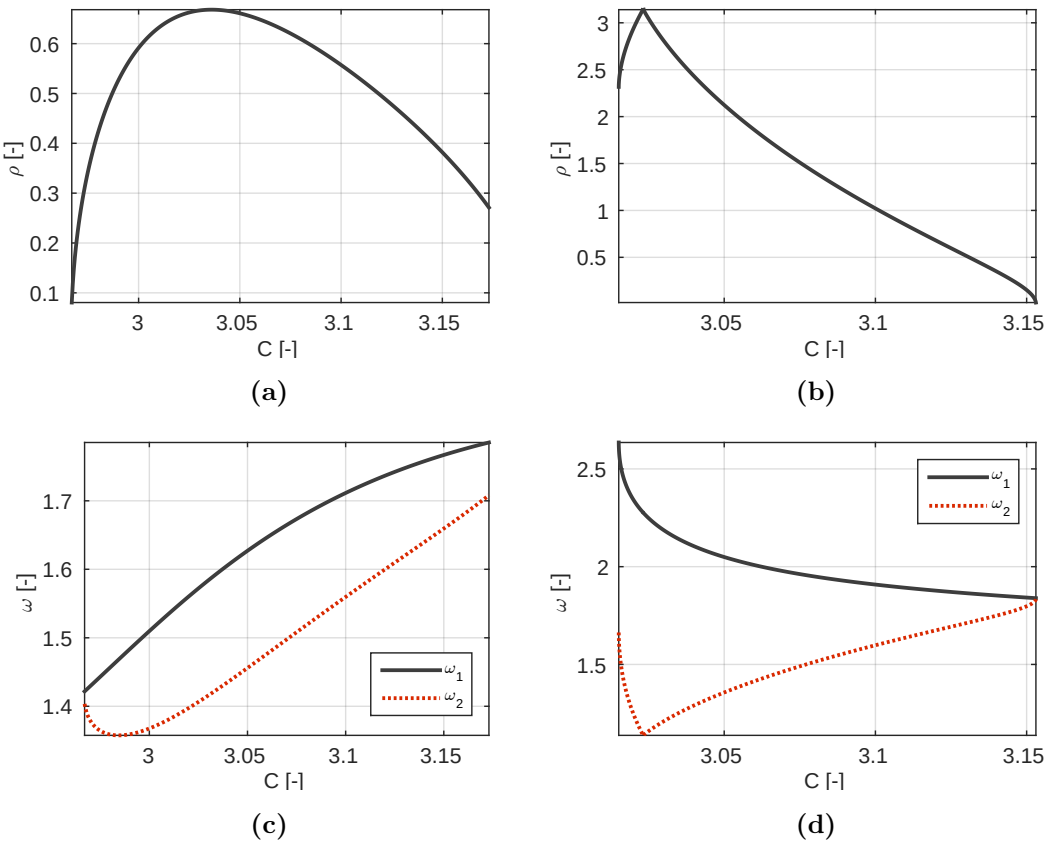

Figure 3.11: Dependency of the rotation number on the Jacobian value and the system frequency ω_1 (a) + (c) for vertical Lyapunov orbits and (b) + (d) for Northern halo orbits around the L_2 Earth-Moon libration point.

libration point L_2, for the vertical Lyapunov orbits, there is a variation between 15.45 and 17.03 days. Here, the notation $\uparrow$ and $\downarrow$ is introduced to describe the behaviour of the named quantities from, when the orbital period increases. The behaviour throughout the orbital set is $C\uparrow, t_p\uparrow, A_z\downarrow$ for halo Northern halo orbits, $C\uparrow, t_p\downarrow, A_z\downarrow$ for vertical Lyapunov orbits and $C\uparrow, t_p\downarrow, A_z\downarrow$ for horizontal Lyapunov orbits, where C is the Jacobian constant, t_p the orbital period and A_i the amplitudes in the direction given by the index. The orbits with large amplitudes possess a lower Jacobian constant than the smaller ones, this is the case for all three classes.

The orbital amplitudes throughout the periodic solutions can be seen from Fig. 3.10a and Fig. 3.10b. The frequencies and the rotation number for the orbital families are shown in Fig. 3.11. Here, the rotation number is defined as $\rho = \frac{2\pi}{\omega_1}$. The behaviour of the system frequency ω_1 differs within the family.

Distant periodic orbits

The second class of periodic solutions are distant retrograde orbits, which only represents one class of distant periodic orbits. Distant retrograde orbits were proposed for missions to Europa, a moon of Jupiter, while their use for the Earth-Moon system just recently appeared (Lam and Whiffen [2005]). Those orbits exist due to a resonance between a primary and secondary body. Most distant periodic orbits are stable and evidence for this is found in a stability analysis of the linearised problem by studying the eigenvalues of the Monodromy matrix. It can be shown that distant periodic orbits provide the largest known region of stable orbits amongst all families in the circular restricted three-body problem (Ming and Shijie [2009], Hirani and Russell [2006]). Those orbits share some characteristics with highly ecliptic Earth orbits and libration point orbits. They are sufficiently high up in the gravitational well of the Earth-Moon system and provide at the same time some benefits of libration point orbits.

Fig. 3.12 shows a planar view of two types of distant retrograde orbit orbiting about the two collinear libration points L_1 and L_2. The 1-period retrograde orbits refer to a periodic orbit symmetric about the rotating x-z plane, this results in crossing the rotating x axis twice for every period. On the contrary, there are also periodic orbits that are 2-period or larger. Apart from the 1-period, the focus here is set to 3-period offering unique properties. Given that a 1-period retrograde orbit exists at a particular energy level, a corresponding 3-period that close after three revolutions around the Moon also exists. Some characteristics are shared, others only exist for a certain period doubling.

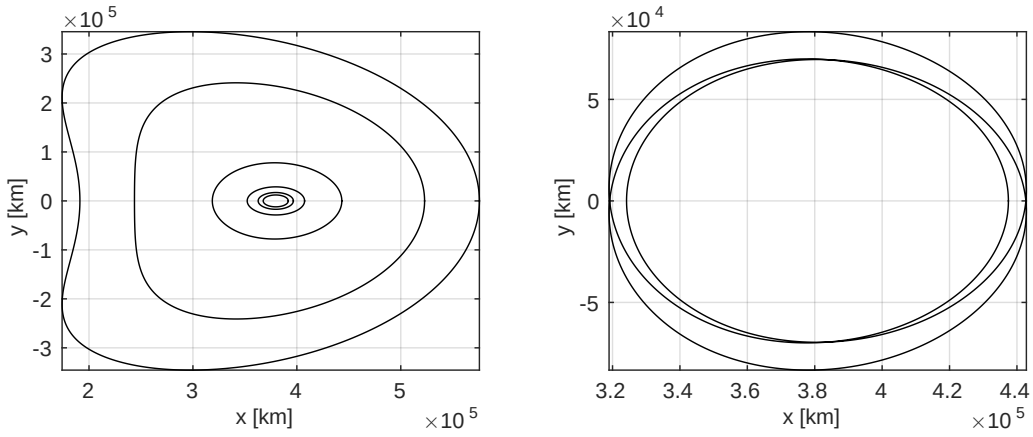

Figure 3.12: Planar view of distant periodic orbits around L_1 and L_2 in the rotating reference frame in natural units. Family of (a) 1-period and (b) 3-period distant retrograde orbits.

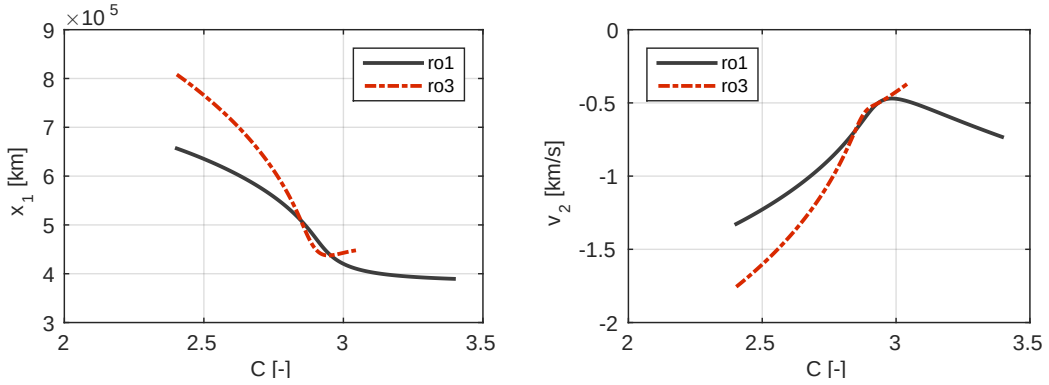

Figure 3.13: Initial (a) positions and (b) velocities for the 1-period and 3-period retrograde orbit families. The transition between Keplerian and distant periodic orbits is evident by the maximal point of the velocity.

In contrast with 1-period retrograde orbits, 3-period ones are linearly unstable. As unstable orbits have associated stable and unstable manifolds, stable distant periodic orbit only possess an associated centre manifold.

The orbital velocity on a distant retrograde orbit increases with its amplitude. This is contrary to Keplerian orbits where the orbital velocity decreases with a rising distance of circular orbits. Fig. 3.13b shows the y component of the velocity of the orbits. All other velocity components are zero as the trajectory crosses the x axis perpendicularly, therefore $\dot{x} = 0$, with a positive y velocity $\dot{y} > 0$. There is a transition between the distant retrograde orbits and pure Keplerian orbits, they are indicated as maximal (turning point) in Fig. 3.13b. The transition between 1-period distant periodic and low lunar orbit take place at a Jacobian value of $C = 2.984$. The 1-period and 3-period distant retrograde orbit intersect when $C = 2.847$ and $C = 2.955$, this points can be

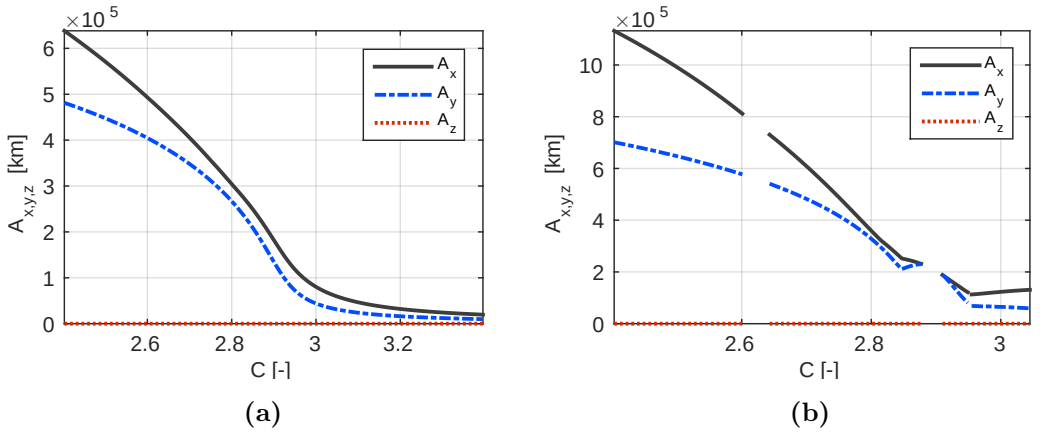

Figure 3.14: Orbital amplitudes for the (a) 1-period and (b) 3-period retrograde orbit families around the Moon in the Earth-Moon three-body problem.

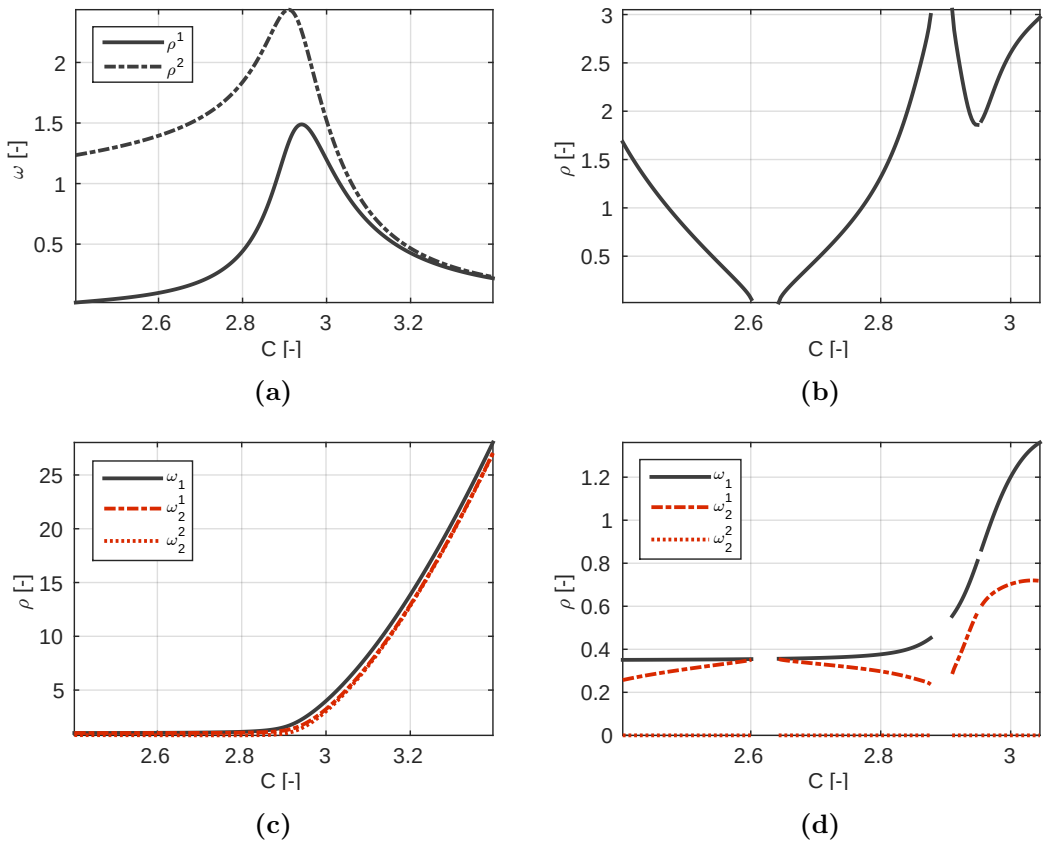

Figure 3.15: Rotation number of (a) 1-period and (b) 3-period retrograde orbits. Frequencies of (c) 1-period and (d) 3-period retrograde orbits.

seen as period-tripling bifurcations as depicted in Fig. 3.13a and Fig. 3.13b.

The orbital amplitudes A_x, A_y, and A_z throughout the families are shown in Fig. 3.14. A_z is zero as only planar solutions are investigated. The orbital amplitudes grow with increasing orbital periods as they pass through the resonance with the Moon. The dependency of the rotation number and associated frequencies on the Jacobian value is seen in Fig. 3.15. The behaviour throughout the orbital set is $C \uparrow, t_p \uparrow, A_z \downarrow$ for 1-period and $C \uparrow, t_p \downarrow, A_z \downarrow$ for 3-period distant retrograde orbits, where C is the Jacobian constant, t_p the orbital period and A_i the amplitudes in the direction given by the index i. The orbits with large amplitudes possess a lower Jacobian constant than the smaller ones, this is the case for all three classes. The orbital periods drop with increasing values of C, they go through $1:3$, $2:3$ and $1:1$ resonance with the Moon, see Fig. 3.15d. The 1-period retrograde orbit family bifurcate from the $1:1$ resonance and disappear when approaching the $2:3$ resonance. The distant periodic orbits have a range from 26.7 to 2.05 days. Periodic orbits and the behaviour around the centre modes are summarised here in detail as they are the starting point for the investigation of quasi-periodic solutions.

CHAPTER 4

Parametric representation of quasi-periodic orbits

The previous chapter outlined equilibrium points and periodic orbits as existing solutions of the equations of motion, see Eq. 3.9-3.11. In this chapter the focus is particularly on a third type of solution, the quasi-periodic orbit or so-called invariant torus. Starting with the description of quasi-periodic motion, a method is proposed to obtain quasi-periodic orbits utilising Fourier series with complex coefficients, stroboscopic maps, invariant curves, and a multiple shooting method. Results are presented as parametric functions containing state vectors, each representing a single quasi-periodic solution. A variety of quasi-periodic orbit families in the Earth-Moon system and their properties are computed.

4.1 Invariant tori and quasi-periodic motion

Invariant tori are fundamental solutions of the equations of motion in Eq. 3.9-3.11. The focus is set to the following general p-dimensional invariant tori:

- Equilibrium points with $p = 0$
- Periodic orbits with $p = 1$
- Quasi-periodic orbits with $p \geq 2$

Equilibrium points and periodic orbits can be regarded as special cases of invariant tori with $p < 2$. A quasi-periodic solution is described as the motion on a two-dimensional torus (2-torus) that is associated with two unique internal frequencies. Mathematically, invariant tori originate from small perturbations of the Hamiltonian. A detailed description of invariant tori and their existence is found in literature (Schilder [2002]).

For an invariant torus with $p = 2$, the surface is densely covered by a trajectory assuming that the trajectory is propagated for $t = \infty$. It is helpful to regard the torus

as an invariant object or for visualisation purposes as a geometric object. Geometrically, a two-dimensional invariant torus can be described as a toroidal surface covering all trajectories for a particular set of parameters with all starting conditions during the dynamical evolution.

Invariant tori posses an important property, which is a global coordinate transformation. This property is used to localise the dynamical system about the invariant manifold. The first step towards generating quasi-periodic orbits is the introduction of angular quantities. The definition of the angle vector is

$$\boldsymbol{\theta} = (\alpha, \beta)\,, \tag{4.1}$$

where α and β are the two phase angles. The torus states are visualised in Fig. 4.1. The states are defined at discrete equidistant angles for each $\boldsymbol{\theta}_{i,j}$ as

$$\boldsymbol{s}_{i,j} = \left(x_{i,j},\, y_{i,j},\, z_{i,j},\, v_{x_{i,j}},\, v_{y_{i,j}},\, v_{z_{i,j}}\right). \tag{4.2}$$

The corresponding torus function is introduced as

$$\boldsymbol{u}\,(\alpha, \beta)\,, \tag{4.3}$$

where $\boldsymbol{u}$ is a six-dimensional state vector in cartesian coordinates representing position and velocity elements. The torus function maps the torus onto a square in an area $[0, 2\pi)^2$ in parameter space. The torus is then described by this *torus function* $\boldsymbol{u}\,(\boldsymbol{\theta})$, which parametrises the state vectors on the torus using phase angles. The torus function $\boldsymbol{u}$ is a map in $\mathbb{R}^6$.

Two further condition must be met: (a) the dynamics must be restricted to the torus surface, and (b) a constant vector field of motion must be satisfied. The constant vector field can be defined by a parallel flow over the entire surface. The corresponding constant vector field is

$$\begin{cases} \dot{\boldsymbol{s}} = \boldsymbol{f}_0(\boldsymbol{s}, \boldsymbol{\theta}) \\ \dot{\boldsymbol{\theta}} = \boldsymbol{\omega}. \end{cases} \tag{4.4}$$

The motion on the torus must be consistent with the vector field $\boldsymbol{f}_0$. An invariant condition must hold over the entire two-dimensional surface of the tori, which can be derived as

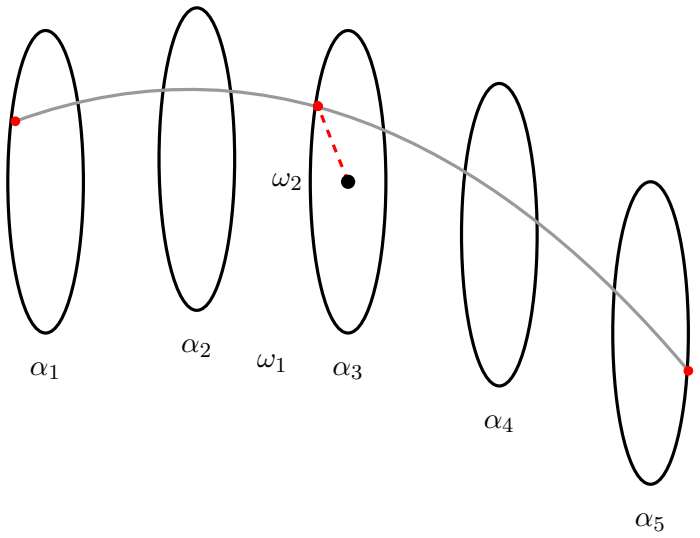

Figure 4.1: Visualisation of the motion on a torus with a two-dimensional frequency base. The black circle represents a cross section of the torus.

$$\omega_1 \frac{\partial \boldsymbol{u}}{\partial \alpha}(\boldsymbol{\theta}) + \omega_2 \frac{\partial \boldsymbol{u}}{\partial \beta}(\boldsymbol{\theta}) = f(\boldsymbol{u}(\boldsymbol{\theta})). \tag{4.5}$$

The solution is an invariant torus, if both conditions are met. All trajectories of this flow are quasi-periodic functions of time and their properties strongly depend on the arithmetical properties of the frequency base. The parallel flow on an invariant torus with the frequency base $\boldsymbol{\omega}$ is non-resonant, if the basic frequencies are rationally independent (no non-trivial linear combination with integers is equal to zero). In this case the torus is densely covered by the quasi-periodic solution. The torus collapses, if the frequencies are rationally dependent (integer k exists that solves the equation $k_1\omega_1 + k_2\omega_2 = 0$).

The two parameters, which are frequencies, are defined as

$$\boldsymbol{\omega} = (\omega_1, \omega_2)\,. \tag{4.6}$$

The period T_i corresponding to the frequency ω_i needed for one rotation is

$$T_i = \frac{2\pi}{\omega_i}. \tag{4.7}$$

The rotation number of a torus is defined as

$$\rho = \omega_2 T_1 = 2\pi \frac{\omega_2}{\omega_1}. \tag{4.8}$$

The rotation number represents the average movement in the ω_2 direction when one revolution is done in ω_1 direction. The values of ρ is defined in a mathematical positive direction. This knowledge of the natural flow is very useful for trajectory and formation design. The motion is directly linked to the frequency base of the torus, and can be described by a particle that is longitudinally moving about the generating periodic orbit with the frequency ω_1, while rotating with frequency ω_2, see Fig. 4.2. The first frequency is associated with the orbital period of the generating periodic orbit. Quasi-periodic orbits *envelop* a *base periodic orbit*.

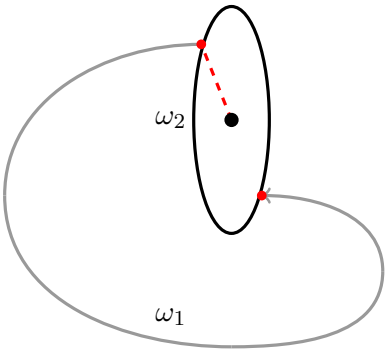

Figure 4.2: Visualisation of the motion on a torus with a two-dimensional frequency base. The black circle represents a cross section of the torus.

A transformation into angular torus coordinates (α, β) enables the introduction of a parametric representation of quasi-periodic trajectories. Furthermore, utilising the parametric representation the location of a spacecraft on the orbit is uniquely defined by two phase angles α and β, see Fig. 4.1. The angles are similar to the true anomaly known from the Keplerian motion, they increase in the direction of motion and vary between 0 and 2π. The study of quasi-periodic orbits, e.g. the transfer design, benefits from a parametric description of trajectories and their associated manifolds, which simplifies the description of departure and arrival conditions along an orbit. The introduction of a parametric representation of quasi-periodic orbits enables the identification of a single orbit by its Jacobian constant C and the two frequencies ω_1 and ω_2. To fully specify the location of a spacecraft on a quasi-periodic orbit, four parameters are required: the Jacobian value, the rotation number and two phase angles.

4.2 Calculation method for quasi-periodic orbits

With the preliminaries on quasi-periodic orbits at hand, a computation method to determine $\boldsymbol{u}$ for quasi-periodic orbits arising from periodic orbits is proposed and stepwise introduced. The computation aims to identify an approximation of the state vector function $\boldsymbol{u}$ described by a Fourier series representation on a two-dimensional angular

grid. The fundamental elements of the method are described in the preceding section, followed by the initial guess generation and the continuation process to generate orbital families.

When discretising the function $\boldsymbol{u}$, points are chosen for a set of angular parameters in an interval. The first step is to find a convenient discretisation of the angles and the function $\boldsymbol{u}$. Consequently, the angular phase definitions are

$$\boldsymbol{A} = (\boldsymbol{\theta}_{1,1}, \boldsymbol{\theta}_{1,2}, \cdots \boldsymbol{\theta}_{1,M}, \boldsymbol{\theta}_{2,1}, \boldsymbol{\theta}_{2,2} \cdots, \boldsymbol{\theta}_{M,N})^T . \tag{4.9}$$

where $\boldsymbol{\theta}_{i,j} = \left\{ \frac{2\pi i}{N}, \frac{2\pi j}{M} \right\}$. The matrix $\boldsymbol{A}$ shows the indexing for a unique element on the torus. The index is used to identify a geometric location on the torus. The definition of the six-dimensional state vectors follows the angles.

Concatenating the state vectors to a single vector yields a $(N \cdot M) \times 6$-dimensional vector, which is defined as

$$\boldsymbol{P} = (\boldsymbol{x}_{1,1}, \boldsymbol{x}_{1,2}, \cdots \boldsymbol{x}_{1,M}, \boldsymbol{x}_{2,1}, \boldsymbol{x}_{2,2} \cdots, \boldsymbol{x}_{N,M})^T . \tag{4.10}$$

A transformation of the matrix $\boldsymbol{P}$ is introduced further use the state vectors. It is defined as

$$\boldsymbol{p} = \boldsymbol{P} \cdot \boldsymbol{I}. \tag{4.11}$$

The resulting vector has a dimension of $(6 \cdot N \cdot M) \times 1$. The discrete Fourier transform matrix can be described for a 6-dimensional vector. A transformation can be applied to shift the matrix $\boldsymbol{Q}$ to one with the following structure

$$q_{i,j} = q_{i,j} \cdot \boldsymbol{I}_6, \tag{4.12}$$

where $\boldsymbol{I}_6$ is an identity matrix multiplying the element $q_{i,j}$ for each of the six-dimensional state vector. Utilising this diagonal matrix the following matrix defines the required transformation

$$\boldsymbol{P} = \begin{pmatrix} q_{1,1} & q_{1,2} & \cdots & q_{1,n} \\ q_{2,1} & q_{2,2} & \cdots & q_{2,n} \\ \vdots & \vdots & \ddots & \vdots \\ q_{m,1} & q_{m,2} & \cdots & q_{m,n} \end{pmatrix}, \tag{4.13}$$

where $\boldsymbol{P}$ is a $(6 \cdot m) \times (6 \cdot n)$ matrix. The operation in Eq. 4.13 must be applied to the following matrices: $\boldsymbol{Q}$, $\boldsymbol{R}$, and $\boldsymbol{P}$.

The invariance condition must hold over the entire two-dimensional torus surface (Schilder [2002]). Several methods are mentioned in literature to solve this equation (Kolemen et al. [2011]). In this work, the method is based on two-dimensional truncated Fourier series of $\boldsymbol{u}$. In this particular case a solution of the invariance condition is not required, and the condition is enforced by a rotation operator. The flow $\boldsymbol{f}_0$ is reduced by converting the flow to a stroboscopic map, which is associated with a time $T = \frac{1}{\omega_1 M}$.

With all the preliminaries explained, this includes the introduction of the definition of state vectors and the arrangement of the corresponding vectors, the calculation method is introduced for two different discretisation schemes:

- Discretisation with $N = M$, immediately leads to the fully described function $\boldsymbol{u}$ (at discretised states). Disadvantage are large memory requirement for fine discretisations. This methodology utilises the two-dimensional Fourier representation. The benefit in calculating the full two-dimensional function $\boldsymbol{u}$ and not, as in many other methods a unique invariant curve is the precise knowledge of additional orbital parameters such as the orbital amplitudes.
- Discretisation with $N < M$, representing a multiple shooting approach working with the one-dimensional Fourier representation.

The process is described a priori, the following steps are required:

1. Take an initial guess of the function $\boldsymbol{u}$ defining the entire quasi-periodic orbit and create the quantities $\boldsymbol{P}$ and $\boldsymbol{p}$, see Eq. 4.10 and Eq. 4.11.
2. Propagate $\boldsymbol{p}$ forwards for a specified time. The rotation operator allows evaluating the invariance condition that must be satisfied for a quasi-periodic solution.
3. Utilise an iterative Quasi-Newton method to satisfy a mapping condition. Within this process certain constraints are implemented to assure a unique solution.
4. Determination of the full function $\boldsymbol{u}$ once a converged solution is determined.
5. Continue the orbital families by either an iso-energetic stepping or a grid-based method.

One-dimensional and two-dimensional Fourier series

Since the function $\boldsymbol{u}$ is 2π periodic in the angular variables α and β, it is natural to discretise it using Fourier series. The idea of a Fourier series representation is the

approximation of $\boldsymbol{u}$ by a sum of decomposed simple periodic sine and cosine functions. For the one-dimensional case the discrete Fourier transform $\boldsymbol{f}$ and its inverse $\widetilde{\boldsymbol{f}}$ are defined as

$$\boldsymbol{f}(\alpha_n) = \sum_{n=-N/2}^{N/2} c_n e^{-i\alpha_n n}, \tag{4.14}$$

$$\widetilde{\boldsymbol{f}}(\alpha_n) = \frac{1}{\sqrt{N}} + \sum_{n=-N/2}^{N/2} k_n e^{i\alpha_n n}, \tag{4.15}$$

where N is the number of harmonics, defined on a domain $[-\frac{N}{2}, \frac{N}{2}]$, k_n are the Fourier coefficients, with each being a complex number representing both amplitude and phase of a sinusoidal component of function $\boldsymbol{x}_n$. The Fourier coefficients k_n build up the vector $\boldsymbol{k_1}$.

For the one-dimensional case the discrete Fourier transform matrix $\boldsymbol{D}$ is defined as

$$\boldsymbol{p}_1 = \mathbf{D}(\alpha) \cdot \boldsymbol{k_1} \text{ , where } d_n = e^{-i\alpha_n n}, \tag{4.16}$$

$$\boldsymbol{k_1} = \mathbf{D}^{-1}(\alpha) \cdot \boldsymbol{p}_1 \text{ , where } d_n^{-1} = \frac{1}{\sqrt{N}} + e^{i\alpha_n n}, \tag{4.17}$$

where $\boldsymbol{p}_1$ is a vector containing the equi-distant samples of a function.

For the two-dimensional case the equations are

$$\boldsymbol{f}(\alpha_n, \beta_n) = \sum_{n=-N/2}^{N/2} \sum_{m=-M/2}^{M/2} k_{n,m} e^{-i\alpha_n n - i\beta_m m}, \tag{4.18}$$

$$\widetilde{\boldsymbol{f}}(\alpha_n, \beta_m) = \frac{1}{\sqrt{NM}} + \sum_{n=-N/2}^{N/2} \sum_{m=-M/2}^{M/2} k_{n,m} e^{i\alpha_n n + i\beta_m m}, \tag{4.19}$$

where $k_{n,m}$ are the elements of a matrix $\boldsymbol{K_2}$ containing the Fourier coefficients. The transform $\boldsymbol{k}_2 = \boldsymbol{K}_2 \cdot \boldsymbol{I}$ builds the corresponding vector. The summation of the discrete truncated Fourier transform is a geometrical progression and can be expressed in a compact form. This matrix transforms Fourier coefficients into coordinate variables. The introduction of the discrete Fourier transform matrix is the first step towards the calculation of quasi-periodic orbits.

For the two-dimensional case, the discrete Fourier transform matrix $\boldsymbol{D}$ that transforms Fourier coefficients to coordinate variables is defined as

$$\boldsymbol{k_2} = \boldsymbol{D}(\alpha, \beta) \cdot \boldsymbol{p_2} \text{ , where } d_{n,m} = e^{-i\alpha_n n - i\beta_m m} \tag{4.20}$$

$$\boldsymbol{p_2} = \boldsymbol{D}^{-1}(\alpha, \beta) \cdot \boldsymbol{k_2} \text{ , where } d^{-1}_{n,m} = \frac{1}{\sqrt{N}} + e^{i\alpha_n n + i\beta_m m}. \tag{4.21}$$

In the two-dimensional case $\boldsymbol{p_2}$ is a vector containing the equi-distant samples of a function. It is important to note that computation variables are the state variables rather than the Fourier coefficients.

The rotation operator

An important part of the method is the introduction of a *rotation operator*. The rotation operator is defined in the form of a rotation matrix. A rotation of the Fourier coefficient, consequently of the corresponding state vectors, can be applied by a matrix operation. A rotation is equivalent to a propagation, if the invariance condition holds true and the appropriate shift is applied. For the two-dimensional case the rotation matrix $\boldsymbol{R}$ is derived in the following. Starting with the rotation of the Fourier coefficients by

$$\boldsymbol{k}_s = \boldsymbol{Q}^{-1}(\alpha) \cdot \boldsymbol{k} \text{ , where } q_n^{-1} = e^{-i\alpha n}. \tag{4.22}$$

$$\tag{4.23}$$

For the two-dimensional case the rotation matrix is defined as

$$\boldsymbol{k}_s = \boldsymbol{Q}^{-1}(\alpha, \beta) \cdot \boldsymbol{k} \text{ , where } q^{-1}_{n,m} = e^{-i\alpha n - i\beta m}. \tag{4.24}$$

Four steps are required to derive a real-valued rotation matrix. The rotation is equivalent to the propagation of the equations of motion up to a given time, if the invariance condition is satisfied. This is the required time to be equivalent to the rotation in both, the α and β direction. The first transformation (matrix manipulation) is introduced to shift the complex Fourier coefficients with

$$\boldsymbol{k_s} = \boldsymbol{Q} \cdot \boldsymbol{k}, \tag{4.25}$$

where $\boldsymbol{k}$ is a vector of complex Fourier coefficients. $\boldsymbol{k_s}$ is a vector containing the shifted Fourier coefficients. The shifted Fourier coefficients in Eq. 4.25 can be transformed backwards to shifted states $\boldsymbol{p_s}$ by

$$\boldsymbol{p_s} = \boldsymbol{D}(\alpha) \cdot \boldsymbol{k_s}. \tag{4.26}$$

Combining the two previous steps, a real-valued rotation matrix $\boldsymbol{R}$ is can be introduced as

$$\boldsymbol{R} = \boldsymbol{D}^{-1} \cdot \boldsymbol{Q} \cdot \boldsymbol{D}. \tag{4.27}$$

The rotation operator is applied as

$$\boldsymbol{R}(-\rho) = \boldsymbol{D}^{-1} \cdot \boldsymbol{Q}(-\rho) \cdot \boldsymbol{D}. \tag{4.28}$$

The arranged state vector is now directly rotated by applying $\boldsymbol{R}$ to $\boldsymbol{p}$, which is expressed as

$$\boldsymbol{p_s} = \boldsymbol{R} \cdot \boldsymbol{p}. \tag{4.29}$$

The rotation operator is a powerful tool and the advantage is that as applied to set of state vectors is that it hides the underlying complex Fourier coefficients.

4.2.1 Methodology for a discretisation with $N = M$

For $N = M$ the torus function $\boldsymbol{u}$ is fully described by the two-dimensional Fourier series. The discretisation is already introduced in the previous section.

Problem definition

Additional to the state vectors defined by $\boldsymbol{u}$, two properties ω_1 and ω_2 must be specified to uniquely define the orbit, for more detailed aspect see Sec. 4.1. Several different pairs of parameters may be used for the unique identification of a single quasi-periodic solution. The two values chosen here are the z component of the position of the state that represents the origin of the parametrisation, and the y component of the velocity of this state, respectively. Two constraints define a member within the family of possible solutions, another two constraints are required to fix the orientation of the phase definition as this is arbitrary chosen. To assure uniqueness of the origin, the y component and the $\dot{x}$ component are set to zero, this fully defines the origin within the parametric function. It would be theoretically possible to remove the two latter constraints by removing the values from the initial state vector list, but for clarification

it is easier to introduce the additional constraints. The solution vector contains the following elements

$$\boldsymbol{q} = (\boldsymbol{p},\, \omega_1,\, \omega_2)^T\,. \tag{4.30}$$

The problem is formulated by

$$\begin{aligned}
\boldsymbol{g}_{1..n-4}(\boldsymbol{q}) &= \boldsymbol{p} - \boldsymbol{R}(\Delta t \cdot \omega_1,\, \Delta t \cdot \omega_2)\boldsymbol{p}_p && (4.31)\\
g_{n-3}(\boldsymbol{q}) &= y_{1,1} - c_1 && (4.32)\\
g_{n-2}(\boldsymbol{q}) &= (x^2 + y^2 + \frac{2(1-\mu)}{r_1} - \frac{2\mu}{r_2} + \mu(1-\mu) - \dot{x}^2 - \dot{z}^2) - c_2 && (4.33)\\
g_{n-1}(\boldsymbol{q}) &= y_{1,1} && (4.34)\\
g_n(\boldsymbol{q}) &= v_{x_{1,1}}. && (4.35)
\end{aligned}$$

Propagation and invariance condition

The state vector $\boldsymbol{p}_s$ representing the function $\boldsymbol{u}$ is propagated for the time that lies between the discretised steps. The state vectors $\boldsymbol{p}_s$ are propagated forward in time and the results are stored in the projection variables that are defined as follows

$$\boldsymbol{p}_p = \boldsymbol{\Phi}_{\Delta t}(\boldsymbol{p}_s), \tag{4.36}$$

where $\boldsymbol{p}_p$ is a vector containing the mapped states. The notation for the flow of the dynamical equations from a given initial state vector here in assembled form containing several single states, propagated for the time interval $\Delta t = \frac{2\pi}{N}\frac{1}{\omega_1}$, is $\boldsymbol{\Phi}_t(p)$. Note that at this state there is no information about the phase angle available for vector $\boldsymbol{p}_p$. The backwards transformation from $\boldsymbol{p}_s$ and $\boldsymbol{p}_p$ into Fourier coefficients is defined by matrix $\boldsymbol{R}$. The error function $\boldsymbol{F}$ is defined as

$$\begin{aligned}
\boldsymbol{F}(\boldsymbol{p}_s, \omega_1,\, \omega_2) &= \boldsymbol{p}_s - \boldsymbol{R}(\Delta t \cdot \omega_1,\, \Delta t \cdot \omega_2)\boldsymbol{p}_p\\
&= \boldsymbol{p}_s - \boldsymbol{R}(\Delta t \cdot \omega_1,\, \Delta t \cdot \omega_2)\phi_{\Delta t}(\boldsymbol{p}_s) = 0,
\end{aligned} \tag{4.37}$$

where $\boldsymbol{R}$ is the rotation operator and $\boldsymbol{p}_s$ and $\boldsymbol{p}_p$ the state vectors. The error function yields zero, if the invariance condition is satisfied. This means for a two-dimensional function $\boldsymbol{u}$ represented by the Fourier approximation that the propagation is equivalent to a rotation of the field corresponding to the two frequencies and the time of propagation. The application of the rotation operator to the state vectors and the utilisation to compensate the effect of a propagation is an aspect that is novel in this work. The

objective is to compute the closed curve $\boldsymbol{p}_s$ and the two frequencies in a way that the error function is zero $\boldsymbol{g}(\boldsymbol{p}_s, \omega_1, \omega_2) = 0$.

Newton loop and constraints

At the beginning of the process the state vector $\boldsymbol{p}_s$ and both frequencies ω_1 and ω_2 are unknown. The objective of the following iterative process is to determine accurate values for $\boldsymbol{p}_s$ such that $\boldsymbol{p}_s$ is identical to $\boldsymbol{p}_p$ under the map $\boldsymbol{R}$. This iterative procedure is mathematically identical to a root finding problem. The algorithm iteratively adjusts the frequency vector in order to transform the set of points at each *section* into a continuous curve. The algorithm continues iterating until a set of constraints is satisfied.

One advantage of this formulation is that it can be solved numerically by a Newton method. The method leads to quadratically convergent solutions assuming a good initial guess is provided. How to find the initial guess is described in a later step. The iteration condition for the Newton method can be written as

$$\boldsymbol{g}(\boldsymbol{q}^0) + D\boldsymbol{g}(\boldsymbol{q}^0)(\boldsymbol{q}^1 - \boldsymbol{q}^0) = 0, \tag{4.38}$$

where $\boldsymbol{g}$ is the vector and $D\boldsymbol{g}$ is the gradient of this function with respect to $\boldsymbol{q}_0$. This condition is iterated until it converges to a sufficient value close to zero. Before the Newton iteration can be applied to the root finding problem, the derivative $D\boldsymbol{g}$ must be defined.

4.2.2 Methodology for a discretisation with $N < M$

The previously introduced method is computational time consuming and a variant of the algorithm is implemented being faster and relying on a one-dimensional Fourier series approximation supported by a multiple shooting method. Possible is $N = 1$, but to overcome difficulties caused by the unstable behaviour of the flow, $N > 1$ reduces the propagation times, which is similar to a multiple shooting method. For $N = M$ the torus function $\boldsymbol{u}$ is fully described by the two-dimensional Fourier series. In the case that only certain invariant curves are modelled for $N < M$, two-dimensional Fourier series are not applicable and each invariant curve is modelled by a one-dimensional Fourier series. The discretisation is already introduced, see Sec. 4.2. Only the differences to the methods for $N = M$ are highlighted here.

Problem definition

In the case that only certain invariant curves are modelled for $N < M$, two-dimensional Fourier series are not applicable and each invariant curve is modelled by a one-dimensional Fourier series. At the beginning of the process the state vector $\boldsymbol{p}_s$ and both frequencies are unknown. The chosen values are accurate, if all states $\boldsymbol{p}_s$ are identical with $\boldsymbol{p}_p$ under the map $\boldsymbol{R}$. This condition is mathematical identical with a root finding problem. The algorithm iteratively adjusts the frequency vector in order to transform the set of points at each *section* into a continuous curve. The algorithm continues iterating until a set of constraints is satisfied. The objective is to find the closed curves $\boldsymbol{p}_s^1$, $\boldsymbol{p}_s^2$, and $\boldsymbol{p}_s^3$, and the two frequencies such that the error function is zero, $\boldsymbol{g}(\boldsymbol{p}_s, \omega_1, \omega_2) = 0$. Overall, the system is formulated as

$$\boldsymbol{g}_{1..m}(\boldsymbol{q}) = \boldsymbol{p}_s^1 - \boldsymbol{R}(\Delta t \cdot \omega_1, \Delta t \cdot \omega_2)\boldsymbol{p}_p^1 \text{ , for all } \boldsymbol{p}_s \tag{4.39}$$

$$\boldsymbol{g}_{m+1..2m}(\boldsymbol{q}) = \boldsymbol{p}_s^2 - \boldsymbol{R}(\Delta t \cdot \omega_1, \Delta t \cdot \omega_2)\boldsymbol{p}_p^2 \text{ , for all } \boldsymbol{p}_s \tag{4.40}$$

$$\boldsymbol{g}_{2m+1..3m}(\boldsymbol{q}) = \boldsymbol{p}_s^3 - \boldsymbol{R}(\Delta t \cdot \omega_1, \Delta t \cdot \omega_2)\boldsymbol{p}_p^3 \text{ , for all } \boldsymbol{p}_s \tag{4.41}$$

$$g_{n-3}(\boldsymbol{q}) = y_{1,1} - c_1 \tag{4.42}$$

$$g_{n-2}(\boldsymbol{q}) = (x^2 + y^2 + \frac{2(1-\mu)}{r_1} - \frac{2\mu}{r_2} + \mu(1-\mu) - \dot{x}^2 - \dot{z}^2) - c_2 \tag{4.43}$$

$$g_{n-1}(\boldsymbol{q}) = y_{1,1} \tag{4.44}$$

$$g_n(\boldsymbol{q}) = v_{x_{1,1}}. \tag{4.45}$$

The condition in Eq. 4.38 may be written with the new vectors in Eq. 4.39 - Eq. 4.45. The constructed linear system appears to be overdetermined, but for the circular restricted three-body problem, which is a Hamiltonian system, a solution exist. Before the Newton iteration can be applied to the root finding problem, the derivative $D\boldsymbol{g}$ must be defined.

Propagation and invariance condition

The state vector $\boldsymbol{p}_s$ representing the function $\boldsymbol{u}$ is propagated for the time that lies between the discretised steps. The state vectors $\boldsymbol{p}_s$ are propagated forward in time and the results are stored in the projection variables that are defined as follows

$$\boldsymbol{p}_p = \boldsymbol{\Phi}_{2\frac{\pi}{N}\omega_1}(\boldsymbol{p}_s), \tag{4.46}$$

where $\boldsymbol{p}_p$ is a vector containing the mapped states. $\boldsymbol{\Phi}_t(x)$ is the notation for the flow of the dynamical equations from a given initial state vector, here, in assembled form containing several single states, propagated for the time interval $\Delta t = \frac{2\pi}{N}\omega_1$. The following assembled vector $\boldsymbol{p}$ is defined as

$$\boldsymbol{p} = \left(\boldsymbol{p}_s^1, \boldsymbol{p}_s^2, \boldsymbol{p}_s^3, \omega_1, \omega_2\right)^T. \tag{4.47}$$

Note that at this state there is no information about the phase angle available for vector $\boldsymbol{p}_p$.

4.2.3 Initial frequencies and Fourier coefficients

A suitable way in finding an initial guess for the function $\boldsymbol{u}$ and for the frequencies ω_1 and ω_2 is to start from a periodic orbit. This guess can be partially derived from properties of the generating periodic orbit and their linear stability, which is obtained from its Monodromy matrix. The argument of the complex eigenvalues of this matrix $\lambda_n = \cos\phi + i\sin\phi$ defines the rotation of the flow. The quantity ϕ is the angular shift on the invariant curve between the outgoing and returning trajectory. The eigenvalues λ_n of Monodromy matrices for a set of periodic orbits are depicted in Fig. 4.3. Fig. 4.3a shows the real valued eigenvalues and Fig. 4.3b the complex ones. The value of the complex eigenvalue is used to create an initial guess for the frequency ω_2.

The initial guess for the two frequencies $\widehat{\omega}_1$ and $\widehat{\omega}_2$ is derived from ϕ and from the orbital period of the generating orbit. It is defined as

$$(\widehat{\omega}_1, \widehat{\omega}_2) = \left(\frac{2\pi}{t_p}, \frac{\pm\phi + 2\pi i}{t_p}\right), \tag{4.48}$$

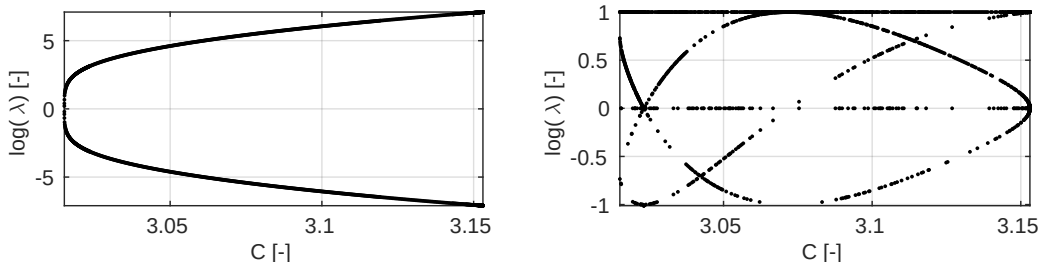

Figure 4.3: Eigenvalue structure of the Monodromy matrix of a periodic orbit. (a) Real eigenvalues and (b) complex ones.

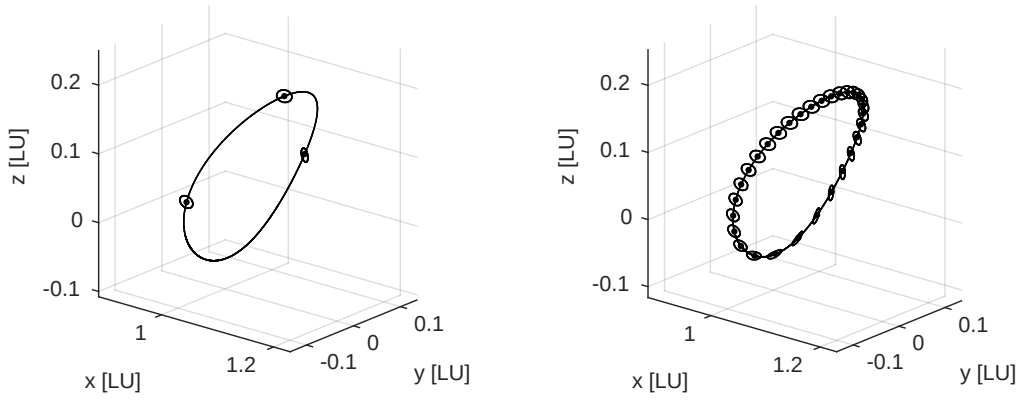

(a) **(b)**

Figure 4.4: Initial guess for the state vector $\boldsymbol{p}$ (a) for a discretisation with $M = 3$ and $N = 40$ and (b) with $M = N = 30$. The periodic base orbit is a Northern halo orbit with an orbital period of $T_p = 11.86\,d$.

where here i is zero and ϕ has a positive value. With these quantities the rotation number $\widehat{\rho}$ is determined. This initial guess is valid for solutions that are close to the periodic orbit. Another option is to determine the system frequencies by means of Fourier spectral methods, such as a Laskar Frequency map analysis and quasi-periodic decompositions, see Laskar [2003].

The complex eigenvectors $\boldsymbol{a}_n$ span a plane on which the initial guess for the state vector function $\boldsymbol{u}(0, \boldsymbol{\beta})$ is defined. The first part of the function $\boldsymbol{u}$ is derived from the complex eigenvectors $\boldsymbol{a}_n$ as

$$\boldsymbol{u}(0, \boldsymbol{\beta}) = \boldsymbol{u}_{periodic}(0) + \epsilon \left\{ \cos(\beta) Re(\boldsymbol{a}_n(\alpha)) - \sin(\beta) Im(\boldsymbol{a}_n(\alpha)) \right\}, \tag{4.49}$$

where $\boldsymbol{u}_{periodic}(0)$ is the the state vector of the periodic orbit. The rest of the function $\boldsymbol{u}$ is determined by propagating the state vectors of $\boldsymbol{u}(0, \boldsymbol{\theta}_2)$ with the following description

$$\begin{cases} \boldsymbol{p}_p & = \boldsymbol{\Phi}_{\frac{\pi}{4}\omega_1} \boldsymbol{p}_s \\ \beta^p & = \beta^s + \omega_2 2\pi/\omega_1 \end{cases} \quad \Leftrightarrow \quad \boldsymbol{\Phi}_t(t, t_0, \boldsymbol{x}_0) : \boldsymbol{x}(t_0) \rightarrow \boldsymbol{x}(t). \tag{4.50}$$

Fig. 4.4 shows the initial state vector $\boldsymbol{p}$ obtained by the Eq. 4.50.

4.2.4 Continuation

Once a converged solution is found and the function $\boldsymbol{u}$ has been obtained, one can compute further orbits starting from this previous solution. This procedure is called *continuation*. For periodic orbits the process is simple as the orbits belong to a one-parameter family. A one-parameter continuation scheme in either the Jacobian value C or the orbital period T_p is implemented to isolate family members. Quasi-periodic orbits are derived in two-parameter families, which requires a different approach. Two continuation schemes are introduced here to achieve different goals: one for generating iso-energetic orbit families and one for the evaluation of quasi-periodic solutions over a two-parameter grid. This allows either to do the continuation by varying both parameters or keeping one and changing the other.

4.2.4.1 Evaluation of iso-energetic series

Iso-energetic orbit series are obtained by fixing the orbital energy and conducting a one-parameter continuation with one of the parameters ω_1, ω_2 or a combination of it. Strict iso-energetic quasi-periodic orbit families enable a comparison with Poincaré maps, which represent a reduced two-dimensional view of existing orbits.

The first continuation method is explained in the following paragraph. The first computed solution with its parameters C^i, ρ^i builds the starting point, see Fig. 4.5. For the next three solutions, the Jacobian $C^{i+1} = C^i$ is fixed and ρ^{i+1} is attenuated. A small step size is used to achieve converged in the next step. Other parameters such as the states $\boldsymbol{p}$ are not extrapolated due to missing data in the first continuation steps. From the fourth solution onwards, a third-order polynomial fit is used to extrapolate the state vectors of $\boldsymbol{u}$, therefore $\boldsymbol{p}$. The result of a linear extrapolation or later a

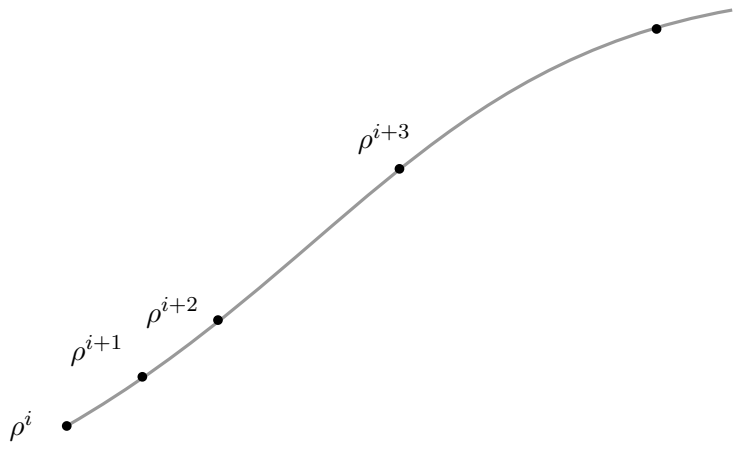

Figure 4.5: Visualisation of the iso-energetic continuation scheme.

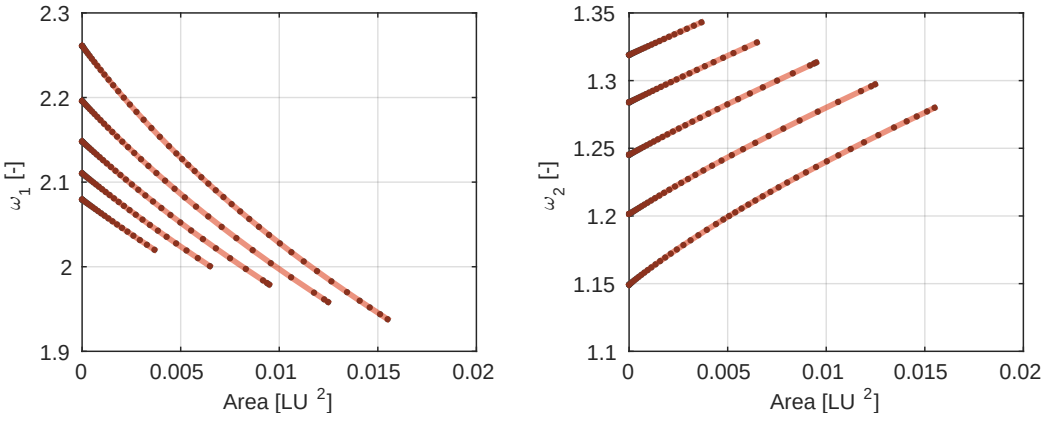

(a) **(b)**

Figure 4.6: (a) The frequency ω_1 plotted as a function of the area confined by the invariant curve. (b) Same relation for ω_2.

polynomial fit serves as initial guess for the next computation run. This process is continued until no new solution can be found. In this case the step size for the previous extrapolation is reduced and the computation restarted. The family continuation is stopped once the step size is smaller than a pre-defined value. Stopping reasons are either a collapse of the torus near resonances or when the number of harmonics are not sufficient to accurately define the state vectors of the function $\boldsymbol{u}$. The downside of continuing quasi-periodic orbits in a single-parameter is that the guess generation for the consecutive step must be sufficient enough to overcome resonance gaps.

First results of the iso-energetic continuation scheme are discussed in the following. Each point represents an individual calculated quasi-periodic orbit. Orbits with the same Jacobian constant are connected by a line segment. Fig. 4.6a and Fig. 4.6b show

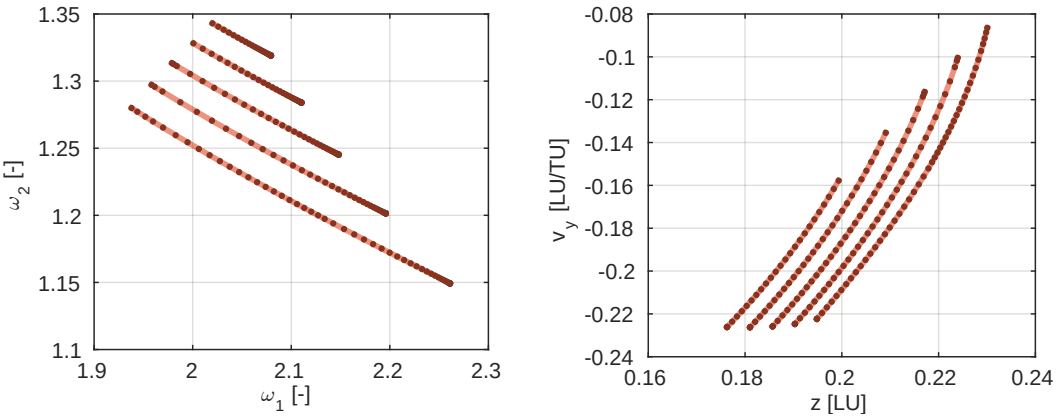

(a) **(b)**

Figure 4.7: (a) Relation between ω_1 and ω_2, and (b) the values for z and $\dot{y}$.

the dependency of the frequencies on the area confined by the invariant curve. Fig. 4.7a shows the relation between ω_1 and ω_2, whereas Fig. 4.7b reveals the spacing on the z-$\dot{y}$ plane.

4.2.4.2 Adaptive grid evaluation on z-$\dot{y}$ plane

The previously introduced continuation method generated iso-energetic orbit families with no constraints on the frequencies. The disadvantage is that a converged solution cannot be found, if the two frequencies approach a resonance. The consequence is that the continuation stops as no previous solution can be utilised for the next step. To overcome this disadvantage, a two-parameter adaptive grid continuation process is proposed.

A two-dimensional grid is introduced to determine pairs of ω_1 and ω_2. The boundaries of the computational domain for the two-parameter range is restricted to a rectangular domain. The computational scheme requires only a first converged solution for a quasi-periodic orbit. For surrounding solutions, the Jacobian $C^{i+1,j+1} = C^{i,j}$ is fixed. The other parameters such as the states $\boldsymbol{p}$ are not extrapolated. A solution is calculated for each of the grid points, with the parameter set $C^{i,j}$, $\omega_1^{i+1,\,j+1}$, and $\omega_2^{i+1,\,j+1}$, see Fig. 4.8. Once a solution failed, the grid is locally refined and for each newly created parameter set a solution is tried to obtain.

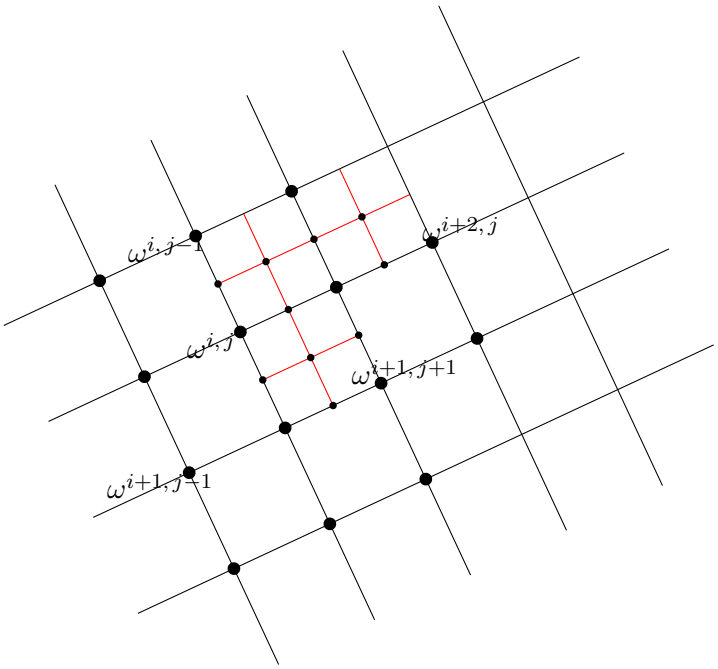

Figure 4.8: Visualisation of the adaptive grid continuation scheme on the ω_1-ω_2 plane.

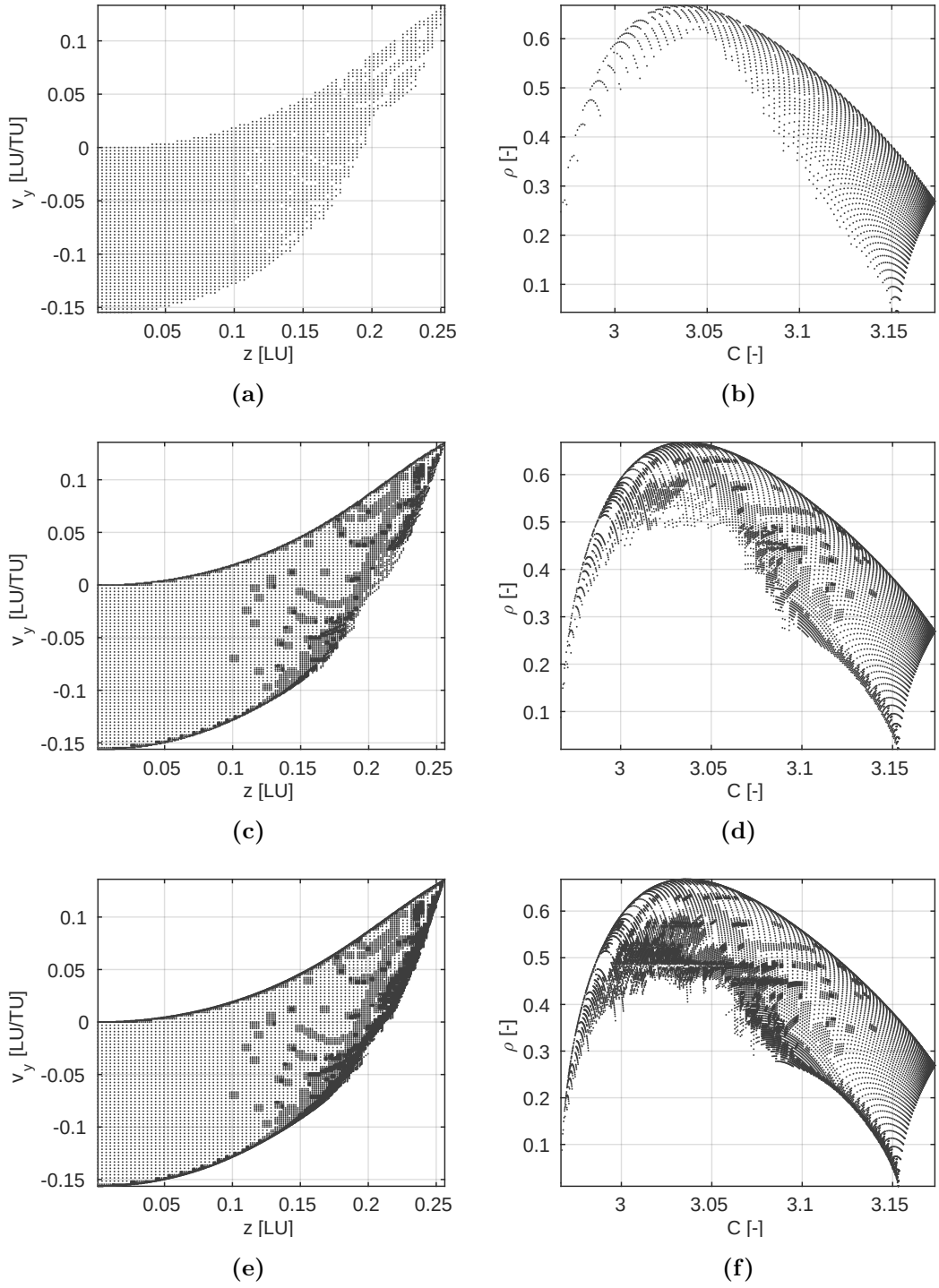

Figure 4.9: Iso-energetic quasi-periodic orbit family around a vertical lyapunov orbit evaluated in five iterative steps utilising the grid adaptation scheme. Each grey dot represents an individual solution. (a) + (b) Results of the first iteration, (c) + (d) third iteration, and (e) + (f) for the fifth iteration.

A huge benefit is that each individual solution is calculated on the basis of its neighbour without interpolation. This continuation method in two-parameters enables to

surround gaps, where no solution exists, from all directions. Therefore, it is likely to reach the entire solution space. In order to prove the performance of the continuation algorithm a set of quasi-periodic orbits around Northern halo orbit are calculated, see Fig. 4.9. Numerical results have been obtained for five grids. The step size has a large impact on the maximal extent of the existence of orbits as one solution is based on the other. For a too large step size the initial guess is not sufficient enough to compute consecutive quasi-periodic orbits.

4.2.5 Stability properties of quasi-periodic orbits

A linear approximation of the flow around a quasi-periodic orbit provides linear stability information. This information is analysed by studying the eigenstructure, i.e. eigenvectors and eigenvalues of a constructed matrix $\tilde{\boldsymbol{M}}$ that possesses similar properties as the Monodromy matrix $\boldsymbol{M}$. The required stability properties are: the stability index λ, the orientation of the subspace defined by the complex eigenvectors, and the stable and unstable direction vectors. The general stable or unstable behaviour of an orbit is not investigated here. The analysis performed here focuses on the stability information for a quasi-periodic orbit that is derived from the eigenvectors of the Monodromy matrix. For a periodic orbit the definition of the Monodromy matrix is straightforward, the variational equations are propagated forward in time with $t = T_p$ creating a linear map, see Sec. 3.3.2.

For quasi-periodic orbits the variational equations can be propagated forward for $t = 2\pi\rho$, but as the returns occur on an invariant curve the created linear map does not directly provide stability information. Therefore, an intermediate step is required to cancel the rotation caused by the dynamics of the invariant torus. The stability calculation is partially a by-product of the previous described iterative calculation of the torus parametrisation. A block diagonal matrix $\boldsymbol{S}_M$ is introduced as

$$\boldsymbol{S}_M = \begin{pmatrix} \boldsymbol{\Phi}_1 & 0 & \cdots & 0 \\ 0 & \boldsymbol{\Phi}_2 & \cdots & 0 \\ \vdots & \vdots & \ddots & \vdots \\ 0 & 0 & \cdots & \boldsymbol{\Phi}_M \end{pmatrix}, \tag{4.51}$$

where $\boldsymbol{\Phi}_i$ are the state transition matrices. The application of the rotation operator enables the definition of a matrix $\tilde{\boldsymbol{M}}$ as

$$\tilde{\boldsymbol{M}} = \boldsymbol{R}(-\rho)\boldsymbol{S}_M, \tag{4.52}$$

where $\boldsymbol{R}(-\rho)$ is the rotation operator and $\tilde{\boldsymbol{M}}$ the new matrix for a quasi-periodic orbit with similar properties to the one of the Monodromy matrix. The eigenvalues and eigenvectors of $\tilde{\boldsymbol{M}}$ contain the required stability information. Finally, a Monodromy matrix is calculated for a non-periodic orbit, the cancellation of the rotation is ensuring that the stability properties are comparable to the ones for a period orbit. Once the stability directions are determined for the first closed curve, the set is complemented by integration with the following definitions

$$\begin{cases} \boldsymbol{\psi}^u_{i,j} & = \lambda^{-\alpha_i/2\pi} \boldsymbol{\Phi}_{2\pi/\omega_1 \alpha_i}(u_{i,j}) \\ \boldsymbol{\psi}^s_{i,j} & = \lambda^{\alpha_i/2\pi} \boldsymbol{\Phi}_{2\pi/\omega_1 \alpha_i}(u_{i,j}) \\ \beta^p & = \beta^s + \omega_2 2\pi/\omega_1 \end{cases} \quad \Leftrightarrow \quad \boldsymbol{\Phi}_t(t, t_0, x_0) : \boldsymbol{x}(t_0) \rightarrow \boldsymbol{x}(t), \tag{4.53}$$

where $\boldsymbol{\psi}^u_{i,j}$ is the directional vectors towards the unstable direction, and $\boldsymbol{\psi}^s_{i,j}$ for the stable direction, respectively. The solutions are stored together with the parametric function for a quasi-periodic orbit. Fig. 4.10 shows a quasi-periodic orbit with the directional components calculated by Eq. 4.53.

Stability properties and directions

Both functions $\boldsymbol{\psi}^u$ and $\boldsymbol{\psi}^s$ are six-dimensional vectors containing directional information on the stable and unstable directions. These directions are defined by the angles between the velocity component of the eigenvectors and the x axis of the rotating coordinate frame. The directions are often derived from the linear Lissajous motion. The

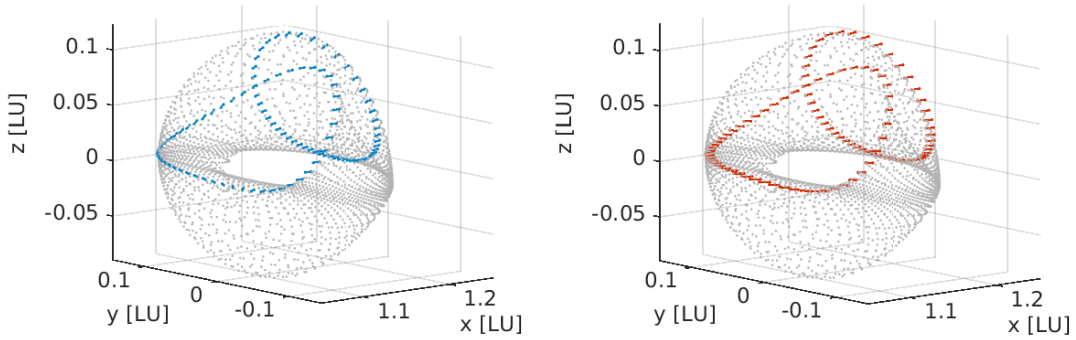

(a) **(b)**

Figure 4.10: Representation of the eigenvectors defining the (a) stable and (b) unstable directions. The grey dots represent a quasi-periodic orbit about the L_2 libration point at discrete positions with the following properties: $C = 3.1188$, $\boldsymbol{\omega} = (1.8175, 1.7383)$.

angle between the stable and unstable direction is 90 deg. At a first approximation for the Earth-Moon L_1 point, the stable direction angle is -65.31 deg and the unstable one 24.69 deg, see **?**. In the majority of the studies the angles are only defined in the x-y plane with no component in z direction.

The defined angles are shown in Fig. 4.10 for a quasi-periodic orbit within in the vertical Lyapunov family ($C = 3.0283$). The information gained is not only important for the calculation of the stable and unstable manifold directions, but for e.g. thruster alignment during early spacecraft mission design.

4.3 Parametric functions

For various design aspects of space mission utilising quasi-periodic orbits it is important to have a parametric description of trajectories and their associated manifolds. Instead of storing a single point on a quasi-periodic orbit representing the entire trajectory, a better representation of a quasi-periodic orbits is the state vector function $\boldsymbol{u}$. A compressed parameterisation using coefficients of the Fourier expansion gained in the orbit generation process is stored instead of the individual state vectors $\boldsymbol{u}$. This compressed parametrisation provides a simple tool for mission analysis purposes to create trajectories. The benefits is that state vectors can be determined independent on the discretisation of $\boldsymbol{u}$. They are written as

$$\begin{aligned} \boldsymbol{u}(\alpha,\beta) &= \sum_{n=-N/2}^{N/2} \sum_{m=-M/2}^{M/2} k_{n,m} e^{-i\alpha_m n - i\beta_m m}, \\ \dot{\boldsymbol{u}}(\alpha,\beta) &= \frac{1}{\sqrt{NM}} + \sum_{n=-N/2}^{N/2} \sum_{m=-M/2}^{M/2} k_{n,m} e^{i\alpha_n n + i\beta_m m}. \end{aligned} \tag{4.54}$$

The parametric representation of quasi-periodic orbits enables the identification of a single orbit by the Jacobian constant C and two frequencies ω_1 and ω_2. Furthermore, utilising the compressed parametrisation, the location of a spacecraft on the orbit is uniquely defined by the phase angles α and β. Three possible representations of a quasi-periodic orbit are shown in Fig. 4.11. A single trajectory is plotted in Fig. 4.11a. In Fig. 4.11b, the compressed parametrisation is used to evaluate the state vectors on a grid of 50×50 elements. Fig. 4.11c shows a mesh representing the torus surface.

With the help of the function $\boldsymbol{u}$, trajectories may be generated for arbitrary time spans with the following expression

$$\boldsymbol{x}(t) = \boldsymbol{u}(\alpha_0 + \omega_1 t,\, \beta_0 + \omega_2 t), \tag{4.55}$$

where α_0 and β_0 are the initial phases. A trajectory generated in this manner is suitable to initiate the transition to an ephemeris model using a process such as multiple shooting. Since the function $\boldsymbol{u}$ can be evaluated efficiently once it is computed, quasi-periodic orbits from various starting points can be generated with minimal computational effort.

Another representation of a quasi-periodic solution is to visualise the function $\boldsymbol{u}$ in angular coordinates in the α-β plane. Fig. 4.12a shows the z components of the function $\boldsymbol{u}$. Fig. 4.12b shows characteristics representing a single quasi-periodic orbit and the phases change along the propagation.

4.4 Sensitivity analysis

Before applying the proposed method, it is required to determine appropriate values for n_{max} and s, which is realised by providing a sensitivity analysis. The convergence behaviours and the quality of the solutions is studied for different values in the following section.

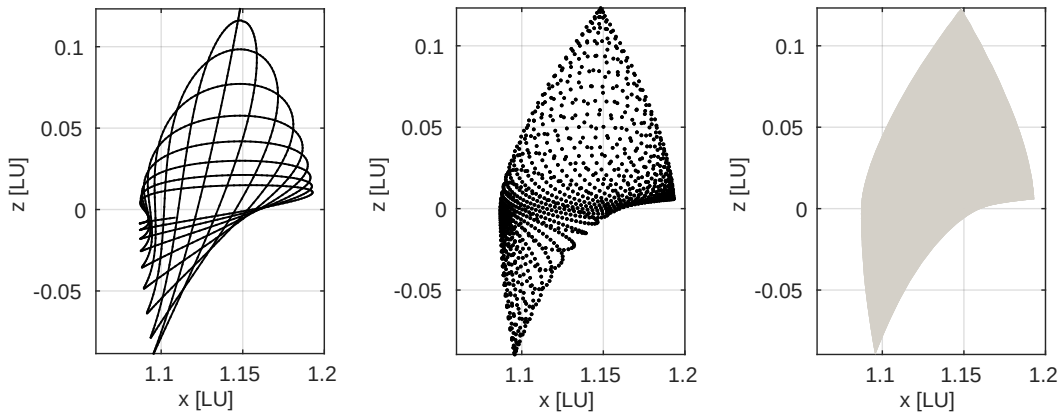

Figure 4.11: Visualisation of three possible representations of a quasi-periodic orbit. (a) A single trajectory. (b) The entity of all state vectors of the orbit. (c) A mesh representing the surface of the torus.

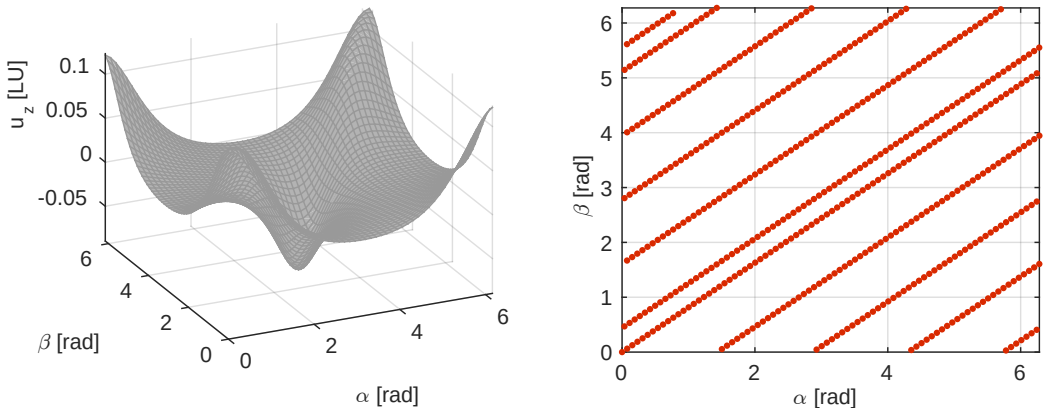

(a) **(b)**

Figure 4.12: (a) Torus function $\boldsymbol{u}$ plotted in two-dimensional angular phase space. (b) Characteristics representing a quasi-periodic orbit in angular coordinates.

Number of harmonics n_{max}

The number of Fourier coefficients n_{max} in the truncated series is one of the main drivers in the continuation process. This value has the largest impact on the maximal extension of the orbit family. The values N and M are directly depended on the number of harmonics, this results form the problem statement. For the sensitivity analysis the case $N > M$ with $N = 3$ is used for the orbit generation, where N defines the number of steps in the multiple-shooting method. This is the minimal number recommended to get a converged solution.

Fig. 4.13 show results for three different values of n_{max}. The lines represent the bound-

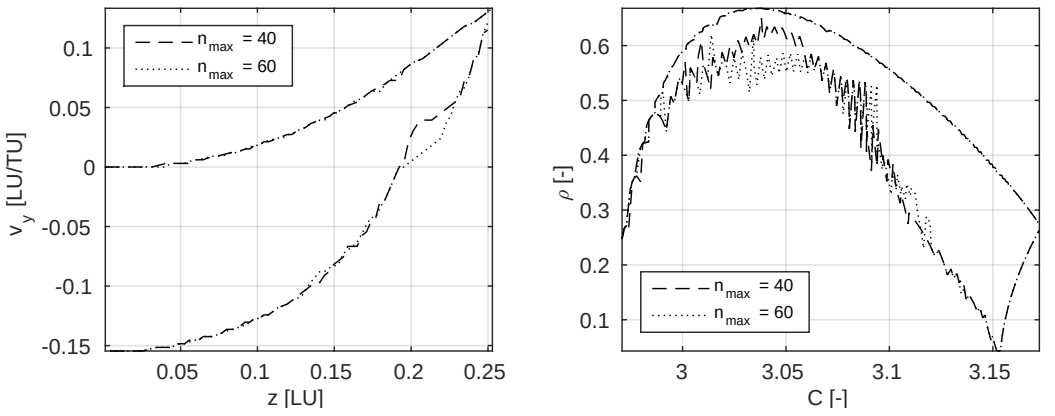

(a) **(b)**

Figure 4.13: Sensitivity of the grid continuation on the number of Fourier coefficients. (a) Maximal extent on the z-v_y plane. (b) Results on the C-ρ plane.

aries of the regions with calculated solutions. To find out whether the borders are caused by the number of harmonics, results are shown for $n_{max} = 40$ and $n_{max} = 60$.

Stepping parameter s

The grid size continuation parameter s affects the calculated solutions. The in-plane stepping on the z-v_y plane defines the distance that lies between the family members. Three value for s are selected to find out whether further solutions can be found once smaller steps between the solutions are allowed. The maps in Fig. 4.14 shows the regions with existing solutions where the generation stopped depending on the stepping parameter s. A uniform mesh has the disadvantage once the orbits pass close to the secondary body with fast changing dynamics with the same step size, either it is too fine for some part or too coarse for others. In some cases, if the initial solution that triggers the grid continuation is in a region that required very small step sizes, the process fails due to a too coarse grid for the first iteration step.

4.5 Extent and boundaries of quasi-periodic orbit families

Various quasi-periodic orbits are computed in the vicinity of the Lagrange points L_1 and L_2 in the Earth-Moon system. The quasi-periodic orbit families emerge from periodic vertical Lyapunov, Northern and Southern halo orbit and families of the 1-period and 3-period distant retrograde orbits. Tab. 4.1 introduces the notation of types of quasi-periodic orbits along with properties of the two-parameter continuation process.

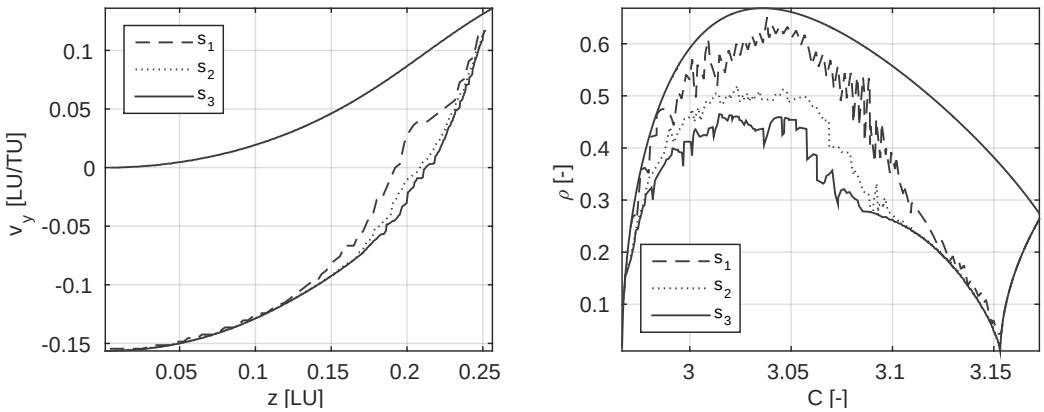

Figure 4.14: Sensitivity analysis for three different stepping parameters s. (a) Maximal extent on the z-v_y plane. (b) Results on the C-ρ plane.

Name	p-type	z		$\dot{y}$	
		min	max	min	max
ro1	distant retrograde 1-period orbits	0.001	2.0	−2.2	1.0
ro3	distant retrograde 3-period orbits	0.001	2.0	−2.2	1.0
l2nh	L_2 Northern halo orbits	0.001	0.3	−0.28	0.1
l2vl	L_2 vertical Lyapunov orbits	0.001	0.35	−0.03	0.2

Table 4.1: Notation of the types of quasi-periodic orbit families. Summary of the bounding boxes for the two-parameter continuation process.

The bounded rectangular domain in z and $\dot{y}$ is restricted to values from $z_{min} < z < z_{max}$ and $\dot{y}_{min} < \dot{y} < \dot{y}_{max}$, see first two rows in Tab. 4.1.

4.5.1 Quasi-periodic distant retrograde orbits

Results of the family generation for quasi-periodic orbits originating from 1-period and 3-period distant retrograde orbits in the circular restricted three-body problem are presented. Five iteration steps are calculated for the grid continuation process assuring that the convergence of neighbour quasi-periodic orbits is achieved. A total of 5000 orbits are calculated for the 1-period case and 6000 orbits for the 3-period case. The z value is an indication for the A_z amplitude, as all quasi-periodic distant retrograde orbits are symmetric about the x-y plane.

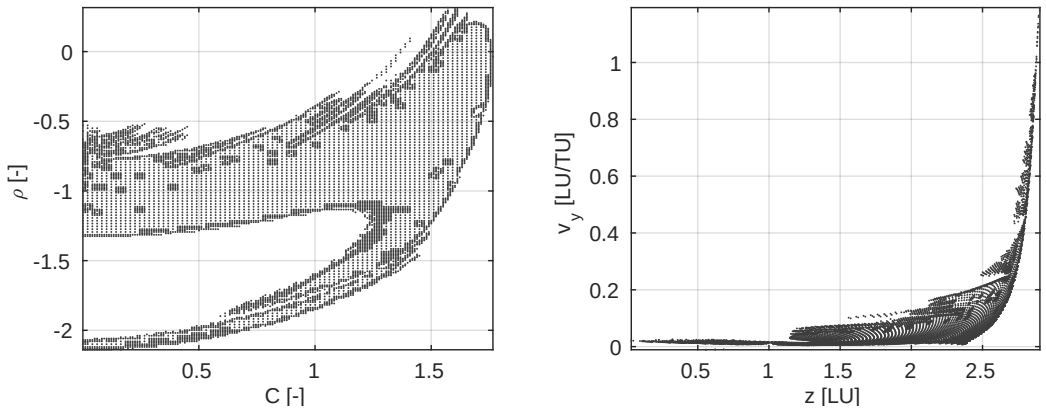

Figure 4.15: Results of the mesh continuation methods for 1-period quasi-periodic distant retrograde orbits. (a) Results shown on the C-ρ plane. (b) Representation of all orbit on the z-v_y plane.

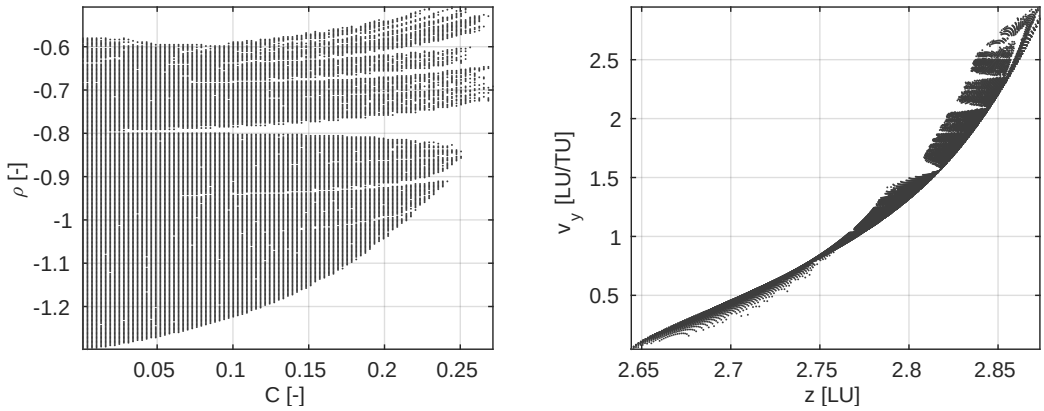

(a) **(b)**

Figure 4.16: Results of the mesh continuation methods for 3-period quasi-periodic distant retrograde orbits. (a) Results shown on the C-ρ plane. (b) Representation of all orbit on the z-v_y plane.

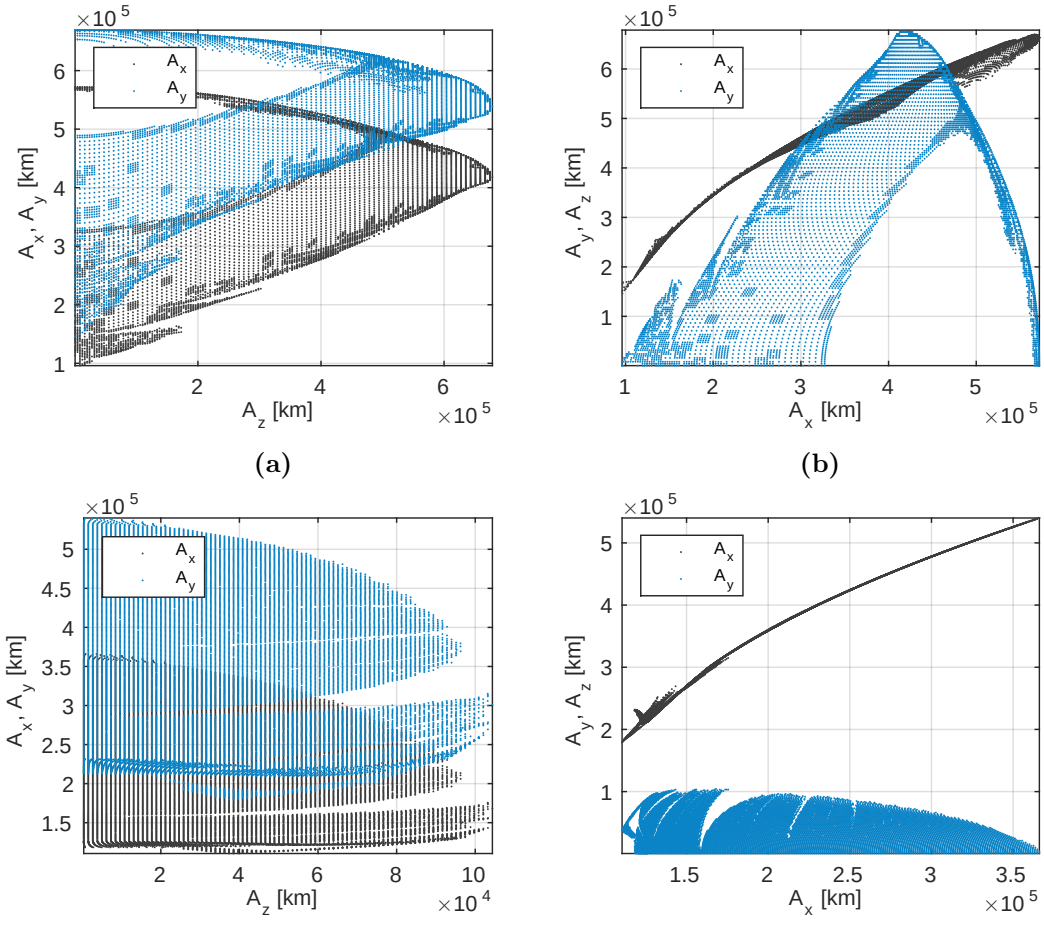

(a) **(b)**

(c) **(d)**

Figure 4.17: Amplitudes for (a+c) 1-period and (b+d) 3-period quasi-periodic distant retrograde orbits.

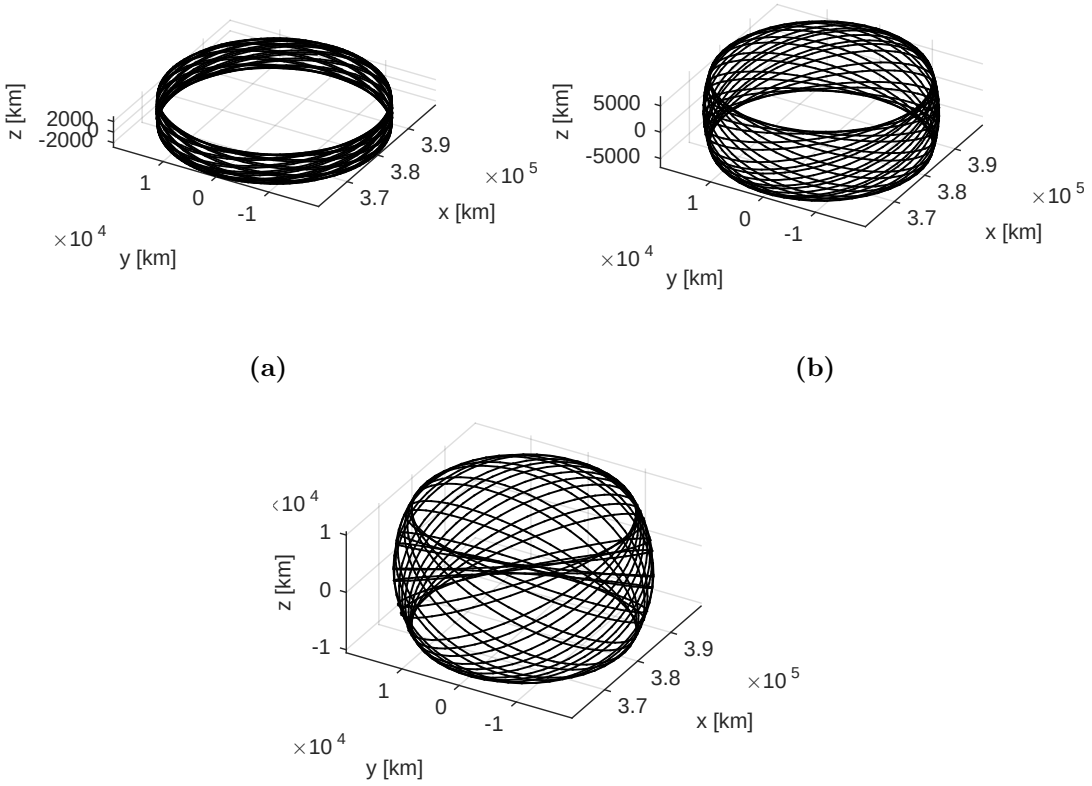

Figure 4.18: Selection of 1-period quasi-periodic distant retrograde orbits in the synodic reference frame. For all three solutions $C = 3.15$. (a) $\boldsymbol{\omega} = (10.88, 9.96)$, (b) $\boldsymbol{\omega} = (10.77, 9.84)$, and (c) $\boldsymbol{\omega} = (10.56, 9.62)$.

The results are presented for the 1-period quasi-periodic distant retrograde orbits in Fig. 4.15a and Fig. 4.15b, drawing the z and $\dot{y}$ values describing the full state of each orbit at the construction point $\boldsymbol{u}(0, 0)$ with $z = 0$, $z > 0$ and $\dot{z} > 0$. The results for the 3-period quasi-periodic distant retrograde orbits are presented in Fig. 4.16a and Fig. 4.16b. The phases start at this point from zero. The boundaries represent the rising line from periodic orbits into quasi-periodic solutions and on the other side the maximal extent. The stability parameters, the energy level and the frequencies are not presented in this figure. For this purpose another figure is introduced combining those parameters.

The amplitudes for the calculated quasi-periodic orbits are summarised in Fig. 4.17. Sample trajectories for both cases are visualised in Fig. 4.18 and Fig. 4.19. The orbital parameters of the solution can be found in the description of the figures.

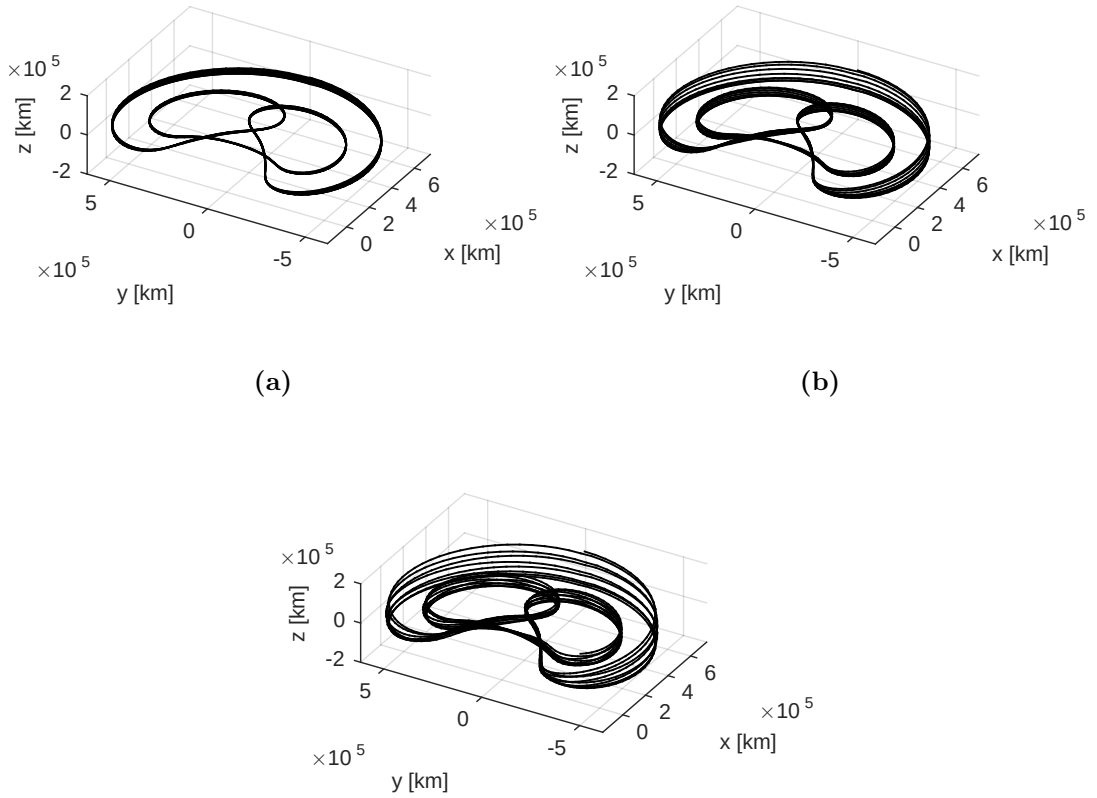

Figure 4.19: Selection of 3-period quasi-periodic distant retrograde orbits in the synodic reference frame. For all three solutions $C = 2.55$. (a) $\boldsymbol{\omega} = (0.3530, 0.3283)$, (b) $\boldsymbol{\omega} = (0.3533, 0.3258)$, and (c) $\boldsymbol{\omega} = (0.3537, 0.3193)$.

4.5.2 Quasi-periodic libration point orbits

Results of the family generation for quasi-periodic orbits originating from periodic libration point orbits are presented in this section. Results are shown for the libration point L_2, but the method can be applied in the same way to the L_1 or other libration points. Five iteration steps for the grid continuation process are sufficient to assure that the convergence of neighbour quasi-periodic orbits is achieved. A total of 5000 quasi-halo orbits around a Northern halo are calculated. Another 6000 lissajous orbits around the vertical Lyapunov orbit are presented. The z value is an indication of the A_z amplitude, as all quasi-periodic libration point orbits are symmetric about the x-z plane.

In Fig. 4.20 and Fig. 4.21 the region covered by quasi-periodic orbits is illustrated. The existence is restricted by the orbital period of the generating periodic orbit and

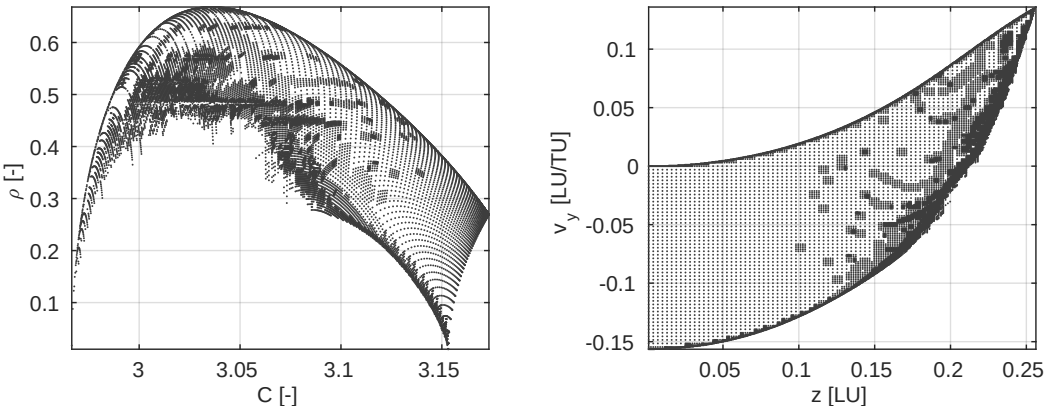

(a) **(b)**

Figure 4.20: Results of the mesh continuation method for quasi-periodic solutions around periodic vertical Lyapunov orbits. (a) Results shown on the $C\,\rho$-plane. (b) Representation of all orbit on the $z\,\dot{y}$- plane.

the corresponding ω_2 as the argument of the complex eigenvalue of the Monodromy matrix. The amplitudes of all calculated solutions are summarised in Fig. 4.22. The orbits here are sorted by ascending orbital amplitudes in x direction.

Some trajectories for both cases are visualised in Fig. 4.23 and Fig. 4.24. The orbital parameters of the solution can be found in the description of the figures.

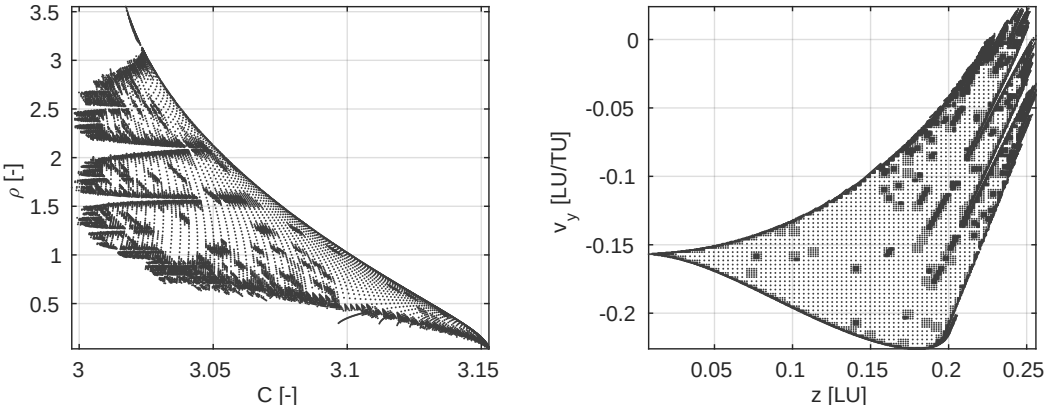

(a) **(b)**

Figure 4.21: Results of the mesh continuation method for quasi-periodic solutions around periodic Northern halo orbits. (a) Results shown on the ρ-C plane. (b) Representation of all orbit on the z-$\dot{y}$ plane.

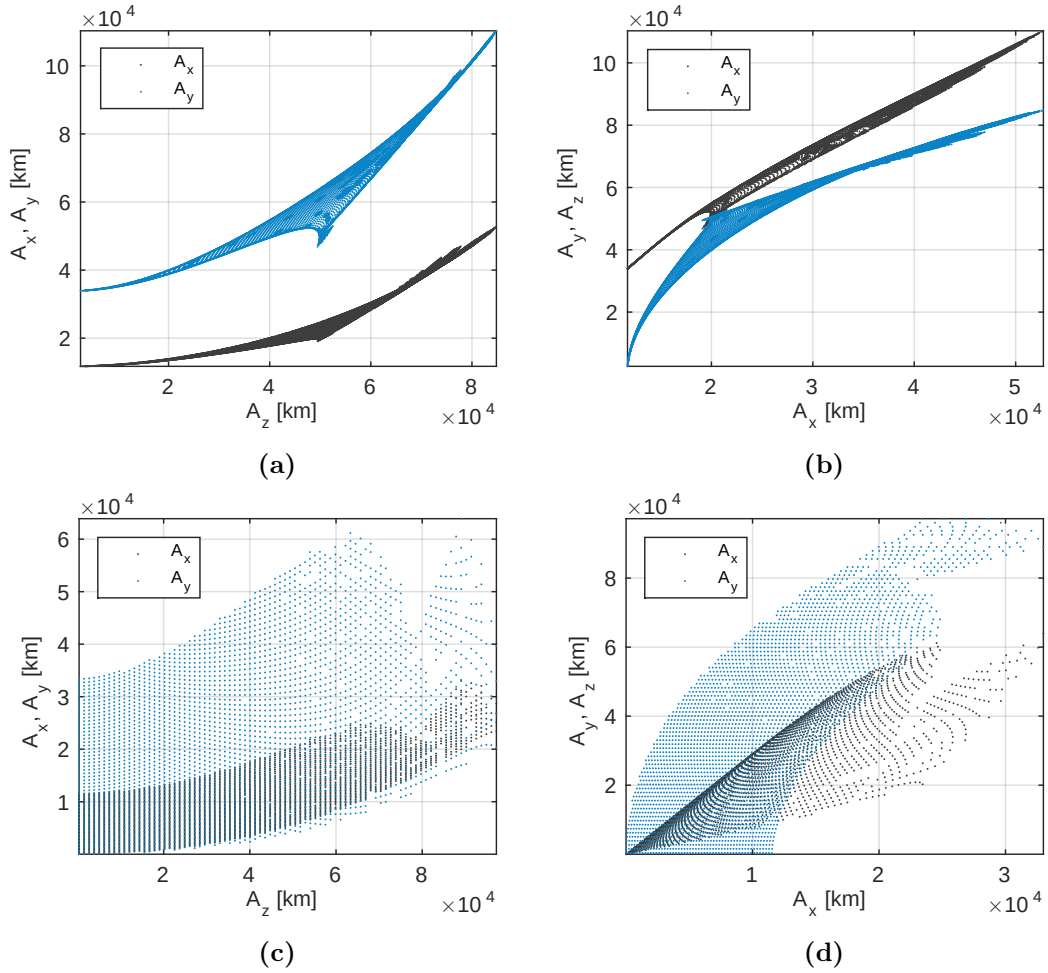

Figure 4.22: Amplitudes A_x, A_y, and A_z for quasi-periodic solutions. Results with ascending amplitudes (a) A_z, and (b) A_x for quasi-halo orbits. Amplitudes (c) A_z,and (d) A_x for lissajous orbits.

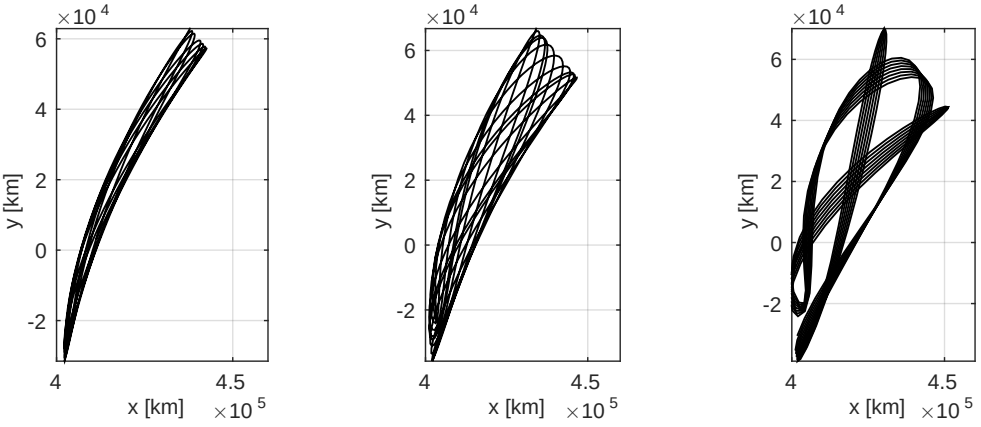

Figure 4.23: Selection of quasi-periodic orbits around periodic Northern halo orbits in the synodic reference frame. For all three solutions $C = 3.0641$. (a) $\boldsymbol{\omega} = (1.9910, 1.4378)$, (b) $\boldsymbol{\omega} = (1.9745, 1.4453)$, and (c) $\boldsymbol{\omega} = (1.9411, 1.4613)$.

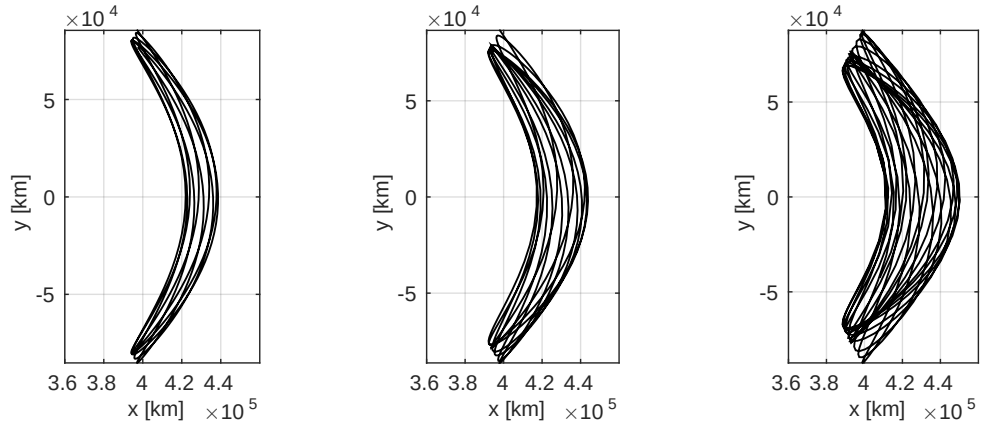

Figure 4.24: Selection of quasi-periodic orbits around periodic vertical Lyapunov orbits in the synodic reference frame. For all three solutions $C = 3.0175$. (a) $\boldsymbol{\omega} = (1.5533, 1.3967)$, (b) $\boldsymbol{\omega} = (1.5519, 1.4025)$, and (c) $\boldsymbol{\omega} = (1.5485, 1.4128)$.

4.6 Summary

This chapter presents a method developed to efficiently compute quasi-periodic orbits. The calculation method enabled a characterisation of each solution either by geometric properties or by properties that are related to the inner structure of the quasi-periodic solution. These properties are the amplitudes A_x, A_y, A_z, phase angles α, β, and the frequencies ω_1 and ω_2. Their evolution across quasi-periodic orbit families was explained. The derivation of an initial guess to initiate the calculations was explained in detail. A parametric function was introduced to represent quasi-periodic orbits. A similar concept is the use of the analytical solution to the linear lissajous motion in Canalias Vila [2007], but with a limited application to orbits with small orbital amplitudes. Two continuation methods were introduced to expand a single solution into a family of orbits. The first one was for the generation of iso-energetic orbit families. The second one was a novel grid-based two-parameter continuation with the advantage to picture the entire solution space and find solutions close to resonances of the two frequencies. Another advantage of a grid-based continuation on the z-$\dot{y}$ plane with a focus on application is an equal spacing for e.g. transfer relevant parameters of the orbit is achieved. In a last section, quasi-periodic solutions were obtained for a variety of periodic orbits. The parametric representation of the quasi-periodic orbits is of particular interest for further applications. The next chapters utilise the proposed parametrisation of quasi-periodic orbits for the calculation of orbital transfers, and to study formation flying aspects. Furthermore, a method to cope with quasi-periodic orbits in a more sophisticated dynamical model is proposed.

CHAPTER 5

Station-keeping for quasi-periodic orbits

The dynamically sensitive behaviour of most libration points and distant retrograde orbits prohibits the propagation of multiple orbital revolutions. A technique is required to compensate for perturbations either introduced by gravitational forces or numerical errors in numerical propagations. This chapter presents a novel methodology to maintain quasi-periodic orbits over long time spans. The objective of this methodology is to identify station-keeping manoeuvres in a way that orbital properties are maintained throughout manoeuvre execution. The station-keeping methodology is explained and applied to periodic and quasi-periodic trajectories coming from dynamical models with different accuracy.

Effects of the large orbital eccentricity of the Moon and the perturbations of the Earth destroy orbits that can be identified in the circular restricted three-body problem. For a periodic orbit the identifying parameter is the Jacobi constant, for quasi-periodic orbits there is an additional parameter required, either the frequency ω_2 or the rotational number ρ. The requirement imposed on the algorithm is that those orbital properties are preserved by the station-keeping manoeuvres, when an orbit is propagated for an arbitrary length of time.

5.1 Determination of the orbital lifetime and its maximisation

Before the station-keeping procedure is explained, the focus is set on the basic idea of the algorithm, which is the determination and implementation of manoeuvres that increase the lifetime of an orbit. The objective is to find manoeuvres that maximise the time the trajectory remains within a given region around a libration point. For orbits with larger amplitudes, when the limits of the given region include the secondary body the spacecraft must not fall into the primary. For this purpose an exclusion zone

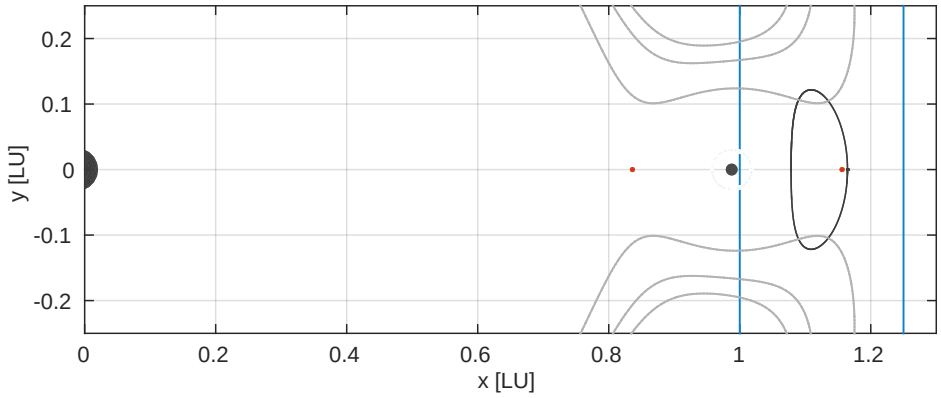

Figure 5.1: Planar view of the bottleneck region with a visualisation of the boundaries (blue) set manually depending on the orbital amplitudes to evaluate the orbital lifetime. The grey lines indicate zero velocity curves. A trajectory of an halo orbit is shown in black.

is added around the secondary body, see Eq. 5.1. The forbidden region defined by the zero velocity curves enables the introduction of limits that are purely defined by the x component of the state vector. The numerical integration stops when the trajectory passes through the boundaries defined by

$$\begin{cases} x & < x_{L2} + \delta_1 \\ x & > x_{L2} - \delta_1 \\ \delta_2 & < \sqrt{(x_1 - x_{1,M})^2 + (x_2 - x_{2,M})^2 + (x_3 - x_{3,M})^2}, \end{cases} \tag{5.1}$$

where δ_1 is the maximal amplitude in x direction of the exclusion zone and $\delta_2 = 10^{-4}\,LU$ builds a sphere around the Moon. These boundaries are visualised in Fig. 5.1. The position vector of the Moon $\boldsymbol{x}_M$ is defined in the synodic reference frame. Assuming that the initial state is already within these limits and on the x-y plane in the synodic reference frame, the state can be perturbed in a way that the orbital lifetime changes. The starting point for the evaluation of the orbital lifetime is a state vector on the x-y plane in positive direction. In order to determine the correction manoeuvre, the trajectory is propagated forward from the initial state. The time until this event is defined as T_{max}. The value T^+_{max} refers to a forward, T^-_{max} to a backward propagation, respectively.

Station-keeping maneouvres

In order to extend the lifetime of an orbit, either the velocity, the position or both can be changed. The implementation of a velocity change is straightforward, whereas changing the position would leave a discontinuity in the trajectory. To cope with this problem a position change is implemented by two velocity changes, the first one to vary the position of a point half a revolution post maneouvre, where the second manoeuvre is applied. The starting point for the station-keeping method is a pre-calculated state vector $\boldsymbol{x}_0 = (x, y, z, \dot{x}, \dot{y}, \dot{z})$.

An optimisation method is utilised to find an optimal Δv applied at the x-y plane crossing to maximise the mean orbital lifetime mean(T^+_{max}, T^-_{max}). This only leads to feasible solutions, if the position vector is accurate. One major difference to the bisection method (Hechler [2002]) is the determination of the mean time mean(T^+_{max}, T^-_{max}) allows to find a balancing between stable and unstable manifold branches. Finding the optimal manoeuvre is closely related to the invariant manifolds, in particular to the centre manifold as this describes the part of the phase space that is neither affected by the attraction of the stable manifold nor the repulsion of the unstable one.

Achieving this point of the state space assures to maintain the properties of the orbit. For all cases the vector elements x and y are fixed, and an optimal Δv is applied at the x-y plane crossing point to maximise the orbital lifetime T_{max} post manoeuvre. Restricting the station-keeping manoeuvre to the in-plane direction and allowing it only at the crossing of the x-y plane reduces the number of parameters to be optimised.

The initial state assuming $z = 0$ is fully defined by

$$\begin{aligned} x_1 &= x \\ x_2 &= y \\ x_3 &= 0 \\ x_4 &= \dot{x} + \Delta v_x \\ x_5 &= \dot{y} + \Delta v_y \\ x_6 &= \sqrt{C + x^2 + y^2 + \frac{2(1-\mu)}{r_1} - \frac{2\mu}{r_2}}, \end{aligned} \tag{5.2}$$

where $\boldsymbol{x}$ is the new state vector. The magnitude of the manoeuvre is determined by the $l2$-norm $\Delta v = \sqrt{\Delta v_x^2 + \Delta v_y^2}$. Both parameters Δv_x and Δv_x are determined by solving the optimisation problem described in the next section.

Maximisation of the orbital lifetime

A differential evolution algorithm for non-linear functions is used to maximise the orbital lifetime due to multiple local maxima. The differential evolution algorithm has two parameters that can be set, the differential weight $F = [0, 2]$ and $CR = [0, 1]$ representing the crossover probability. For details about differential evolution algorithms, see Storn and Price [1997]. The optimisation parameters and the domain of the optimisation variables are listed in Tab. 5.1. The optimisation problem is stated as

$$\underset{\Delta v_x, \Delta v_y}{\text{maximise}} \quad J(\Delta v_x, \Delta v_y), \tag{5.3}$$

where Δv_x and Δv_y are the optimisation parameters. Eq. 5.3 is solved subject to the constraints defined in Eq. 5.1.

Name	constant	range min. value	range max. value
Generations	200		
Population	40		
CR	0.5		
F	0.8		
Δv_x		$-10^{-4}\ \frac{LU}{TU}$	$10^{-4}\ \frac{LU}{TU}$
Δv_y		$-10^{-4}\ \frac{LU}{TU}$	$10^{-4}\ \frac{LU}{TU}$

Table 5.1: Optimisation parameters and the domain of the optimisation variables for the maximisation of the orbital lifetime.

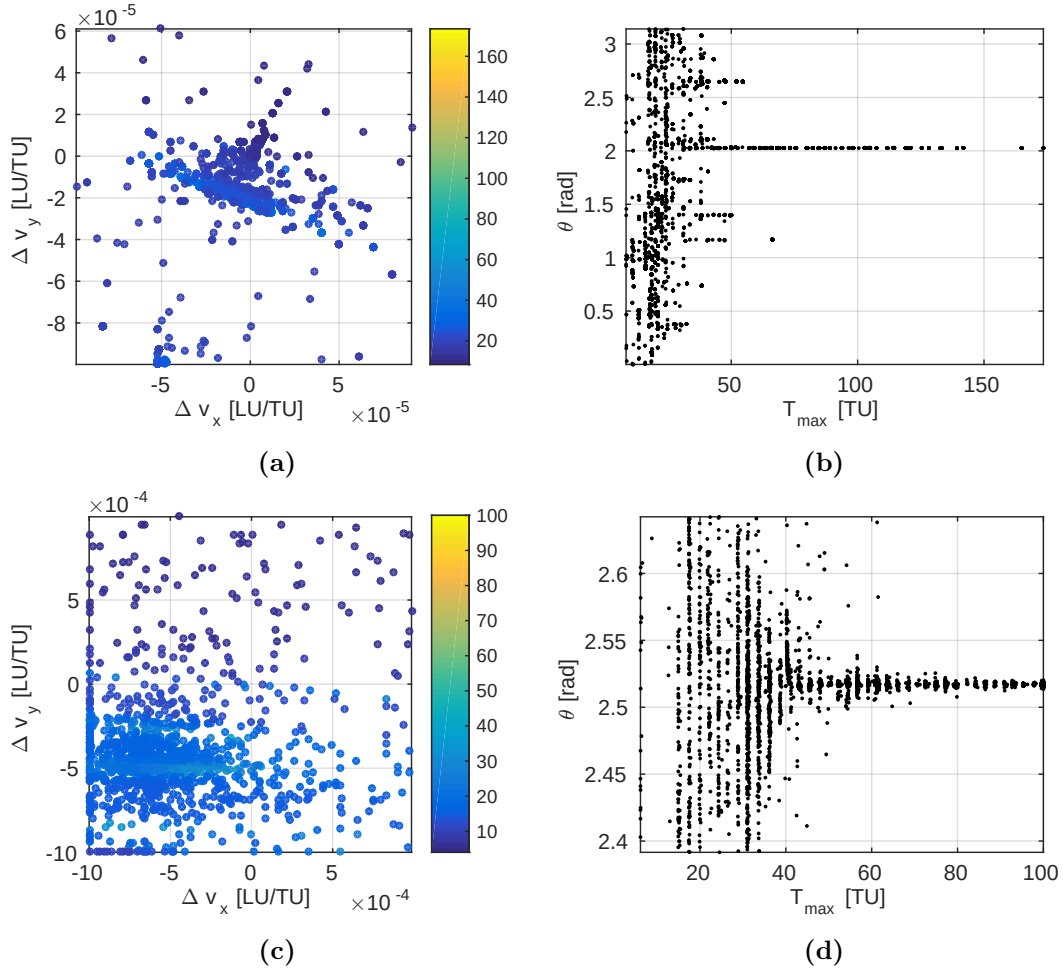

Figure 5.2: (a) + (c) Individual Δv-pairs evaluated during the optimisation process. (b) + (d) Corresponding manoeuvre directions. (a) + (b) Results for a forward propagation with T_m^+ and (b) with a backwards propagation with T_m^-.

Different objective functions are considered, which are:

1. Orbital lifetime $J_1 = \max(T_{max}^+)$ post manoeuvre.
2. Mean lifetime $J_1 = \text{mean}(T_{max}^+, T_{max}^-)$.
3. For a multi-objective optimisation $J_1 = \max(T_{max}^+)$ and $J_2 = \min(\Delta v)$.

The quantities T_{max}^+ and T_{max}^- are evaluated by

$$\boldsymbol{f}_{T_{max}^+} = \boldsymbol{\Phi}_{+\tau_{max}} \left(\boldsymbol{x} \left(\Delta v_x, \Delta v_y \right) \right), \tag{5.4}$$

where $\boldsymbol{\Phi}_{\pm\tau_{max}}$ denotes the propagation. The optimisation of each objective function yields an optimal station-keeping manoeuvre. For the multi-objective case a solution on the Pareto front is chosen that represents a trade-off between the orbital lifetime and the manoeuvre magnitude. During the optimisation process a constant Jacobi value C

is assured by adjusting the Δv_z component, see Eq. 3.14. More specific details on the objective function and constraints will be provided in the following as they might vary from one scenario to the other.

Two optimisation runs show the correlation between Δv_x and Δv_y, one is conducted for a forward and the other one for a backward propagation, indicating the stable and unstable manoeuvre directions, respectively. Fig. 5.2 highlights the results. Fig. 5.2a and 5.2c show individual evaluated Δv pairs in the population during the differential evolution process. The colour code indicates the orbital lifetime. The Δv_x-Δv_y plots show the correlation between manoeuvre components and orbital lifetimes. The best 10 % of the solutions are taken to produce the T_{max}-θ plots in Fig. 5.2b and 5.2d, where θ is the optimal maneouvre direction.

The relation between manoeuvre directions, magnitudes and their corresponding orbital lifetimes T_{max} are further studied as they represent a major step towards the design of the station-keeping algorithm. An initial state vector belonging to a periodic orbit, which is the outcome of the solved two-point boundary value problem, is used.

Remarkable is the smooth behaviour for the manoeuvre direction θ, whereas the orbital lifetime indicates a chaotic pattern. A reason for this is the fact that the location where the trajectory escapes moves along the boundary planes. In some cases the is also the switching between the two boundaries as introduced in Eq. 5.1 is visible.

5.2 Station-keeping applied to the circular restricted three-body problem

The determination of the optimal manoeuvre to extend the orbital lifetime is equivalent to finding the next downstream centre manifold. Targeting the next downstream centre manifold implies that no stable or unstable component is introduced and the spacecraft evolves on the *same* orbit as prior to the manoeuvre. It is significant for a station-keeping algorithm that on the one side orbital properties are maintained and on the other side that no pre-calculated reference trajectory is required.

5.2.1 Trajectory extension

In mission design it is desirable to extend the lifetime of an existing orbit to fulfil primary and secondary mission requirements. An unstable libration point orbit usually escapes after one to three revolutions and leaves the desired path on one of the hyperbolic invariant manifolds. Therefore, a method is implemented in the following to extend the orbital lifetime by utilising the previously introduced station-keeping manoeuvres. Out of all investigated objective functions, the optimisation with $J = \text{mean}(T_m^+, T_m^-)$

has been proven to be the most effective approach for the identification of the centre manifold. The extension of the lifetime maintains the spacecraft in the vicinity of the original orbit.

The fundamental idea of increasing the orbital lifetime is explained in the previous section. The algorithmic formulation of the procedure to create quasi-periodic orbit families consists of the following steps:

1. Take a point $\boldsymbol{f}^n$ along the nominal orbit.
2. Optimise and apply station-keeping manoeuvre to extend the trajectory for two x-y plane crossings.
3. The optimal manoeuvre is determined and executed and the trajectory with the state vector $\boldsymbol{f}^{n+1}$ is propagated for a full revolution (two x-y plane crossings). Once a return point is identified it is used as starting condition for the next manoeuvre evaluation.
4. Take this new state vector and continue with step 2 and 3 until the required orbital lifetime is achieved.

In the following station-keeping costs are computed for periodic and quasi-periodic cases following the proposed approach. In general, the station-keeping algorithm is applicable to all libration point and distant retrograde orbits that possess an invariant hyperbolic manifold. The numerical algorithm is purely used to continue and extend the orbital lifetime of orbits. Applying this algorithm in a dynamical regime modelled by the circular restricted three-body problem accounting neither for uncertainties nor a navigation budget leads to very small manoeuvres that simply compensate numerical errors introduced by the propagation scheme.

Example for a periodic orbit

The performance of the method is validated on a periodic orbit with a Jacobian value of $C = 3.0641$. Fig. 5.3a shows the x-y plane with several returns locations where the manoeuvres take place. The bold markers present returning locations after each station-keeping manoeuvre. The grey (dotted) rings present the centre manifold structure for this particular periodic orbit. The trajectories associated to those rings correspond to quasi-periodic solutions with the same Jacobian as the periodic orbit. The representation of the centre manifold by those curves is widely used and enables a reduction of the parameters for a better visualisation on the x-y plane. The resulting halo orbit is plotted in Fig. 5.3b.

For the periodic case the station-keeping error can be easily evaluated as the trajectory returns to the same point on the x-y plane. A first study evaluates the manoeuvre magnitude and direction of the station-keeping strategy that is applied every second crossing of the x-y plane. The manoeuvre history is shown in Fig. 5.4a. The velocity increments are all in the range of a few $\frac{mm}{s}$ up to $\frac{cm}{s}$. The optimisation shows that all station-keeping manoeuvre are conducted in the same direction (or 180 deg shifted), see the value of θ in Fig. 5.4b. The maintenance effort in terms of Δv is determined for halo orbits with an orbital period between 13.3 to 14.8 days. A total of 30 station-keeping manoeuvres are evaluated leading to an orbital lifetime of about a year. To be noted that the manoeuvre direction θ is aligned with the direction of the stable mode eigenvectors of the orbit. This is not surprising as station-keeping methods incorporating Floquet analysis utilise manoeuvres that are aligned with the unstable

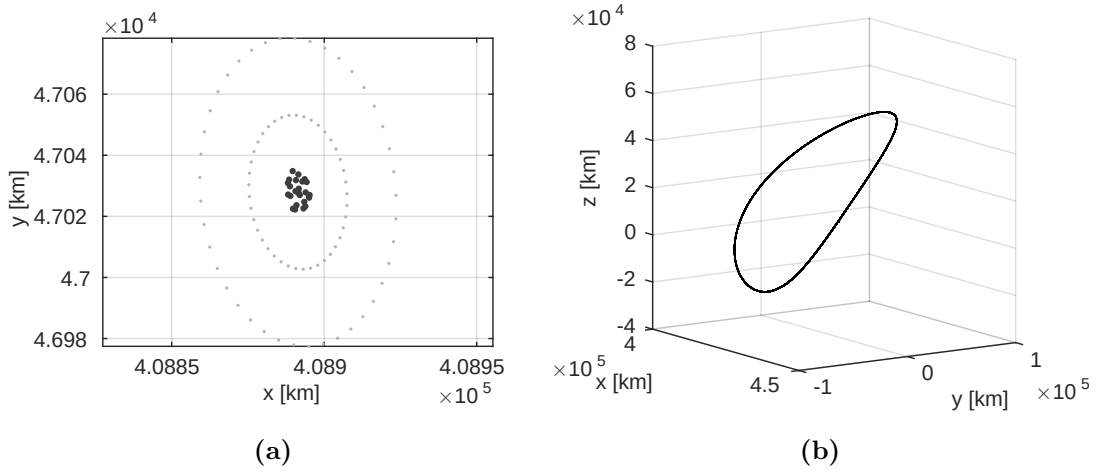

(a) **(b)**

Figure 5.3: (a) Return map on the ...created during the station-keeping process. Initial state belongs to a periodic Northern halo orbit with $C = 3.0641$. (b) Extended trajectory for a lifetime of about 400 days.

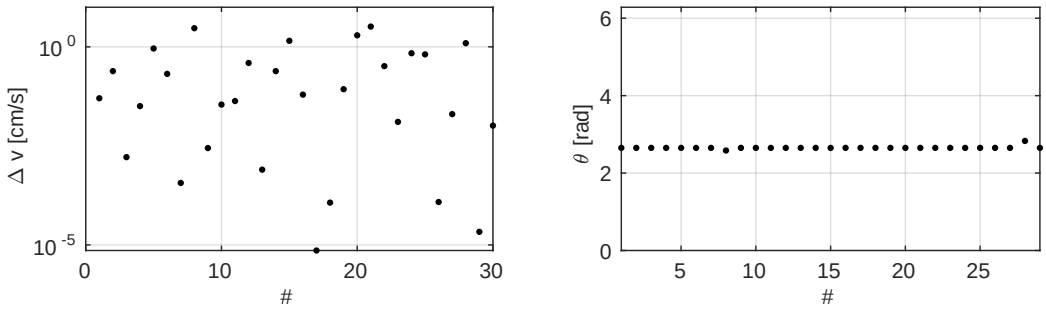

(a) **(b)**

Figure 5.4: Station-keeping manoeuvre history for the orbit in Fig. 5.3. The (a) magnitude and (b) in-plane direction is given for each manoeuvre.

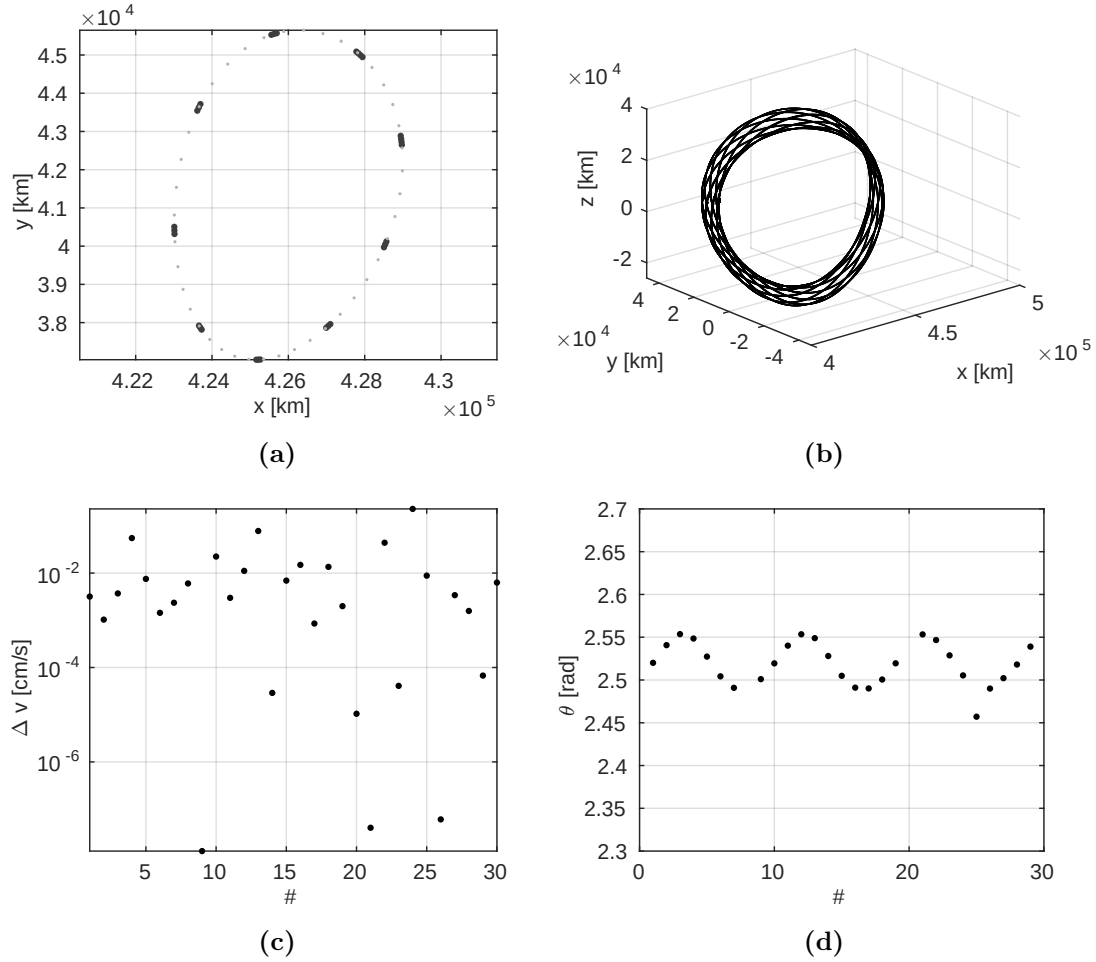

Figure 5.5: Trajectory extension for a quasi-periodic quasi-halo orbit with $C = 3.1180$. (a) Return map on the x-y plane for an initial state on a periodic orbit and (b) the trajectory. Station-keeping manoeuvres are visualised by their (c) magnitude and (d) direction.

mode aiming for a cancellation of the unstable component.

Example for a quasi-periodic orbit

The station-keeping method for quasi-periodic orbits is the same as for the periodic example shown above. The periodic and quasi-periodic case differ only in the return map on the x-y plane which is now described as invariant curve instead of a point as for the periodic case. This means that the optimal-station keeping direction varies depending on the return direction on the invariant curve. Fig. 5.5 and Fig. 5.6 show the locations of the crossings on the x-y plane. For this purpose multiple crossing are evaluated to extend the orbit for a one year lifetime.

The station-keeping is applied to two families of quasi-periodic orbits with an energy

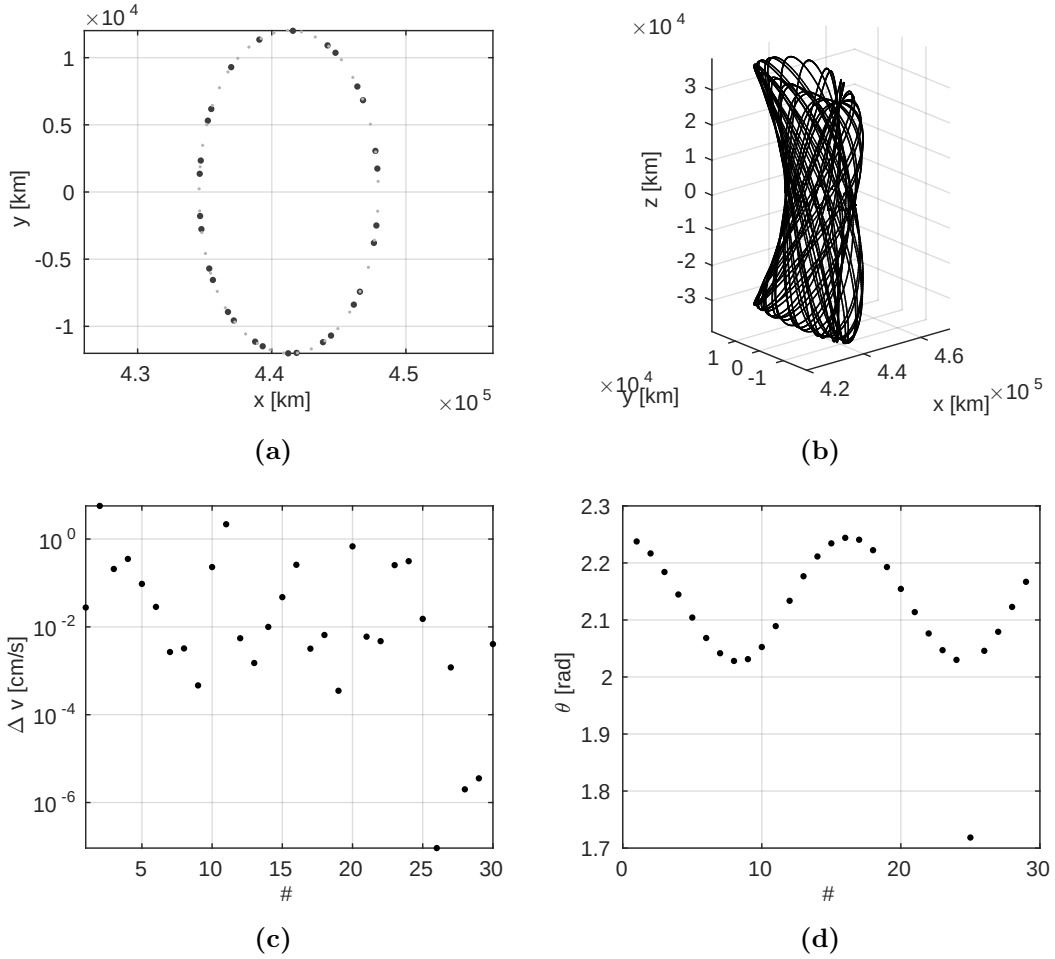

Figure 5.6: Trajectory extension for a quasi-periodic lissajous orbit with $C = 3.1411$. (a) Return map on the x-y plane for an initial state on a periodic orbit and (b) the trajectory. Station-keeping manoeuvres are visualised by their (c) magnitude and (d) direction.

$E = -\frac{C}{2} = -1.559$. Quasi-periodic orbit families share the same orbital energy but differ in the rotation number ρ. The manoeuvre magnitude is below $0.1\,\frac{mm}{s}$ for all cases having only the purpose to cancel out the numerical error. Fig. 5.5a shows the locations of the crossings on the x-y plane. The bold markers are the returning points after each station-keeping manoeuvre. The grey (dotted) rings present the centre manifold structure around the initial state vector. The maintenance effort in terms of Δv is determined for the quasi-periodic orbit with $C = 3.1180$. Here, multiple station-keeping manoeuvres are implemented leading to an orbital lifetime of about one year. For two cases the corresponding trajectories are plotted in Fig. 5.5b and Fig. 5.6b.

5.2.2 Extension algorithm for orbital families

In the circular restricted three-body problem, quasi-periodic orbits occur in families, and for a certain value of the Jacobian there are a variety of orbits. These families of quasi-periodic orbits might be described by a Poincaré section at the x-y plane. In Chap. 4 a method is introduced to compute the families of the quasi-periodic orbits. In the following an algorithm is described to generate families of quasi-periodic orbits without calculating the invariant curves and assuring the invariance condition.

The previously introduced station-keeping method allows for a calculation of consecutive crossings on the x-y plane. Assuming that sufficient crossings are evaluated the invariant curve is accuracy modelled giving a picture of the orbit. Once a single solution is identified, a hopping strategy is required to get the initial condition for the next run leading to the introduction of a continuation parameter.

The extension algorithm consists of the following steps:

1. Take a point $\boldsymbol{f}^n$ along the nominal orbit.
2. Optimise and apply station-keeping manoeuvre to extend the trajectory for two x-y plane crossings.
3. The state vector $\boldsymbol{f}^{n+1}$ at this crossing is the next centre manifold location.
4. Take this new state vector and continue with step 2 and 3 until enough points are calculated to picture the invariant curve.
5. Attenuate the state vector $\boldsymbol{f}^{,} = \boldsymbol{f}^n + (\Delta x, \Delta y, 0, 0, 0, 0)$ and continue with step 2 to 4.
6. The extension algorithm is either stopped once the optimisation fails to converge converge in step 2 or the desired extent of the orbital family is achieved.

The novelty here is the simplicity of the algorithm to generate quasi-periodic orbit families in different dynamical frameworks without extensively implementing the matrix operations as introduced in Chap. 4. This algorithm is a major contribution of this work and can be applied to any orbit in the three-body problem. The only requirement as for the station-keeping is that the orbits possess centre components and an unstable behaviour.

Fig. 5.7 shows the results of the continuation process for a family of quasi-halo and Lissajous orbits. Each dot in the figure corresponds to a x-y plane crossing. Circular patterns can be recognised, if multiple return are determined. Each of these circular sets belong to one quasi-periodic solution.

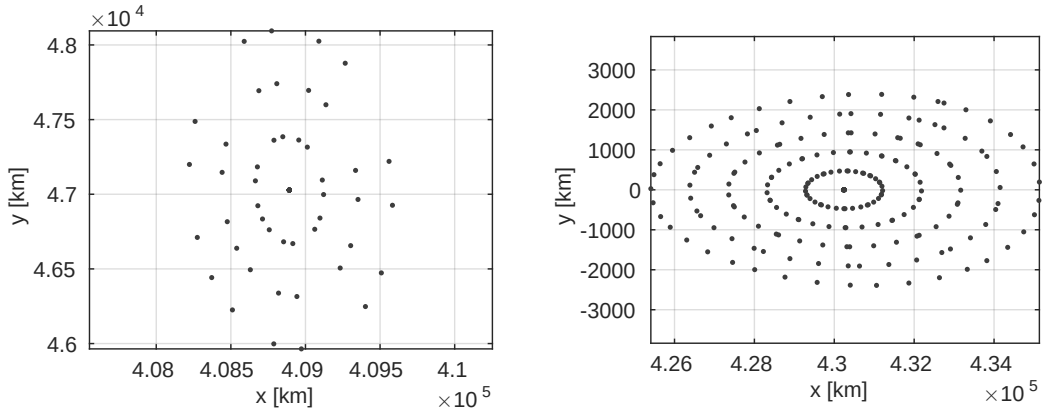

(a) **(b)**

Figure 5.7: Continuation of quasi-periodic orbit families. (b) Solution for a family of quasi-periodic Northern halo orbits. (b) Solution for a family of vertical Lyapunov orbits.

5.3 Application to the full planetary ephemeris problem

Previously, the orbit generation was studied for an autonomous dynamical system. Advantage of the circular restricted three-body problem is that there is no dependency on the epoch nor on variations of the distance between Earth and Moon. This is not the case once an accurate position and velocity of the planets are considered in the dynamical modelling. To cope with this new circumstances, the station-keeping process is redefined to apply it to a time-depended and more accurate dynamical model. The strategy is to control the unstable character by means of discrete thrust impulses remains identical.

5.3.1 Station-keeping methodology

The station-keeping in the full planetary model is straightforward, the difference to the algorithm introduced in Sec. 5.2.2 is the handling of the boundary conditions within the propagation. A coordinate transformation is required as the positions and velocities are required in the rotating reference frame where the boundaries are defined. Starting from an initial state that lies on the x-y plane at a given epoch the transformation of coordinates is applied, the optimal manoeuvre is calculated.

The trajectory is integrated in the heliocentric MEE2000 frame. After each integration step, the position of the spacecraft is transformed into the rotating reference frame and the boundary conditions are evaluated. The boundary condition constrains the final distance from L_2 and prevents the trajectory from escaping.

In the previous section for each station-keeping manoeuvre the direction and magnitude were coming from optimisation. The results showed a constant well defined value for the optimal manoeuvre direction. This result allows one to exclude this information in the optimisation, leaving the magnitude as only parameter. The key outcome of this study is the identification of an optimal manoeuvre direction that pushes the spacecraft towards the invariant stable or unstable manifolds. For the determination of this optimal manoeuvre directions, the manoeuvre magnitude is set to $10^{-3}\,LU$. Forward (unstable) or backward (stable) propagation is required in the lifetime assessment.

Three options are considered to handle the directional orientation of the velocity increment, which are:

1. An analytic linear direction obtained from the linear Lissajous motion.
2. A mean manoeuvre direction ψ.
3. A precise varying direction for quasi-periodic orbits.

Evaluation of the manoeuvre directions

The optimisation results in this study for the halo orbit family are shown for an escape towards the stable (red) and unstable (blue) hyperbolic manifold, see Fig. 5.9 and Fig. 5.10. The results plotted with thin markers correspond to the x and y components of the position vectors determined by Floquet subspaces (Gómez et al. [1998]). The discrepancies between the Floquet mode approach and the station-keeping algorithm proposed in this chapter increase with growing orbital amplitudes. The explanation for this is the linearisation that is required for the Floquet approach. Fig. 5.8 highlights the identified dominant manoeuvre direction for the halo orbit family with parameters.

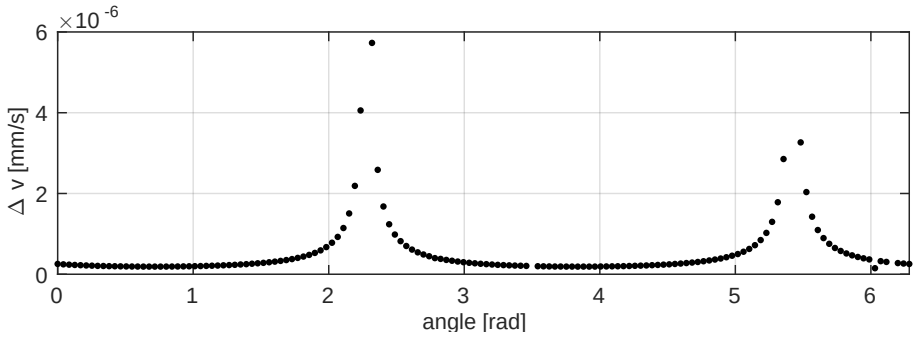

Figure 5.8: Parametric evaluation of the relation between the manoeuvre magnitude and direction.

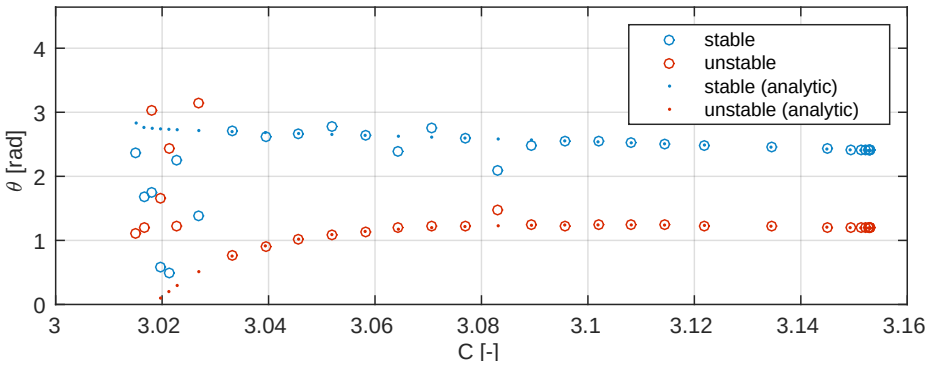

Figure 5.9: Comparison of optimal manoeuvre directions with results obtained from Floquet subspaces, evaluated for the Northern halo orbit family for an escape towards the stable (red) and unstable (blue) hyperbolic manifold.

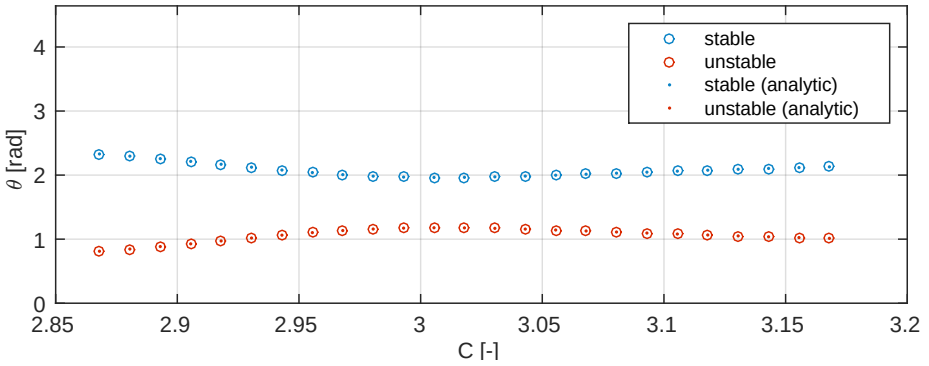

Figure 5.10: Comparison of optimal manoeuvre directions with results obtained from Floquet subspaces, evaluated for the vertical Lyapunov orbit family for an escape towards the stable (red) and unstable (blue) hyperbolic manifold.

Optimisation with a pre-defined manoeuvre direction

The evaluation of the precise direction and magnitude of the station-keeping manoeuvre is time consuming, therefore the direction is pre-defined as the direction is predictable once the desired orbital properties are known. A differential evolution algorithm is used to search for solutions with minimum norm of the Δv manoeuvre. The parameters for the differential evolution algorithm are summarised in Tab. 5.2. The optimisation problem is stated as

$$\underset{\Delta v}{\text{maximise}} \quad J(\Delta v), \tag{5.5}$$

where the manoeuvre magnitude Δv is the only optimisation parameters. Eq. 5.5 is solved subject to the constraints defined in Eq. 5.1.

The initial state vector is assembled similar to Eq. 5.2 but accounting for the direction and magnitude instead of Cartesian vectors. Different objective functions are considered, which are:

1. The orbital lifetime $J = \max(T^+_{max})$.
2. The mean lifetime $J = \text{mean}(T^+_{max}, T^-_{max})$.
3. For a multi-objective optimisation $J_1 = \max(T^+_{max})$ and $J_2 = \min(\Delta v)$.

The quantities T^+_{max} and T^-_{max} are propagated and evaluated

$$\boldsymbol{f}_{T^+_{max}} = \boldsymbol{\Phi}_{\pm\tau_{max}}\left(\boldsymbol{x}\left(\Delta v\right)\right), \tag{5.6}$$

where $\boldsymbol{\Phi}_{\pm\tau_{max}}$ denotes the propagation. The objective functions are assessed yielding the optimal station-keeping manoeuvres, for the multi-objective case a solution on the Pareto front is chosen representing a trade-off between the orbital lifetime and the manoeuvre magnitude.

Name	constant	range min. value	range max. value
Generations	200		
Population	20		
CR	0.5		
F	0.8		
Δv		$-10^{-4}\,\frac{LU}{TU}$	$10^{-4}\,\frac{LU}{TU}$

Table 5.2: Optimisation parameters for the maximisation of the orbital lifetime.

Comparison of the different station-keeping strategies

The three different station-keeping strategies are applied to a quasi-periodic orbit. The results of the station-keeping process in the general case are very similar to the ones for the circular restricted three-body problem. The station-keeping is applied to one quasi-periodic orbit with an energy of $E = -C/2 = -1.5313$. The velocity corrections on each correction point are shown Fig. 5.11. Applying a precise manoeuvre direction depending on the return angle leads to similar manoeuvre magnitudes. When applying a mean manoeuvre direction the range of the magnitude is larger.

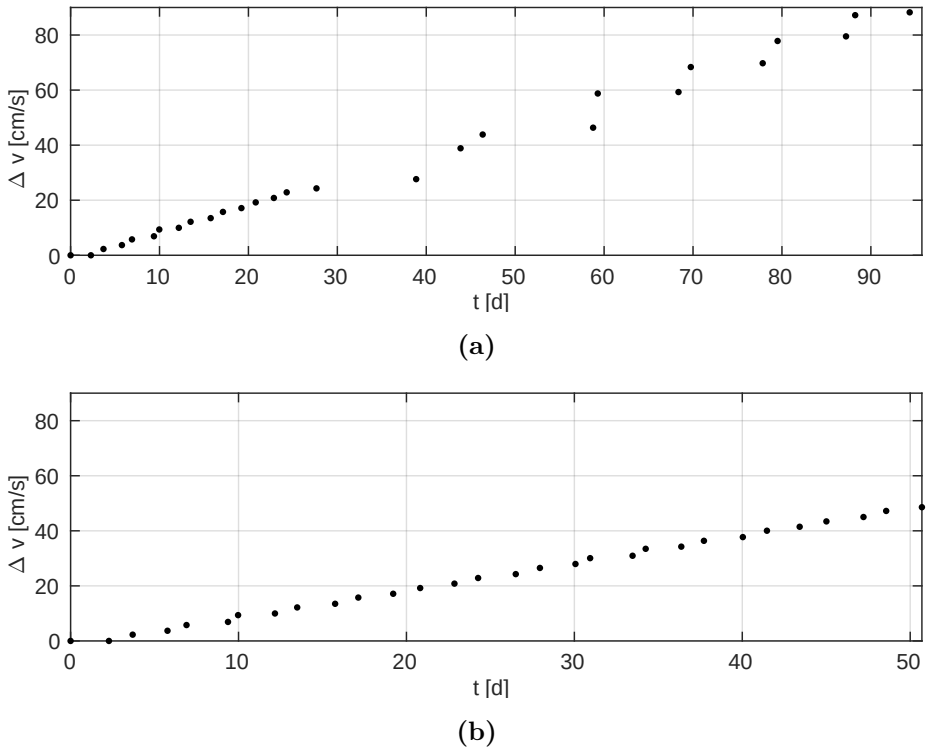

Figure 5.11: Station-keeping costs for three different strategies for the evaluation of the manoeuvre direction. (a) Mean manoeuvre direction. (b) Precise direction varying depending on the return angle.

5.4 Summary

This chapter presented a method to generate quasi-periodic orbits in the framework of an ephemeris based dynamical model by maintaining the orbit for long durations. This method used manoeuvres to compensate for perturbations either introduced by gravitational forces or errors in numerical propagations. The advantage of this proposed method was that there is no need to evaluate the finite arithmetic as developed in Chap. 4. A similar methodology is already applied in the past utilising a linearisation of the equations of motion (Hechler [2002]). For periodic orbits dominant manoeuvre directions can be determined by the eigenvectors of the monodromy matrix, see Simo et al. [1987]. The method proposed in this thesis takes this idea and expands it by taking into account amplitudes and frequencies of quasi-periodic motion. The presented method is a powerful tool to generate quasi-periodic orbit families in different dynamical frameworks without extensively implementing the matrix operations introduced in Chap. 4. Another constraint that was introduced is to identify station-keeping manoeuvres in such a way that orbital properties are maintained. The only requirement as for the station-keeping was that the orbits possess centre components and an unstable behaviour. Apart from the determination of quasi-periodic orbit families, the algorithm can be applied to develop station-keeping algorithms. First studies show that the station-keeping budget is significantly reduced once the direction of manoeuvres is taken into account. Under the assumption that the orbital parameters are known, a pre-defined manoeuvre direction can be determined. This enables an optimisation with a single parameter, the manoeuvre magnitude. A study showed that the assumption of a mean manoeuvre direction is valid and reduces the computational costs significantly.

CHAPTER 6

Transfer options between quasi-periodic orbits

The preceding chapters treated fundamental aspects of quasi-periodic motion and techniques were proposed to create quasi-periodic orbits in different dynamical frameworks. Since libration point and distant retrograde orbits reside together in the lunar vicinity and each orbit possesses characteristic properties, transfers among them are of special interest. A method for the construction of optimal orbital transfers from one orbit to another is proposed in this chapter. Since the circular restricted three-body problem provides useful tools for the design of transfers this formulation of the dynamics is utilised, but results are presented for the full ephemeris model, too. Orbit-to-orbit transfers are optimised for several scenarios and parameters influencing the solution, e.g. transfer costs, are investigated.

6.1 Orbit-to-orbit transfer and manoeuvre design

Transfers are now studied among a wide range of orbits whose properties were assessed in Chap. 4. The focus is set on transfers that utilise the hyperbolic invariant manifold, with the benefit that the transfer comprise of an individual manoeuvre at departure and an asymptotic approach to the final orbit. The idea is to construct transfers by connecting the initial and final orbit by coast phases along the unstable and stable invariant manifold branches, therefore utilising the same effects as used for low energy transfers from Earth. The arrival and departure conditions are determined by the introduced phase angles, two are required per orbit. An additional parameter is the transfer time τ along the stable and unstable invariant manifold. The parametric representation of quasi-periodic orbits in Chap. 4 enables to use predefined locations on departure or arrival orbits depending on the phases α and β as in other studies (Yárnoz et al. [2013], Marsden and Ross [2005]).

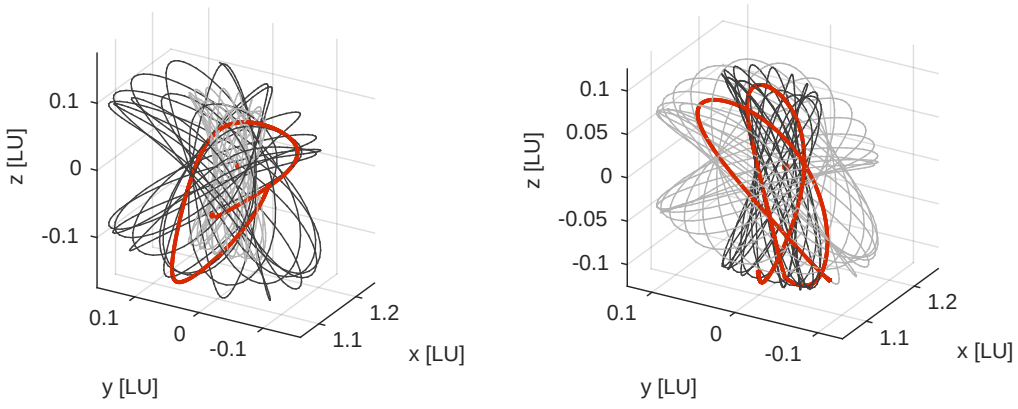

Figure 6.1: The transfer trajectories in the synodic reference frame connect the final (black) and initial (grey) orbit. (a) For a single-manoeuvre transfer utilising the coasting phase along the stable manifold to the final orbit. (b) For a single-manoeuvre transfer utilising both, the coasting phase (red) along the stable and unstable manifold to the final orbit.

Transfers from either periodic or quasi-periodic orbits to other orbits of this type are investigated. Those transfers are relevant from a mission design perspective, used to change the operational orbit or re-phase spacecraft on their orbit. Depending on the combination of initial and final orbit, the transfer changes the properties of the trajectories. Only the location of the spacecraft along its path is changes, if final and initial orbit are the same. Compared to other studies (Gómez et al. [2004], Davis [2009]) there is no constrained posed on the Jacobian constant of the initial and final orbit.

When introducing orbit-to-orbit transfers the following options exist:

- One-manoeuvre transfers utilising stable hyperbolic invariant manifolds to arrive at the final orbit. The result is that a manoeuvre is conducted at time t, and after the velocity change the spacecraft continues its path along a stable manifold leading to the target orbit, see Fig. 6.1a.
- One-manoeuvre transfers utilising unstable hyperbolic invariant manifolds to leave the initial orbit. The conducted manoeuvre sets the spacecraft onto a stable hyperbolic invariant manifold to arrive at the final orbit, see Fig. 6.1b.

A method is proposed in the following for both types of transfers. Before utilising the unique properties of unstable quasi-periodic orbits to design orbit-to-orbit transfers, the accessibility of the libration point and lunar regions from Earth orbit is investigated. The proposed methods thoroughly and reliably explores the space of orbit-to-orbit transfers.

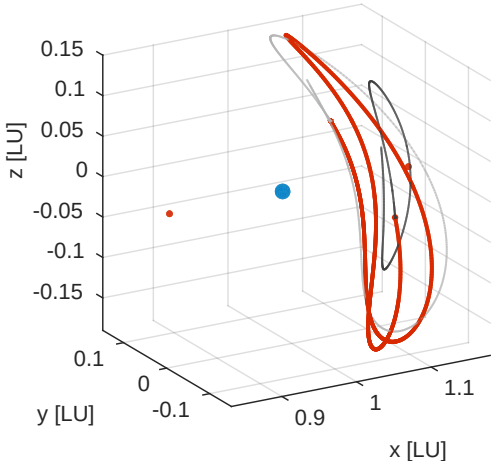

Figure 6.2: Transfer trajectory in the rotating reference frame. The transfer trajectory (red) connects the initial (black) orbit with the targeted one (grey).

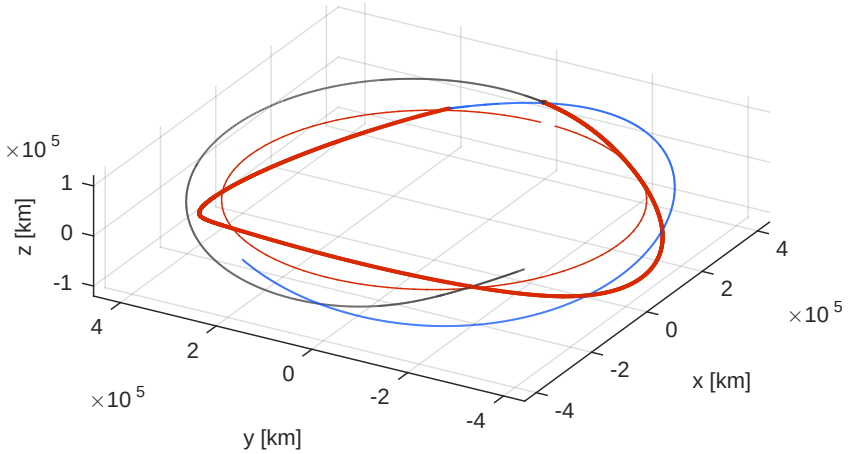

Figure 6.3: Transfer trajectory in the inertial reference frame. The transfer trajectory (red) connects the initial (black) orbit with the targeted one (blue). Trajectory of the Moon is plotted (light red) for a better orientation.

Fig. 6.2 and Fig. 6.3 show the trajectories in the inertial and rotating reference frame of such a transfer. This method offers lower Δv expenses for the transfer compared to two-impulse transfer arcs. The benefit of one-manoeuvre transfers is on the one side the complexity of operations and at the same time this technique will reduce the associated costs. The spacecraft will be transferred to another orbit of interest of the mission.

The following sections outlines the procedure that combines the parametric representation of the orbit with the ones of the manifolds. The orbits and their stable manifolds are represented by discrete parametric functions.

6.1.1 Accessibility of libration point regions from Low Earth Orbit

The comparison of orbit-to-orbit transfers requires a common origin, which, here, is an Earth departure from a Low Earth Orbit (LEO). The transfer optimisation is conducted in the full ephemeris model accounting for the launch dependencies on the actual geometry of the orbit epoch and phases. The Earth departure from LEO is defined with an apogee and perigee altitude $h_a = h_p = 400\,km$, with an inclination fixed at 51.7 deg. At the appropriate time, the spacecraft performs a major manoeuvre of about 3.2 $\frac{km}{s}$. This injects the spacecraft onto a transfer trajectory. The construction point for quasi-periodic orbits is ideally used as target location in the vicinity of the Moon. At this location the motion is perpendicular to the x-z plane and the $\dot{y}$ component is zero.

The most obvious way to transfer from Earth to the lunar vicinity is to use a classical Hohmann like direct transfer or pro-grade and retro-grade gravity assisted transfers. The insertion would then occur tangentially at the x-z plane crossing providing a low Δv opportunity. The arrival phases are studied in detail for a range of quasi-halo orbits. Fig. 6.6 shows the variations in the transfer Δv caused by the arrival phase of the orbit and the departure epoch. The time of flight increased from 5 to 7 days. Another form include flyby geometries at the Moon to reduce the transfer costs. For the flyby geometries at the Moon the minimal flyby distance above the surface of the Moon is $100\,km$. The flyby method offers remarkable energy savings compared to the direct Hohmann like approach. Fig. 6.4 and Fig. 6.5 present direct and flyby transfer geometries for selected arrival orbits.

Due to the variation in the distance from the Earth to the Moon there are small

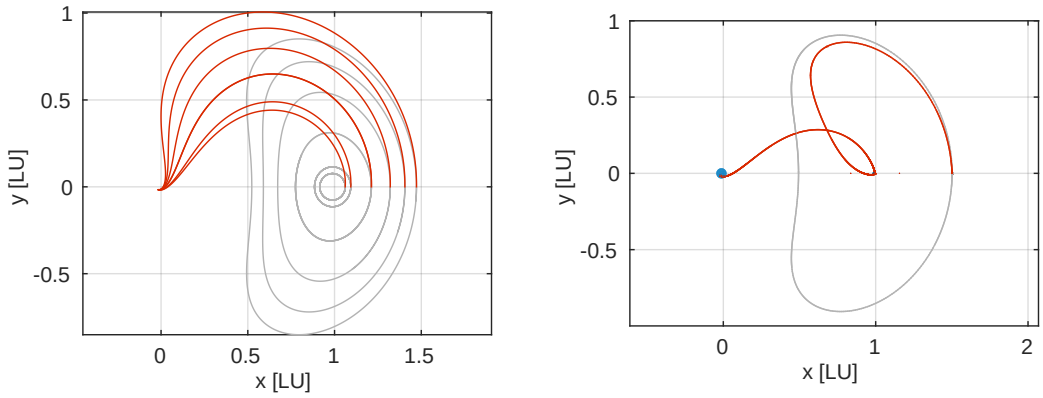

Figure 6.4: (a) Direct and (b) flyby transfers from Low Earth Orbit (LEO) to distant retrograde orbits (grey trajectories). The transfer arcs are shown in red.

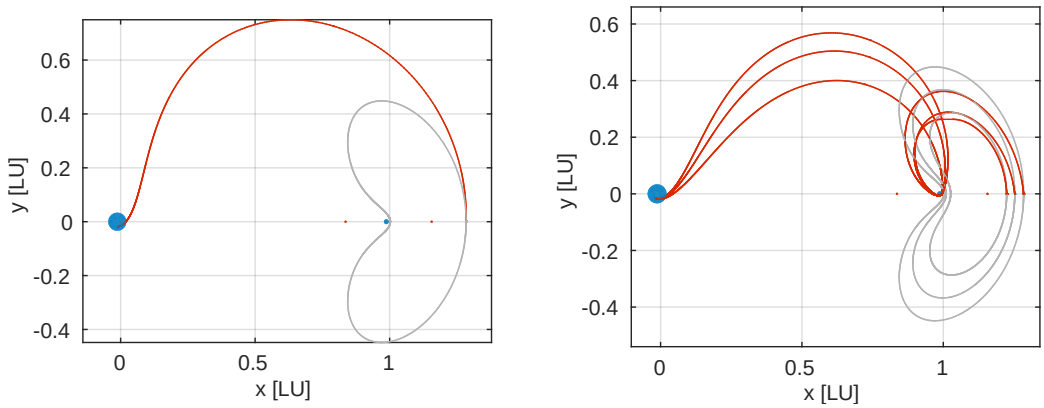

Figure 6.5: (a) Direct and (b) flyby transfers from Low Earth Orbit (LEO) to libration point orbits (grey). The transfer arcs are shown in red.

differences between the dynamical ephemeris model and the circular restricted three-body problem. This causes an impact of the departure epoch on the transfer costs. Only very simple transfers are highlighted here, a more detailed description is available in literature, see Renk [2008].

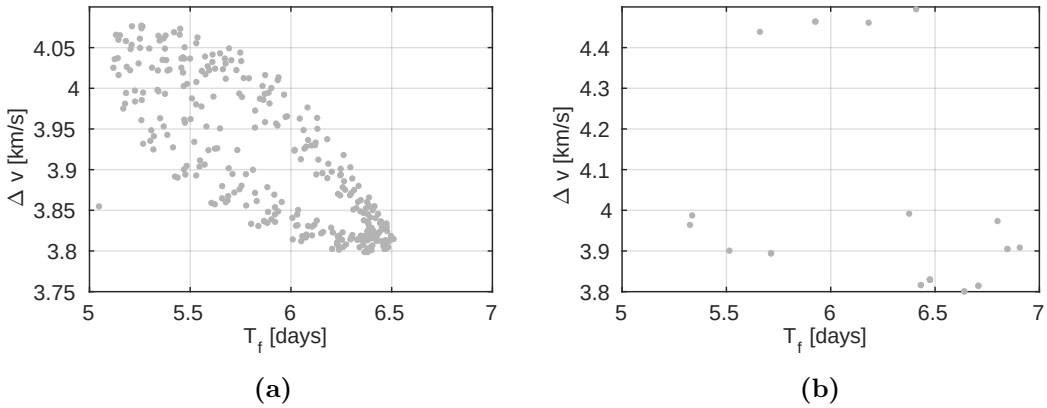

Figure 6.6: (a) Dependency of the transfer Δv on the launch epoch. (b) Impact of orbital phasing upon arrival on the transfer Δv.

6.1.2 Exclusion of lunar flybys

Orbits around L_1 and L_2 are close to the Moon and a spacecraft theoretically could use a considerable change of the velocity and energy of the spacecraft introduced by a lunar flyby. This behaviour is excluded in the following transfers. Numerically the exclusion is realised during propagation by a sphere around the Moon as stopping condition. In most of the cases, the exclusion radius is defined as $r = 0.001\,LU$.

6.1.3 Identification of feasible transfer parameter sets

The use of the hyperbolic invariant manifold increases the number of parameters to be determined by the optimisation process. This causes a heavier computational effort than in the case of periodic orbits, but on the other side it gives additional possibilities for the transfer. Additional phases allow for a wide range of possibilities to connect the two orbits. The parameters strongly depend on each other and islands of local minima exist. Therefore, it is critical to identify and carefully select the initial conditions. A differential evolution method is used to identify the initial conditions. In order to get a continuous transfer trajectory, the determined initial conditions are refined by a gradient-based optimisation method.

The location of the spacecraft at arrival and departure are evaluated with the help of the parametric function $\boldsymbol{u}$. This enables the use of α and β as optimisation variables without numerical integration of the final trajectory. The initial and target locations of the spacecraft on a quasi-periodic trajectory are represented by four angular coordinates α^i, β^i, α^f and β^f. The following two functions are used to calculate feasible regions of the five-dimensional solution space. The function subject to minimisation for the transfer case with one transfer arc along the unstable manifold is

$$\boldsymbol{f}_1 = \boldsymbol{u}\left(\alpha^i,\, \beta^i\right) - \boldsymbol{\Phi}_{-\tau_1}\left(\boldsymbol{u}\left(\alpha^f,\, \beta^f\right) + \epsilon\psi\left(\alpha^f,\, \beta^f\right)\right), \tag{6.1}$$

where $\boldsymbol{u}$ is the parametric function for the orbit, ϵ defines the offset to initiate the path onto the manifold branches, see Eq. 3.31. The time that is required to reach a particular location on the manifold relative to the original orbit is defined as τ_1. The vector field $\boldsymbol{\Phi}_{-\tau_1}$ denotes the backward propagation along the stable invariant manifold.

The function for the case with two transfer arcs, with one on the stable and the other one on the unstable manifold branch, is defined as

$$\boldsymbol{f}_2 = \boldsymbol{\Phi}_{\tau_1}\left(\boldsymbol{u}\left(\alpha^i,\, \beta^i\right) + \epsilon\psi\left(\alpha^i,\, \beta^i\right)\right) - \boldsymbol{\Phi}_{-\tau_2}\left(\boldsymbol{u}\left(\alpha^f,\, \beta^f\right) + \epsilon\psi\left(\alpha^f,\, \beta^f\right)\right). \tag{6.2}$$

The distance $\delta x = \sqrt{f^{1^2} + f^{2^2} + f^{3^2}}$ is an indicator for the feasibility of the solution, and the velocity offset $\Delta v = \sqrt{f^{4^2} + f^{5^2} + f^{6^2}}$ is a first approximation of the expected Δv budget. The results obtained by the initial search might contain a gap between the transfer arcs. As long as this gap is within some limits, it is later removed in the optimisation using a gradient-based method. The main task of this first step is the identification of feasible transfer sets for the phases and transfer times that serve as initial guess. The aim is to find a favourable insertion point on the quasi-periodic orbit satisfying all constraints.

Before the optimisation is initialised a consolidated guess is required for the phases and transfer times. This is achieved by a differential evolution algorithm. The transfer construction process starts with the determination of feasible parameter combinations. Instead of using numerical propagation, state vectors on the quasi-periodic orbit are obtained by using the analytic function $\boldsymbol{u}$ that describes a quasi-periodic orbit, see Eq. 4.3.

The optimisation problem is stated as

$$\underset{\alpha^i,\beta^i,\alpha^f,\beta^f,\tau,l}{\text{minimise}} \quad J(\alpha^i,\beta^i,\alpha^f,\beta^f,\tau_1,l), \tag{6.3}$$

where α^i and β^i are the phase angles on the initial orbit. The phase angles of the target orbit are α^f and β^f. The transfer time along hyperbolic invariant manifold branch is defined as τ_1. The value $l \in \{-1, 1\}$ is a switch function to specify the hyperbolic invariant manifold branch. The domain of the optimisation variables is defined in Tab. 6.1.

Two options for the cost function and constraint handling are considered:

1. Minimisation of the distance δx with no constraint imposed on the Δv.
2. Multi-objective optimisation with $J_1 = \Delta v$ and $J_2 = \delta x$.

The entire set of feasible transfers, with their parameter sets (α^i, β^i, α^f, β^f, τ_1, l, $\delta x, \Delta v$) are evaluated. The corresponding values for $\boldsymbol{f}_1$ and $\boldsymbol{f}_2$ are calculated. The results are shown in Fig. 6.7 and Fig. 6.8 for a scenario with the function f_1. The corresponding Δv for the transfers are plotted in Fig. 6.8a and Fig. 6.8b. A first filter constraints the position and velocity offset to $3000\,km$ and $200\,\frac{m}{s}$ threshold. With this filter solutions are selected that potentially converge at the optimisation step. The next step is to identify similar islands within the parameter sets. In order to find the optimal time for such a transfer, the optimal final phases on the quasi-periodic orbit after the transfer are evaluated, see Fig. 6.8b.

Name	constant	range min. value	range max. value
Generations	200		
Population	20		
CR	0.5		
F	0.8		
α^i		0	2π
β^i		0	2π
α^f		0	2π
β^f		0	2π
τ_1, τ_2		0	10
l		-1	1

Table 6.1: Optimisation parameters for the determination of orbital transfers among quasi-periodic orbits.

This pre-optimisation and filtering gives reasonably good approximations of the feasible parameters that are used in the optimisation. Note that the use of the parametric functions $\boldsymbol{u}(\alpha, \beta)$ and $\boldsymbol{u}(\alpha, \beta, \tau_1)$ are only approximations intended for the pruning of the infeasible sets and retaining the feasible ones.

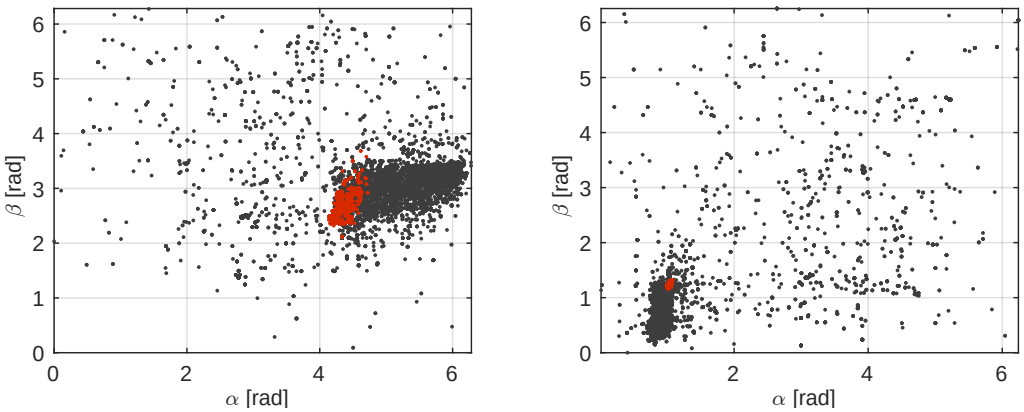

(a) **(b)**

Figure 6.7: Results of the initialisation with initial and final orbit parameter sets. Each black dot corresponds to an evaluated set. Filtered feasible transfer sets (red) with corresponding (a) position and (b) velocity offsets.

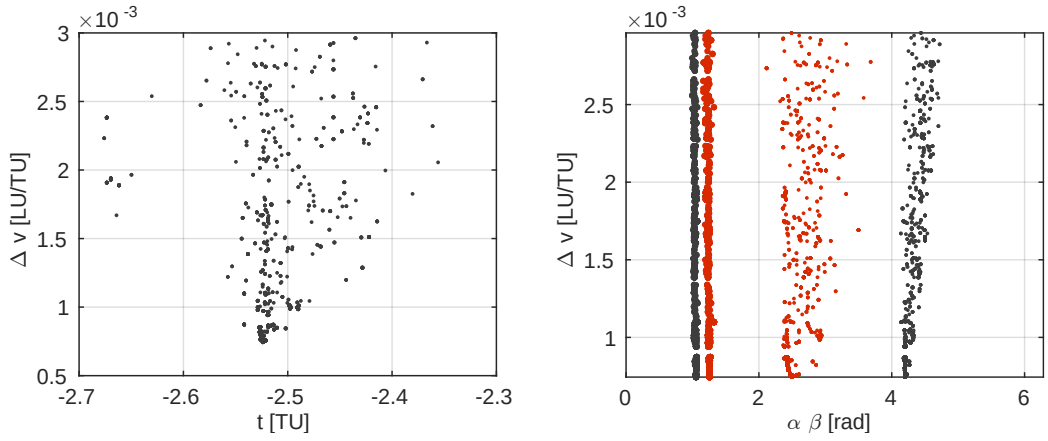

Figure 6.8: Results of the initialisation with initial and final orbit parameter sets. Each dot corresponds to an evaluated set. (a) Dependency of the transfer time and the Δv. (b) Dependency of the initial (red) and final (black) phases on the Δv.

6.1.4 Formulation of the transfer optimisation

Once a feasible transfer set is identified, a gradient-based optimisation is finally used to construct a continuous transfer arc. The problem is formulated as a matching of a forward and a backward propagated arc with the initial and final phases generated by the guess generation. The manoeuvre is indirectly defined as the velocity offset at the end of both transfer arcs. The cost function is the magnitude of the first manoeuvre to set the spacecraft onto the transfer trajectory.

The optimisation problem can be stated as follows:

1. Determine an initial and final orbit.
2. Find a location on the orbits such that a departing stable manifold branch connects reaches the final orbit. This is achieved with the method proposed in Sec. 6.1.3.
3. Vary the initial and final phases, and the transfer time such that an optimal Δv is found, and a continuous transfer arc is created.

The optimisation problem is stated as

$$\underset{\alpha^i,\beta^i,\alpha^f,\beta^f,\tau,l}{\text{minimise}} \quad J(\alpha^i,\beta^i,\alpha^f,\beta^f,\tau,l), \tag{6.4}$$

where α^i and β^i are the phase angles on the initial orbit. The phase angles of the target orbit are α^f and β^f. The value τ defines the transfer time along hyperbolic invariant

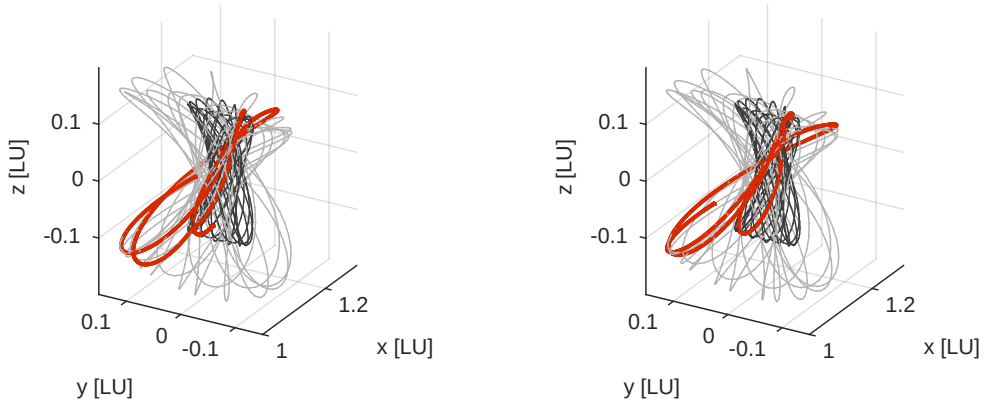

Figure 6.9: The transfer trajectories in the synodic reference frame connect the final (grey) and initial (black) orbit for a single-manoeuvre transfer utilising the coasting phase (red) along the stable manifold to the final orbit. (a) Converged and (b) non-converged solution.

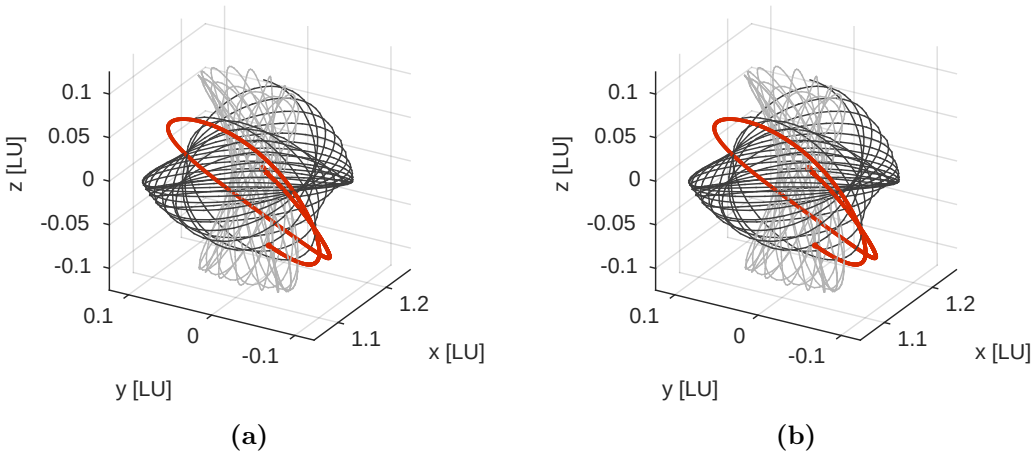

Figure 6.10: The transfer trajectories in the synodic reference frame connect the final (grey) and initial (black) orbit for a single-manoeuvre transfer utilising both, the coasting phase (red) along the stable and unstable manifold to the final orbit. (a) The initial non-converged and (b) the converged solution.

manifold branch. The value $l \in \{-1, 1\}$ is a switch function to specify the hyperbolic invariant manifold branch. The domain of the optimisation variables is defined in Tab. 6.1.

The cost function considers the Δv.

The outcome of the optimisation are locally optimal transfers, with associated arrival and departure conditions, the transfer time, and Δv expenses. Fig. 6.10a shows the unmatched trajectory, whereas the Fig. 6.10b highlights the converged solution.

The main purpose of the proposed method is to find the appropriate phase conditions for the departure and arrival location. The minimal cost transfer is only found, if the departure as well as the arrival phasing conditions are free parameters.

The method delivers orbital transfers within the region of the libration points without accepting flybys at the secondary body (Moon). Other scenarios are possible but not studied in this work, possible applications range from heteroclinic and homoclinic connections to the design of transfer arcs from the primary and secondary body to the orbit that is investigated.

6.1.5 Employing the full planetary dynamics

The study of transfers in the circular restricted three-body problem is the first step towards finding transfers in a full dynamical model. The orbit-to-orbit transfers are based on the dynamics of the circular restricted three-body problem. This is due to the fact that the time-independent property allows for a generalisation of the trajectories and invariant manifolds. In a final step the trajectories are transferred into an inertial reference frame and used in a patching process to find a continuous trajectory when the full dynamics is acting.

The computation scheme implemented in the previous section is employed to translate the transfer trajectories into a more precise model. The positions and velocities are mapped to inertial coordinates, taking the circular restricted three-body problem as initial guess, the aim is to find the a corresponding natural orbit in the full ephemeris model that has similar properties. For the numerical construction of transfer scenarios,

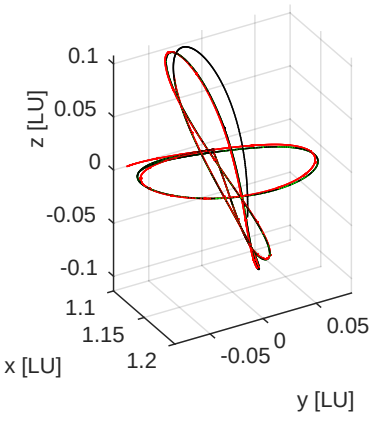

Figure 6.11: Overlay of the transfer trajectory calculated in the simplified dynamical model (black) and the accurate solution (red). Transfer trajectory from Lissajous to a periodic halo orbit as seen from Earth in the rotating frame ($\Delta v = 127.18\ \frac{m}{s}$).

employing full planetary dynamics, a patching is envisioned. The transition from the simplified dynamical model to the full planetary dynamics follows a two step approach. A first guess generation is obtained by a patching process aiming to find a very close solution the full transfer trajectory. Merely patching constraints are employed at this stage and no other constraints.

The following steps are required:

- The resulting trajectory is split into subintervals, and the time and states are defined at each point.
- Each state is then propagated for a time interval $t_{i+1} - t_i$ and when each trajectory segment matches with the consecutive one, a solution is found.

The matching conditions will not be fulfilled for the initial guess and in order to have trajectories without discontinuities a Newton procedure is employed to reduce the error. In the case of no additional constraints a minimum norm solution is found. Fig. 6.11 shows the trajectory in both dynamical systems.

6.2 Results

The method previously introduced is applied to a wide range of arrival and departure orbit combinations out of the family of orbits around the Earth-Moon far-side libration point L_2 and optimised transfers are presented. The dependency of the solution on the arrival and departure conditions and transfer times is studied.

The transfers converged during the optimisation, although they may not represent the global minimum in terms of the total Δv expenses. A transfer trajectory with lower costs may be achieved by allowing Moon flybys or propagating the manifolds for a longer duration.

6.2.1 One-manoeuvre transfers among quasi-periodic orbits

Trajectories will now be constructed to transfer spacecraft from halo orbits to their quasi-periodic extensions with larger out-of-plane and in-plane amplitudes. The extension orbits have the same Jacobian constant as the periodic halo orbit. The z amplitude of the initial orbits varies from $2.65 \cdot 10^4$ km to $8.32 \cdot 10^4$ km. Three transfer scenarios are discussed. For all three cases the transfer trajectories are plotted together with the arrival and departure orbits in Fig. 6.12. The optimised transfer trajectories are shown in the Earth-Moon rotating frame including the paths of the spacecraft before and after the transfer. The transfer arcs from the manoeuvre execution onwards until the asymptotic arrival at the final orbit are highlighted, the final trajectory and the initial

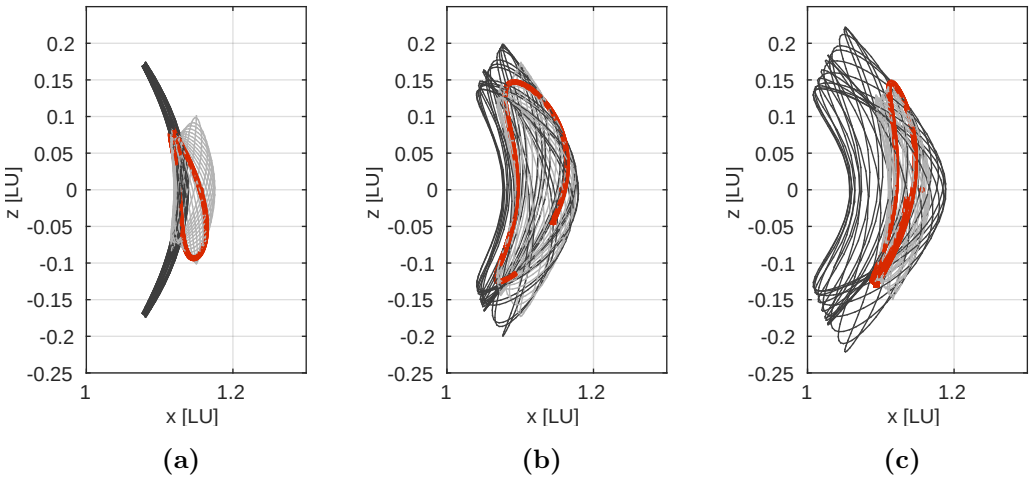

Figure 6.12: Transfers from an initial orbit (black) to an arrival orbit (grey). Transfer trajectories are shown in red. Parameters of the arrival and departure orbit and properties of the transfer trajectories are found in the text. The costs range from (a) $\Delta v = 38.93 \frac{m}{s}$ and (b) $\Delta v = 77.08 \frac{m}{s}$ to (c) $\Delta v = 107.86 \frac{m}{s}$.

one. The transfer duration for each case in Fig. 6.12 is (a) $t_f = 21.86$, (b) $t_f = 24.06$, and (c) $t_f = 23.52$ days. The costs range from $\Delta v = 38.93 \frac{m}{s}$, and $\Delta v = 77.08 \frac{m}{s}$ to $\Delta v = 107.86 \frac{m}{s}$.

Fig. 6.13 shows the Δv requirement to increase the in-plane and out-of-plane amplitudes from a halo orbit to their quasi-periodic orbits with the same Jacobian constant C. A quasi-periodic orbit with $C = 3.057$ and $\boldsymbol{\omega} = (1.57, 1.47)$ is chosen and the transfers are evaluated to orbits throughout the rest of the orbit family. Transfers do not exist for all cases, for some cases the stable invariant manifold branches do not intersect with the initial orbit and no solution can be determined. In those cases two-impulse transfers are required. With the selection of a set of quasi-periodic orbits, the design space can be accessed and transfers evaluated.

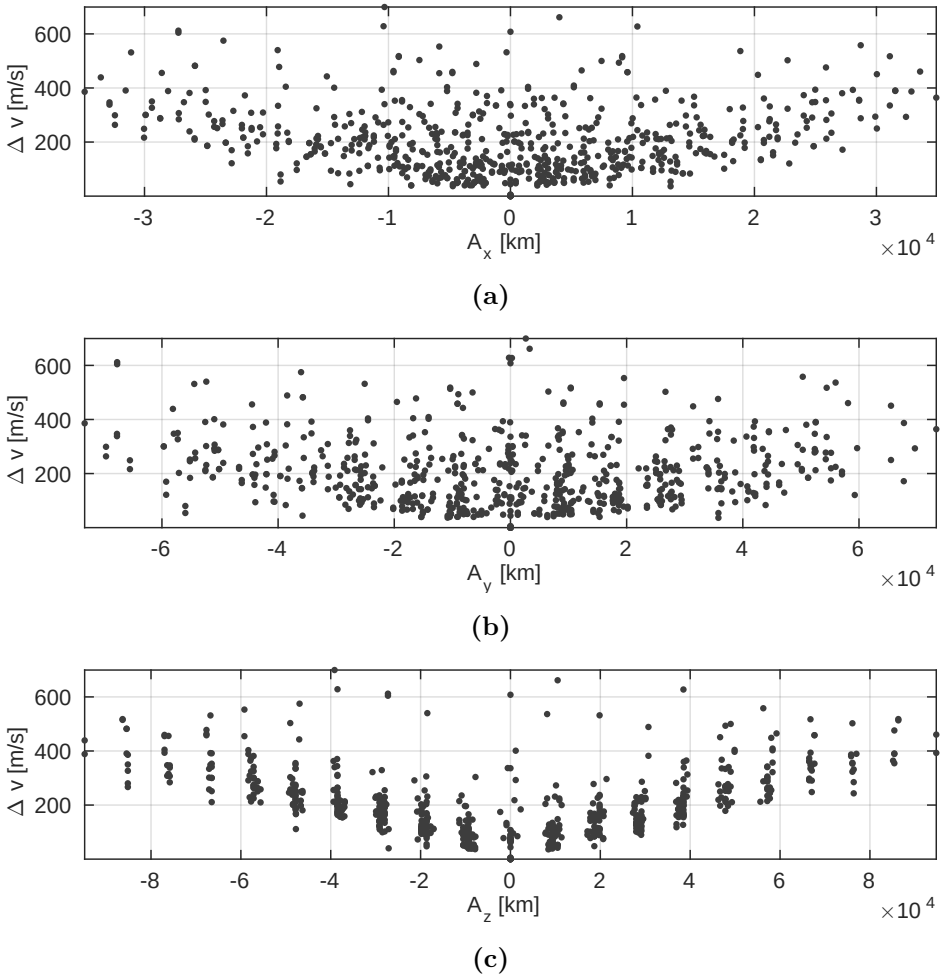

Figure 6.13: Costs of amplitude changes among quasi-periodic orbits. Summary of the Δv requirement to change (a) A_x, (b) A_y and (c) A_z.

6.3 Scenarios

The design of future European contributions to the exploration space transportation infrastructure will benefit from the flexible design of reference missions involving weakly bound destination orbits like distant periodic and libration point orbits. The flexibility of quasi-periodic orbits its amplitude as well as the transfer options open the possibility to combine the mission elements in order to adjust the system to the capabilities of the spacecraft and the objectives of the mission. It is straightforward to apply the knowledge gained in the previous sections to scenarios with the aim to obtain parametric analyses, figures of merit and establish realistic Δv budgets. The notation of each orbit in the scenarios is $g_i(\alpha, \beta)$, where the index i indicates different orbital parameters.

The elements of the journey and operations in the lunar vicinity are outlined here:

- Direct and linked transfer trajectories are addressed in the first scenario in Sec. 6.3.1. The journey starts with a transfer to an orbit around the libration point L_2, as outlined in Sec. 6.1.1 this can be accomplished easily by direct transfers or via lunar flybys. The mission objective is to enter a libration point orbit and loop around the libration point.
- In Sec. 6.3.2, the mission objective is to rendezvous with an uncrewed vehicle that has been placed in an halo orbit.
- The mission objective is to operate an uncrewed vehicle on the surface of the back side of the Moon, see Sec. 6.3.3.
- In Sec. 6.3.4, the mission objective is to create an outpost in a L_2 orbit serving as transportation node to support missions to and from lunar orbit and e.g. to the lunar surface.

6.3.1 Linked transfer combinations from Earth

The first scenario aims to find transfer combinations that offer cheaper access to certain orbits than directly from Low Earth Orbit. The conceptual idea of manoeuvring from one orbit to the other with a one-manoeuvre strategy is explained previously, see Sec. 6. Apart from the obvious in finding an orbital transfer consisting of a Low Earth Orbit to Earth-Moon L_2 transfer plus intermediate orbit to orbit transfers with a cheaper Δv than a direct Earth to final orbit transfer, the flexibility in splitting a transfer in several arcs offer potentialities and possibly increases e.g. launch windows and ground station visibilities.

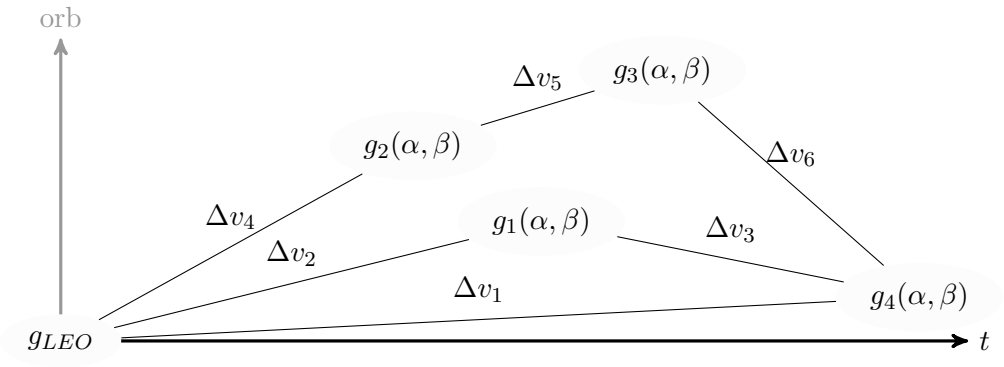

Figure 6.14: Visualisation of three different transfer scenarios. The orbit g_{LEO} represents the origin being a Low Earth Orbit. Options are a direct, 1-stage, and 2-stage transfer.

The schematic picture in Fig. 6.14 shows three solutions to arrive at a target orbit g_{LEO}. The first one is a direct insertion with Δv_1, the second solution results in a $\Delta v = \Delta v_2 + \Delta v_3$ with one intermediate stage at Earth-Moon L_2 orbits g_1. The third solutions utilises two intermediate stages at g_2 and g_3 with a $\Delta v = \Delta v_4 + \Delta v_5 + \Delta v_6$. Note, that the direct transfer option excludes flybys and do not guarantee optimal and cost efficient transfers.

The first step is the evaluation of the transfer costs for each orbit from Low Earth Orbit. Due to the exponential rising combinations and its associated high computational effort, a pre-selection of orbits is favoured. Here, a small set of 100 potential orbits is selected, which includes quasi-periodic Lissajous orbits. The resulting Δv requirement is as seen in Fig. 6.15. The rotation number of the selected orbits is plotted on the abscissa as an orbit identifier.

Fig. 6.16 enables one to choose transfers leading to an overall transfer scenario from an origin to a target orbit. The two start and end point of the solid line segments

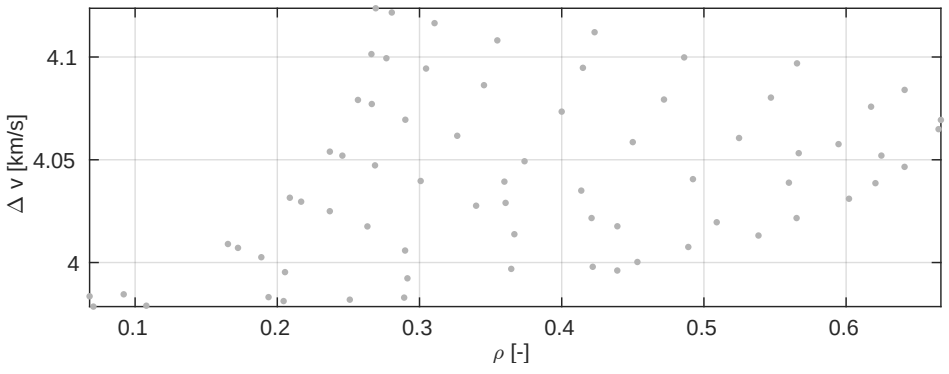

Figure 6.15: Costs associated with a direct transfers from LEO to the Earth-Moon libration point (L_2) orbits and its dependency on the orbital parameter ρ.

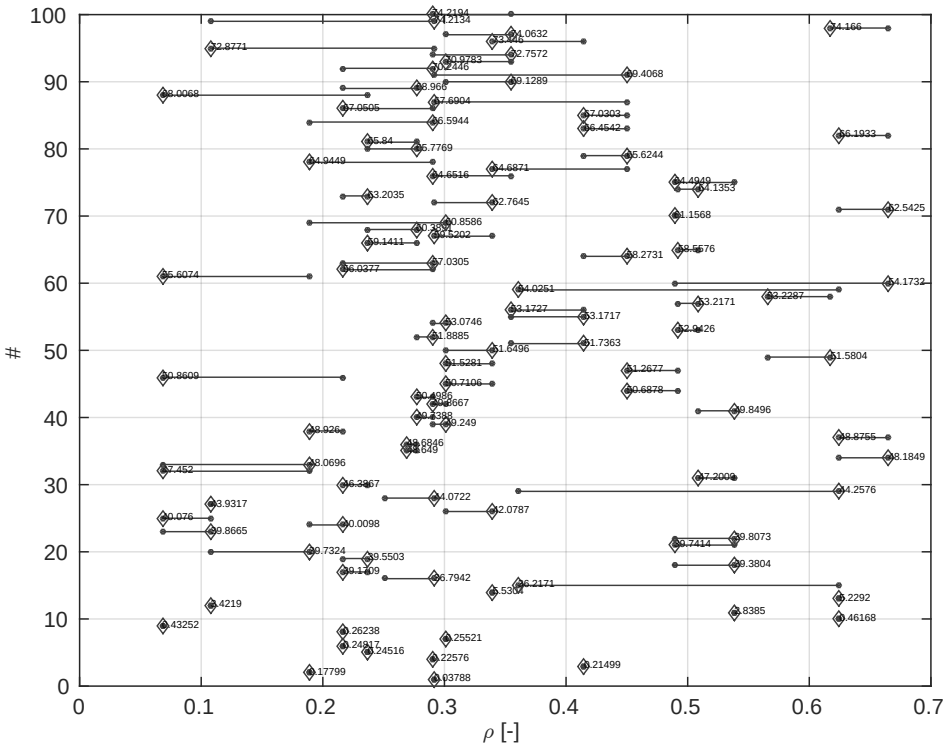

Figure 6.16: Orbit to orbit transfers (the hashtag is the transfer identifier) between selected orbits, orbit identifier is ρ. The transfers are sorted in ascending order according to the Δv demand. The number next to the diamonds is the Δv in $\frac{m}{s}$.

represent the orbital properties of the initial and final quasi-periodic orbit. Each line segment possesses a label indicating the Δv of the transfer in $\frac{m}{s}$. The diamonds show the original orbit and the location where the manoeuvre is applied. The dot connected with a line segment indicates the target orbit, which is reached asymptotically. The length of the line segment does not represent the length of the transfer, but the change of the orbital parameters. Fig. 6.17 shows the Δv demand for transfer combinations with one orbit-to-orbit transfer within the overall sequence.

For this particular selection of 100 orbits, the results yields no one-stage transfer combination is cheaper than launching from Low Earth Orbit directly into the final orbit. In some cases a transfer costs less Δv, if an intermediate orbit is targeted. The same parameter study can be conducted to find transfers between different types of orbit, e.g. a Lissajous and a Northern halo orbit.

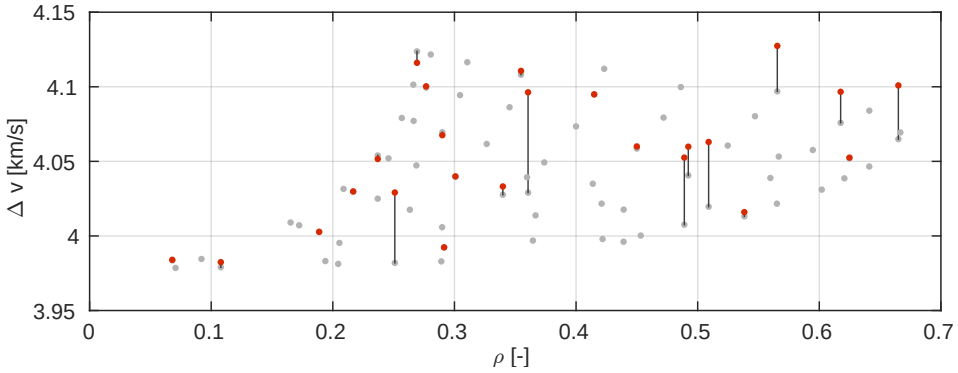

Figure 6.17: 1-stage combinations for a transfer from Low Earth orbit to selected Earth-Moon L_2 Lissajous orbits.

6.3.2 Spacecraft deployment and separation into different orbits

The distribution of spacecraft from a halo orbit onto a quasi-periodic is studied. When focusing on launch scenarios, an efficient way has to be found to separate the satellites either during transfer or once they are inserted into orbit around the Lagrangian point. A single launch with a later deployment enables an increased operational flexibility in terms of launch windows and phasing requirements. Apart from such a separation scenario, transfers to nearby orbits become relevant for formation deployment. Those transfers are designed in the same way as in this scenario.

The scenario assumes two spacecraft launched and injected into a halo orbit g_1 with an orbital period of $T = 3.36\,TU$ $(14.59\,d)$. The objective is to distribute them on a quasi-periodic orbit g_2 in such a way that the phase difference in the ω_2 direction is 210 deg. This scenario is visualised in Fig. 6.18.

In order to find the optimal time for the two transfer manoeuvres, the optimal final

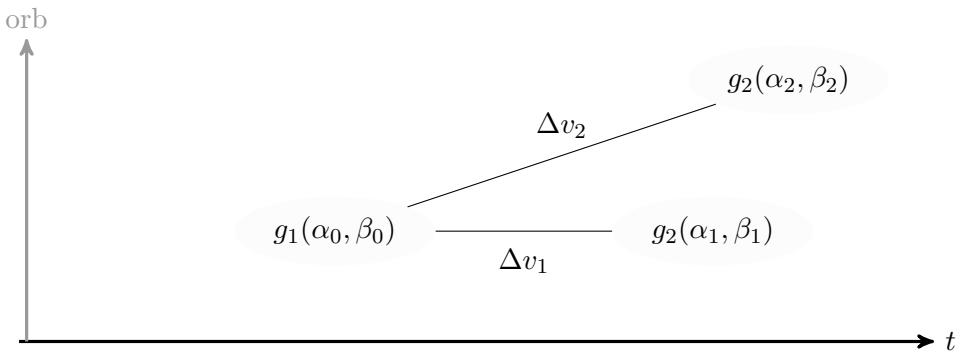

Figure 6.18: Visualisation of the deployment of spacecraft, g_1 is the common orbit before separation and the final orbits and phasing is given by $g_2(\alpha_1, \beta_1)$ and $g_2(\alpha_2, \beta_2)$.

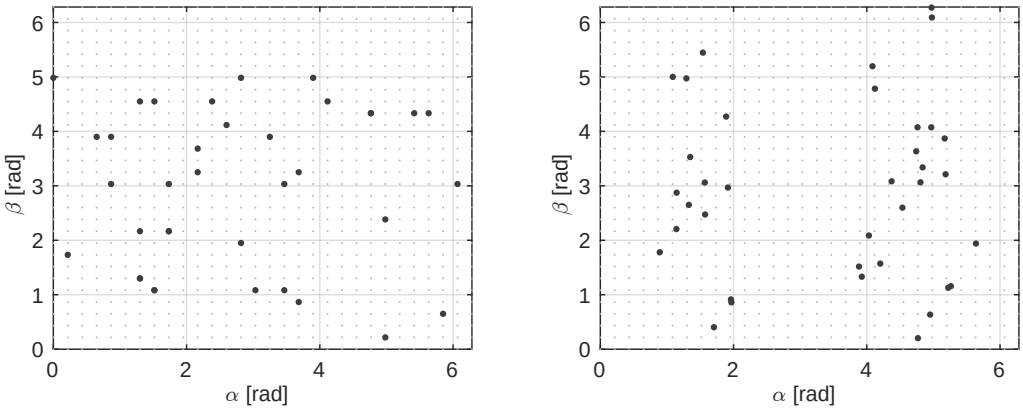

Figure 6.19: Results of a parametric study of transfer options among quasi-periodic orbits, here the orbital parameters are: initial orbit $\boldsymbol{\omega} = (1.7844, 1.7058)$, final orbit $\boldsymbol{\omega} = (1.7823, 1.7000)$. (a) Initial phase pairs and (b) final phases.

phases on the quasi-periodic orbit after the transfer are evaluated. For the scenario a feasible transfer solution is highlighted in Fig. 6.19.

Two transfer options are chosen from the feasible transfers in Fig. 6.19. The manoeuvre phase angles are $(3.538\,rad, 4.865\,rad)$ and $(2.845\,rad, 4.623\,rad)$. The time when the manoeuvres are executed is, for both solutions, $t_i = 2.799\,TU$. Both spacecraft are transferred at the same time, but the time they reach the final orbit is $t_f^1 = 2.70$ for the first spacecraft and $t_f^2 = 1.73$ for the second one. The resulting phase difference of the spacecraft on its new orbit is $\Delta\alpha = 0.019\,rad$ and $\Delta\beta = 3.665\,rad$. Fig. 6.20 shows the trajectory of the spacecraft. The two transfer arcs to the quasi-periodic orbits and

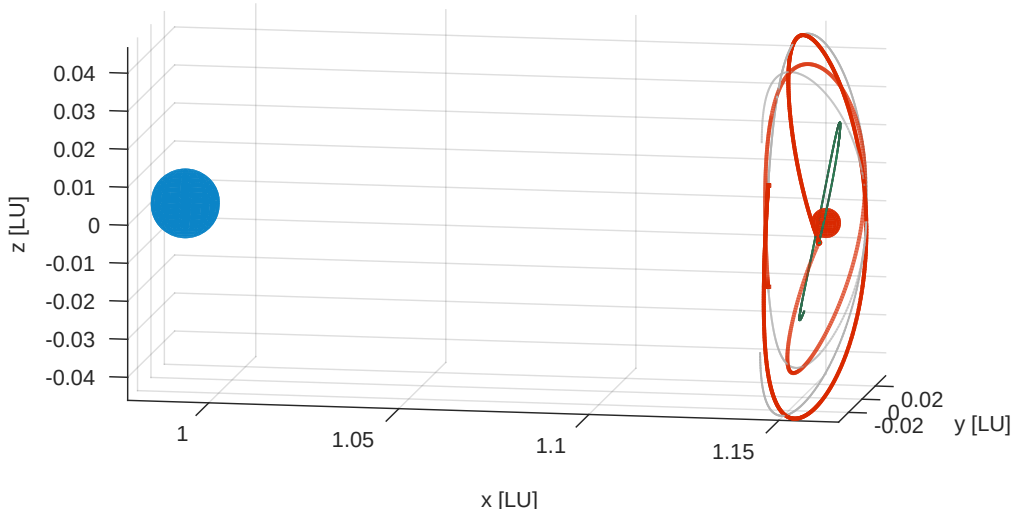

Figure 6.20: Transfer trajectory, initial and final orbit for the separation scenario.

the final trajectories are highlighted.

The deployment phase lasts several days. The two satellites are manoeuvred to reach their final positions on the same orbit but with a phase difference.

6.3.3 Adjusting orbital amplitudes of a Lissajous orbit

The separation sequence left us with two spacecraft moving on the same orbit with a phase difference of $(3.538\,rad,\ 4.865\,rad)$. Since specific mission performance specifications require a Lissajous orbit for the first spacecraft. The seconds spacecraft is parked in its original orbit. Investigations are performed into the relationship between orbital amplitudes and the required Δv. The study is conducted for various amplitude values.

Mission specifications demand precise geometric constraints on the operational orbit. Here, orbital transfers are performed to adjust orbital amplitudes. Starting from a Lissajous orbit with $A_y = A_z = 5000\,km$ transfers leaving towards periodic halo and rectilinear orbits are studied. Furthermore, arrivals at the Lissajous orbit are investigated to complement the accessibility study. This scenario is visualised in Fig. 6.21.

The trajectory of the Lissajous orbit is presented in Fig. 6.22.

Fig. 6.23 and Fig. 6.24 show the transfer costs for a variety of quasi-periodic orbits. The costs depend on the amplitudes, here the dependency is shown for A_x and A_y.

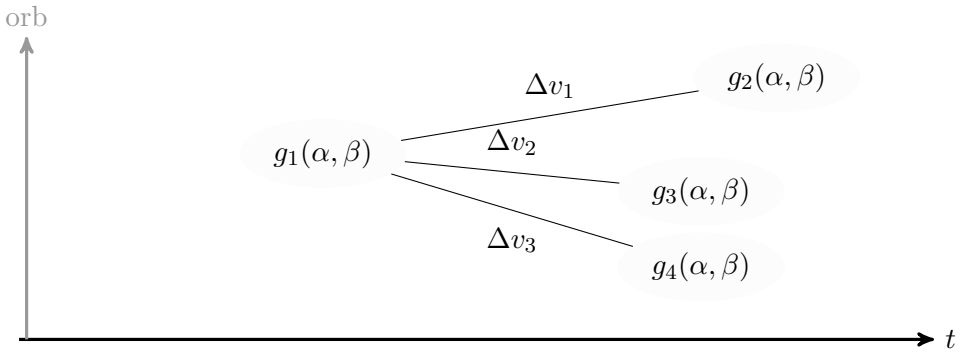

Figure 6.21: Visualisation of different orbit-to-orbit transfers aiming to adjust orbital amplitudes of a Lissajous orbit. The initial orbit is notated as g_1, whereas g_2 to g_4 possess the targeted orbital amplitudes.

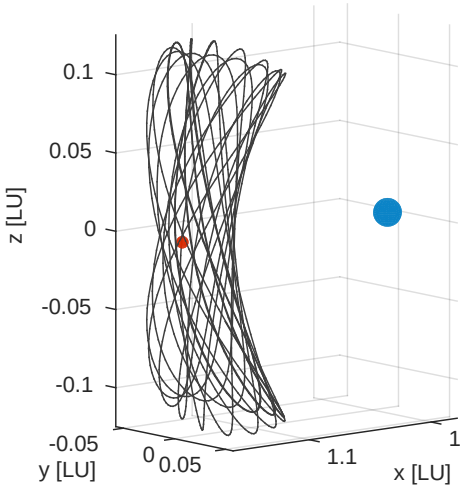

Figure 6.22: Original L_2 Lissajous orbit as basis for the accessibility study with $C = 3.1248$ and $\boldsymbol{\omega} = (1.7459, 1.6208)$.

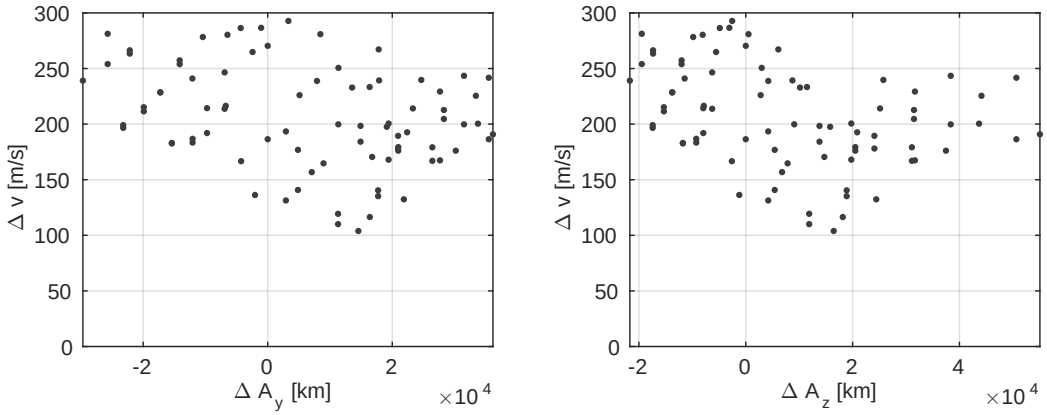

Figure 6.23: Transfer costs associated to adjusting orbital amplitudes for L_2 Northern halo orbits. (a) Dependency on A_y and (b) on A_z.

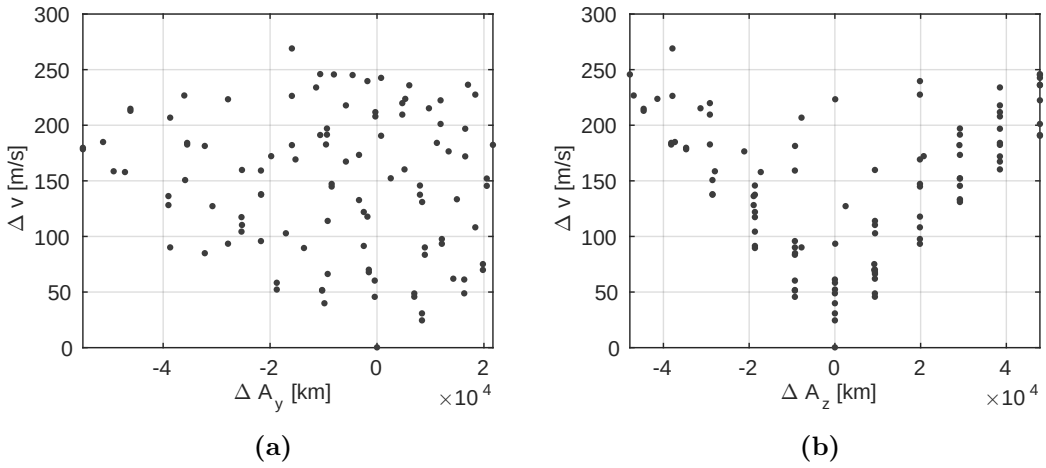

Figure 6.24: Transfer costs associated to adjusting orbital amplitudes for L_2 Lissajous orbits. (a) Dependency on A_y and (b) on A_z.

6.3.4 Accessibility study for a Lissajous orbit with $A_y = A_z = 5000\,km$

In the following transfers are studied originating at the Lissajous orbit with the axis oriented amplitudes $A_y = A_z = 5000\,km$. This orbit might be a suitable choice to do certain in-orbit measurements, but a transfer to another orbit might be required to e.g. include polar regions in successive observations. This emphasises the usefulness and applicability of orbit-to-orbit transfers. The trajectory of the Lissajous orbit is the one already presented in Fig. 6.22. The scenario is visualised in Fig. 6.25.

The first results presented here are transfers leaving the Lissajous orbit towards a range of periodic halo orbits. The range is defined by the orbital amplitude $A_z = 1100 - 1600\,km$. Notable is, at relatively small amplitude Lissajous orbits no halo orbit exists with the same orbital energy, which has the consequence of large transfer costs as feasible transfers are more likely to exist between similar energies.

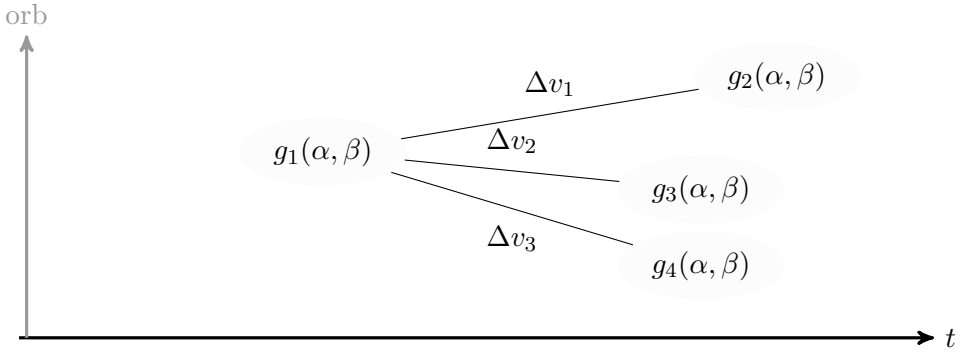

Figure 6.25: Visualisation of orbit-to-orbit transfers. g_1 represents the initial orbit and g_2 to g_4 accessible target orbits.

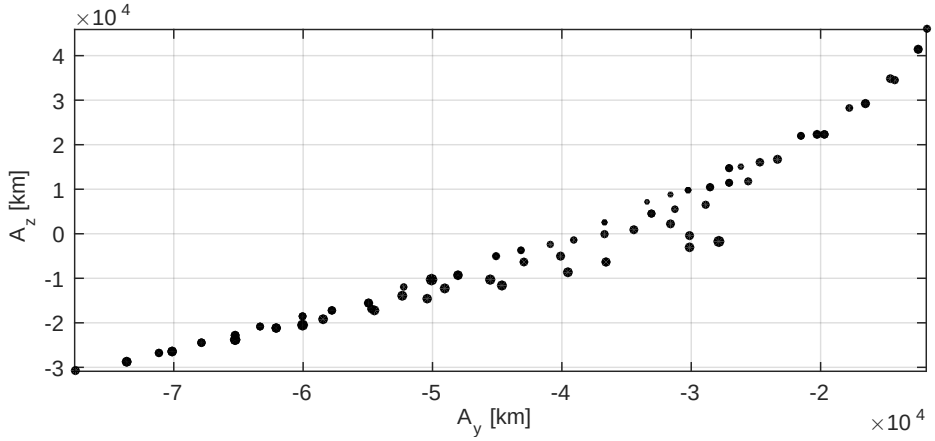

Figure 6.26: Transfer options from the initial orbit utilising the 1-manoeuvre method from a Lissajous orbit with $A_y = A_z = 5000\,km$ to L_2 quasi-periodic Northern halo orbits with $2.4 \cdot 10^4\,km > A_x > 0.6 \cdot 10^4\,km$.

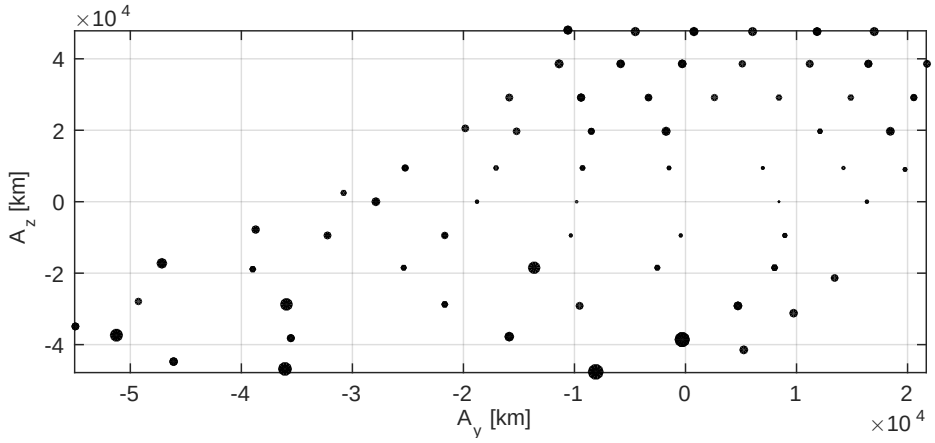

Figure 6.27: Transfer options from the initial orbit utilising the 1-manoeuvre method from a Lissajous orbit with $A_y = A_z = 5000\,km$ to quasi-periodic L_2 Lissajous orbits with $2.4 \cdot 10^4\,km > A_x > 0.6 \cdot 10^4\,km$.

Fig. 6.26 shows the resulting Δv for transfers from the Lissajous orbit to a range of small vertical Lyapunov orbits (rectilinear motion) with $2.4 \cdot 10^4\,km > A_x > 0.6 \cdot 10^4\,km$ to the Lissajous orbit. The size of the dots in the figure indicates the magnitude of the maneouvre relative to the other solutions. Fig. 6.27 highlights transfers from the same Lissajous orbit to quasi-periodic Lissajous ones. Representative solutions are transitioned to an accurate ephemeris model, the transfer costs are given for both dynamical models.

6.3.5 In-orbit rendezvous - a phasing problem

In a previous section optimal manoeuvres from one orbit to another were investigated. Apart from a propellant-optimal solution other transfer arcs exist that might require a higher transfer Δv, but increase flexibility in scheduling manoeuvres. It might be required to phase the spacecraft for a following rendezvous manoeuvre. It is important to reconfigure spacecraft in such a way that a on-orbit rendezvous is achieved for docking activities. In the past, phasing manoeuvres are used to fulfil mission requirements, e.g for the implementation of eclipse avoidance strategies as quasi-periodic Lissajous suffer of longer eclipse periods compared to halo orbits.

In contrast to the amplitude changes of a quasi-periodic orbit, phase changes maintain the geometric properties of a quasi-periodic orbit. The manoeuvre only affects the position of an orbiting spacecraft along the trajectory. This implies that the orbit before and after a successful transfer is described by the same parameter function $\boldsymbol{u}$, see Chap. 4.

A scenario with two spacecraft travelling, only with a phase difference, on the same quasi-periodic orbit is studied, see Fig. 6.28. The initial orbits are g_1 and g_2. A pair of spacecraft is inserted onto the same quasi-periodic orbit with initial phases of $\alpha_1 = 1.63$ and $\beta_1 = 0.40$ and $\alpha_2 = 3.10$ and $\beta_2 = 0.78$. The objective is that both spacecraft meet at a time t at a common location. To provide a parametric analysis on phase changes along a quasi-periodic trajectory, the manifold connections are evaluated, see Fig. 6.29. Both spacecraft follow their nominal path until $t = 1.45$ days with an initial separation of $2.2 \cdot 10^4\, km$. One spacecraft conducts a manoeuvre at $t = 1.45$ and the other one continues on its nominal path. Both spacecraft rendezvous 13.55 days later and follow the quasi-periodic orbit. The Δv requirement for the rendezvous is $83.38\, \frac{m}{s}$. Fig. 6.30 shows the trajectory of both spacecraft.

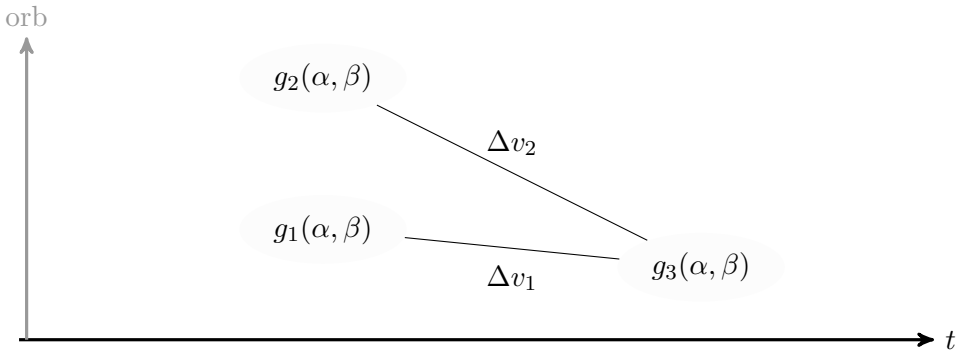

Figure 6.28: Visualisation of a rendezvous scenario. The initial orbits are g_1 and g_2, whereas the rendezvous location lies on orbit g_3.

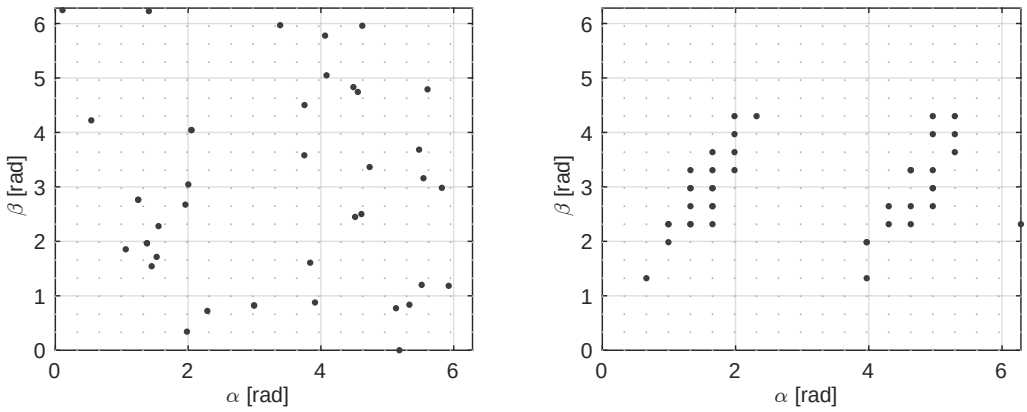

Figure 6.29: Results of a parametric study of transfer options among quasi-periodic orbit, here the orbital parameters are ($\omega_1 = 2.01$ and $\omega_2 = 1.40$). (a) Initial phase pairs and (b) final phases.

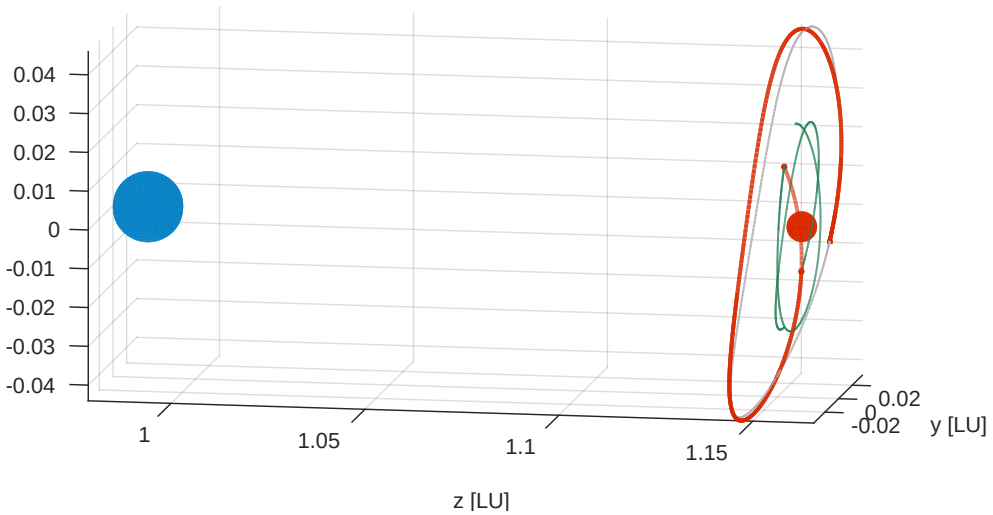

Figure 6.30: Transfer trajectory, initial and final orbit for the rendezvous scenario.

6.4 Discussion and conclusions

This chapter outlined a method for the construction of orbit-to-orbit spacecraft transfers by utilising quasi-periodic orbits and their invariant manifolds. The orbit-to-orbit transfers were introduced as a simple strategy to change orbital parameters of operational orbits for spacecraft missions. The optimisation approach combined a differential evolution algorithm with a gradient-based method. The formulation of the dynamics was used in the form of the circular restricted three-body problem, but results are also presented for the full ephemeris model. Transfers were optimised for several scenarios and transfer costs are investigated. The method proposed in this thesis enables to find energy efficient transfers between quasi-periodic orbits. Compared to work in other publications (Gómez et al. [2004], Davis [2009], Canalias Vila [2007], and Marsden and Ross [2005]) no focus is set on a certain energy level. This method is applicable to find transfers between quasi-periodic solutions, figure of merits can be derived showing the feasibility to transfer spacecraft between a set of orbits. The applicability of the proposed method has been shown by applying it to spacecraft rendezvous and separation scenarios. This method offered lower Δv expenses for the transfers compared to two-impulse transfer arcs. The total cost of the optimal transfer using invariant manifolds was less expensive than the cost of the transfer that did not employ manifolds. It may be possible to lower the transfer cost by allowing for longer manifold propagation. Given longer times of flight, the manifolds may come into better alignment.

CHAPTER 7

Conclusions and future directions

This final chapter concludes the dissertation, presents a summary of this thesis work, and provides an outlook on future work.

7.1 Conclusions

The central research question is how quasi-periodic orbits can support future space missions. Starting from a description of quasi-periodic orbits, this thesis work identified suitable operational orbits, transfer opportunities among those orbits that are potentially useful for next generation of space missions. In this thesis, techniques for the design of quasi-periodic orbits are proposed relying on the simplifications of the circular restricted three-body problem. When appropriate, a more accurate dynamical model was employed to prove new techniques and their applicability. This dissertation lays the foundation to study and utilise quasi-periodic trajectories for future space projects. The following research questions were derived from the central one:

1. How can quasi-periodic orbits be calculated and their parameters be evaluated?
2. How to apply station-keeping to quasi-periodic orbits?
3. What is an appropriate method to design orbital transfers?

To address the first research question, a computation method is proposed, which is suitable for the calculation of quasi-periodic orbits, together with their invariant manifold structure and linear stability characteristics. A better understanding of quasi-periodic motion is given by a parametric function $\boldsymbol{u}$ and the introduction of amplitudes A_x, A_y, A_z, frequencies ω_1 and ω_2, and corresponding phases α and β.

The station-keeping has been investigated for different scenarios in order to address the second research question. The proposed station-keeping algorithm is based on

an orbital lifetime analysis combined a maximisation of the orbital lifetime, which is achieved by a differential evolution algorithm. The orbital lifetime optimisation exploits the natural interaction between the centre and hyperbolic invariant manifolds. It is demonstrated that the combination of a life-time analysis and evolutionary optimisation is a robust method to design station-keeping manoeuvres. It is fast in implementation and flexible in the application to a variety of orbits. For orbits with small amplitudes, the results of the proposed method are comparable to the modal control that can be derived from Floquet modes. When non-linearities are more consistent, with growing amplitudes, the optimisation approach performs better than Floquet. A detailed study will be required to account for navigation and manoeuvring uncertainties. This station-keeping approach is transferable into a non-autonomous high-fidelity dynamical model. Furthermore, the method can be used to generate families of orbits by introducing a simple family continuation scheme.

To focus on the third research question, a method is proposed to construct transfers between quasi-periodic orbits utilising a parametric representation of the orbit and their manifolds. The dynamic behaviour of the libration point regions allows one to create transfers performed by an individual manoeuvre. The transfer trajectories are characterised by the transfer times, initial and final phase shifts and the Δv requirement. The proposed methods utilises a differential evolution method to identify feasible parameter sets, in particular identifying the orbital properties and the initial phases of the spacecraft. A gradient-based optimisation method in finally used to create the continuous transfer arc. This refinement of the trajectory has the objective of computing an orbit continuous both in position and velocity. This method is applicable to find transfers between quasi-periodic solutions, figure of merits can be derived showing the feasibility to transfer spacecraft between a set of orbits.

This hybrid optimisation approach combining a differential evolution algorithm with a gradient-based method provides good results for the highly complex problem of finding the appropriate parameters of such transfers. These transfers are beneficial to increase the in-plane and out-of-plane amplitudes of an orbit, the associated cost range from a few meter per seconds to 150 $\frac{m}{s}$. The cost of the transfers are almost proportional to the amplitude increase in the z direction. The capability to manoeuvre among quasi-periodic orbits was developed and tested on several scenarios.

The work in this thesis shows what can be achieved with quasi-periodic orbits. The parametric representation of a quasi-periodic orbit is valuable to characterise the orbits and incoorporate this description in further studies, e.g. transfers, spacecraft formation and mission concepts studies in general.

7.2 Future directions

The main issue to investigate in further studies are ascent and decent trajectories and how these trajectories connect to quasi-periodic orbits. The method for the transfer design can be extended to find heteroclinic and homoclinic connections or transfer arcs to the primary and secondary body. There are many areas that are of value to be investigated regarding the control of long lifetime science orbits. The most logical extension of the science orbits designed in this thesis is to incorporate precise navigation and detailed models of all of the forces acting on the system. In this work the focus is set to a Earth Moon vicinity, however, the same methods are applicable to different central bodies. In this case, parametric studies of existing orbits and transfers can be valuable.

Bibliography

D. R. Adamo, J. D. Giorgini, P. A. Abell, and R. R. Landis. Asteroid destinations accessible for human exploration: A preliminary survey in mid-2009. *Journal of Spacecraft and Rockets*, 47(6):994–1002, 2010.

E. M. Alessi. *The Role and Usage of Libration Point Orbits in the Earth-Moon System.* PhD thesis, Universitat de Barcelona, 2010.

B. T. Barden and K. C. Howell. Fundamental motions near collinear libration points and their transitions. *The Journal of the Astronautical Sciences*, 46(4):361–378, 1998.

N. Bosanac, K. C. Howell, and E. Fischbach. Exploring the impact of a three-body interaction added to the gravitational potential function in the restricted three-body problem. *AAS/AIAA Space Flight Mechanics Meeting, Kauai, Hawaii*, 148:1829–1848, 2013.

E. Canalias Vila. *Contributions to Libration Orbit Mission Design using Hyperbolic Invariant Manifolds.* PhD thesis, Universitat Politècnica de Catalunya, 2007.

A. K. Catlin and C. A. McLaughlin. Earth-Moon Triangular Libration Point Spacecraft Formations. *Journal of Spacecraft and Rockets*, 44(3):660–670, 2007.

S. R. Chesley, P. W. Chodas, A. Milani, G. B. Valsecchi, and D. K. Yeomans. Quantifying the risk posed by potential Earth impacts. *Icarus*, 159:423–432, 2002.

K. Danzmann, LISA Study Team, et al. Lisa: Laser interferometer space antenna for gravitational wave measurements. *Classical and Quantum Gravity*, 13(11A):A247, 1996.

K. E. Davis. *Locally optimal transfer trajectories between libration point orbits using invariant manifolds.* PhD thesis, University of Colorado at Boulder, 2009.

K. E. Davis, R. L. Anderson, D. J. Scheeres, and G. H. Born. Optimal transfers between unstable periodic orbits using invariant manifolds. *Celestial Mechanics and Dynamical Astronomy*, 109(3):241–264, 2011.

V. Domingo and A. I. Poland. SOHO: an observatory to study the solar interior and the solar atmosphere. *Bulletin of the American Astronomical Society*, 24:781, 1992.

J. R. Dormand and P. J. Prince. A family of embedded runge-kutta formulae. *Journal of Computational and Applied Mathematics*, 6(1):19 – 26, 1980.

D. Dunham and R. Farquhar. *Libration Point Missions, 1978 - 2002.* 2003.

R. W. Farquhar. The utilization of halo orbits in advanced lunar operations. *NASA-TN-D-6365, G-1025*, 1971.

R. W. Farquhar et al. A halo-orbit lunar station. *Astronautics and Aeronautics*, 10:59–63, 1972.

A. Farrés and À. Jorba. Station keeping of a solar sail around a Halo orbit. *Acta Astronautica*, 94(1):527–539, January 2014.

W. M. Folkner, J. G. Williams, and D. H. Boggs. The planetary and lunar ephemeris DE 421. *JPL IOM 343R-08-003*, 2008.

G. Gómez and J. Masdemont. Some zero cost transfers between libration point orbits. *Advances in the Astronautical Sciences*, 105(Part 2):1199–1216, 2000.

G. Gómez, K. C. Howell, J. Masdemont, and C. Simó. Station-keeping strategies for translunar libration point orbits. *Advances in Astronautical Sciences*, 99(2):949–967, 1998.

G. Gómez, A. Jorba, and J. Simó, C .and Masdemont. *Dynamics and Mission Design Near Libration Points - Advanced Methods for Collinear Points*, volume 3 of *World Scientific Monograph Series in Mathematics*. World Scientific Publishing, Singapore, 2001.

G. Gómez, W. S. Koon, M. W. Lo, J. E. Marsden, J. Masdemont, and S. D. Ross. Connecting orbits and invariant manifolds in the spatial restricted three-body problem. *Nonlinearity*, 17 (5):1571, 2004.

G. Gómez, JM. Mondelo, and C. Simó. A collocation method for the numerical fourier analysis of quasi-periodic functions. i. numerical tests and examples. *Discrete and Continuous Dynamical Systems - B*, 14(1):41–74, 2010.

M. Hechler. Herschel, Planck and Gaia orbit design. *ESA Report*, 2002.

A. Héritier. *Exploration of the region near the sun-earth collinear libration points for the control of large formations*. PhD thesis, Purdue University, 2012.

A. Héritier and K. C. Howell. Natural regions near the Sun-Earth libration points suitable for space observations with large formations. *Knowledge Creation Diffusion Utilization*, pages 1–18, 2011.

A. Héritier and K. C. Howell. Regions Near the Libration Points Suitable to Maintain Multiple Spacecraft. *AIAA/AAS Astrodynamics Specialist Conference*, 2012.

A. N. Hirani and R. P. Russell. Approximations of distant retrograde orbits for mission design. *AAS/AIAA Space Flight Mechanics Meeting, Tampa, Florida*, 2006.

K. C. Howell. Formations near the libration points: Design strategies using natural and non-natural arcs. *of GSFC 2nd International Symposium on*, pages 1–25, 2004.

K. C. Howell and H. J. Pernicka. Station-keeping method for libration point trajectories. *Journal of Guidance, Control, and Dynamics*, 16(1):151–159, January 1993.

S. I. Infeld. *Optimization of Mission Design for Constrained Libration Point Space Missions*. PhD thesis, Stanford University, 2005.

A. Jorba and J. Masdemont. Dynamics in the center manifold of the collinear points of the restricted three body problem. *Physica D: Nonlinear Phenomena*, 132(1):189–213, 1999.

M. L. Kaiser, T. A. Kucera, J. M. Davila, O. C. Cyr, M. Guhathakurta, and E. Christian. The stereo mission: An introduction. In *The STEREO Mission*, pages 5–16. Springer, 2008.

N. S. Kardashev, V. V. Andreyanov, V. D. Gromov, V. I. Buyakas, A. S. Gvamichava, A. N. Kotik, V. G. Kurt, G. S. Lazareva, E. N. Mironova, N. V. Myshonkova, et al. The millimetron project. In *Radioastronomical Tools and Techniques*, volume 1, page 111, 2007.

E. Kolemen. *Optimal Configuration of a Planet-Finding Mission Consisting of a Telescope and a Constellation of Occulters*. PhD thesis, Princeton University, 2008.

E. Kolemen, N. J. Kasdin, and P. Gurfil. Multiple Poincaré sections method for finding the quasiperiodic orbits of the restricted three body problem. *Celestial Mechanics and Dynamical Astronomy*, 2011.

T. Lam and G. J. Whiffen. Exploration of distant retrograde orbits around europa. 2005.

J. Laskar. Frequency map analysis and quasiperiodic decompositions. *arXiv Mathematics e-prints*, 2003.

M. W. Lo, R. Serban, L. Petzold, W. S. Koon, S. D. Ross, J. Marsden, and R. Wilson. Halo Orbit Mission Correction Maneuvers Using Optimal Control. *Automatica*, 38(4):571–583, April 2000.

B. G. Marchand. *Spacecraft formation keeping near the libration points of the Sun-Earth/Moon system*. PhD thesis, 2004.

J. E. Marsden and S. D. Ross. New Methods in Celestial Mechanics and Mission Design. *American Mathematical Society*, 43(1):43–73, 2005.

X. Ming and X. Shijie. Exploration of distant retrograde orbits around Moon. *Acta Astronautica*, 65(56):853–860, 2009.

G. Mingotti, F. Topputo, and F. Bernelli-Zazzera. Exploiting distant periodic orbits and their invariant manifolds to design novel space trajectories to the moon. *AAS/AIAA Space Flight Mechanics Meeting, San Diego, California*, 2010.

J. L. Nayler. Soviet rocketry. first decade of achievement. *The Aeronautical Journal (1968)*, 75 (730):743–743, 1971.

Z. P. Olikara. *Computation of quasi-periodic tori and heteroclinic connections in astrodynamics using collocation techniques*. PhD thesis, University of Colorado at Boulder, 2016.

M.T. Ozimek and K.C. Howell. Low-thrust transfers in the earth-moon system, including applications to libration point orbits. *Journal of Guidance, Control, and Dynamics*, 33(2): 533–549, 2010.

T. Pavlak. Mission Design Applications in the Earth-Moon System: transfer Trajectories and Stationkeeping. Master's thesis, Purdue University, 2010.

T. Pavlak and K. C. Howell. Strategy for Optimal, Long-Term Stationkeeping of Libration Point Orbits in the Earth-Moon System. *AIAA/AAS Astrodynamics Specialist Conference*, pages 1–16, August 2012.

G. D. Racca, A. Marini, L. Stagnaro, J. Van Dooren, L. Di Napoli, B. H. Foing, R. Lumb, J. Volp, J. Brinkmann, R. Grünagel, et al. Smart-1 mission description and development status. *Planetary and space science*, 50(14):1323–1337, 2002.

F. Renk. *Mission Analysis for Exploration Missions Utilizing Near-Earth Libration Points*. PhD thesis, University of Stuttgart, 2008.

D. L. Richardson. Analytic construction of periodic orbits about the collinear points. *Celestial Mechanics*, pages 241–253, 1980.

D. J. Scheeres. Satellite dynamics about asteroids: computing poincaré maps for the general case. In *Hamiltonian Systems with Three or More Degrees of Freedom*, pages 554–557. Springer, 1999.

F. Schilder. Computation and continuation of quasiperiodic solutions. *Equadiff 10*, pages 363–377, 2002.

C. Simo, G. Gomez, J. Llibre, R. Martinez, and J. Rodriguez. On the optimal station keeping control of halo orbits. *Acta Astronautica*, 15(6-7):391–397, June 1987.

A. V. Smirnov, A. M. Baryshev, S. V. Pilipenko, N. V. Myshonkova, V. B. Bulanov, M. Y. Arkhipov, I. S. Vinogradov, S. F. Likhachev, and N. S. Kardashev. Space mission millimetron for terahertz astronomy, 2012.

P. D. Spudis. The Moon : Port of Entry to Cislunar Space. 2011.

P. D. Spudis and A. Lavoie. Mission and implementation of an affordable lunar return. 2010.

R. Storn and K. Price. Differential evolution–a simple and efficient heuristic for global optimization over continuous spaces. *Journal of global optimization*, 11(4):341–359, 1997.

D. R. Tolbert. *Spacecraft formation flight at Sun-Earth/Moon libration points*. PhD thesis, Missouri University of Science and Technology, 2009.

D. García Yárnoz, JP. Sanchez, and C.R. McInnes. *Opportunities for Asteroid Retrieval Missions*. Springer Berlin Heidelberg, Berlin, Heidelberg, 2013.